PART I

THE STABILITY OF A MEMBRANE IN A SUBSONIC FLOW

PART II

THE STABILITY OF A GRID OF PANELS IN A SUPERSONIC FLOW

Thesis by

Ronald Oran Stearman

In Partial Fulfillment of the Requirements

For the Degree of

Doctor of Philosophy

California Institute of Technology

Pasadena, California

1961

ACKNOWLEDGMENT

The author wishes to express his sincere appreciation to Dr. Y. C. B. Fung for his encouragement and guidance throughout the course of the investigation. He also wishes to thank Dr. E. E. Sechler for his continued interest and suggestions.

Appreciation is expressed also to Miss Helen Burrus for her typing and general preparation of the manuscript, and to Mrs. Dorothy Eaton and the California Institute of Technology Computing Center for carrying out the numerical calculations in the report. Thanks are also due to Mr. Marvin Jessey concerning the experimental program, to Mr. Milton Wood for the photographs, and to Mrs. Betty Wood for her rendition of the graphs and figures.

This study has been financed by the Air Force Office of Scientific Research which is currently sponsoring a research program in panel flutter at the Institute. This aid is gratefully acknowledged.

PART I

THE STABILITY OF A MEMBRANE IN A SUBSONIC FLOW

ABSTRACT

An experimental investigation has been made on the stability of small aspect ratio rectangular membranes in a subsonic flow. The leading and trailing edges of the membrane were attached to rigid streamlined supports while the two streamwise edges were free. Both surfaces of the membrane were exposed to the airstream, and the membrane tension was applied through the trailing edge.

The results of the test show that two types of flutter (instability) occur. The first to appear as the wind speed was increased from zero, with a fixed tension level in the membrane, was a small amplitude flutter which has a shallow wave like motion traveling in the streamwise direction. At higher wind speeds this motion was damped out. A narrow equilibrium zone or boundary existed which separated the first type of flutter from a second type of motion having a traveling wave of larger amplitude and greater speed. This second type of flutter had no tendency to damp out, but became more violent as the wind speed was increased.

The span of the slender membrane is the physical parameter that uniquely determines and controls the first flutter boundary; its mass plays no part here, but does affect the equilibrium zones.

Appendix A contains an obvious formulation of the slender membrane flutter problem.

TABLE OF CONTENTS

LIST OF FIGURES

LIST OF SYMBOLS

AR	$\frac{S}{\ell}$ aspect ratio
a	$(\mu + \frac{1}{\sigma_n \pi})$ see equation 8 - Appendix A
b	$\frac{1}{\sigma_n \pi}$ see equation 8 - Appendix A
c	$(-\frac{N_x}{Sq} + \frac{1}{\sigma_n \pi})$ see equation 8 - Appendix A
C	wave speed of the membrane in an airstream
C_o	$\sqrt{\frac{N_x}{\gamma}}$ = wave speed of the membrane in a vacuum
f	frequencies - cycles per second
g_n	eigen function - see equation 6 - Appendix A
h	lateral deflection of the panel
H	$\frac{h}{\ell}$ = non-dimensional lateral deflection
K	$\frac{\omega \ell}{U}$ = non-dimensional frequency - reduced frequency
L	kernel function - see page 13 - Appendix A
ℓ	membrane length
M	free stream Mach number
m	integer (positive)
n	integer (positive)
N_x	$\frac{W}{S}$ = membrane tension per unit span
P_a	aerodynamic pressure induced by lateral deflection

q	$(1/2)\,\rho_a U^2$ free stream dynamic pressure
S	membrane span
t	membrane thickness
t	time
U	speed of flow at infinity
w	downwash
W	tension load applied to the membrane trailing edge
x	streamwise coordinate
y	spanwise coordinate
z	vertical coordinate, positive down
α	$\frac{b}{c}$
β	$\sqrt{1 - \frac{ac}{b^2}}$
$\bar{\beta}$	$\sqrt{-1 + \frac{ac}{b^2}}$
γ	mass per unit area of membrane
δ	ratio of amplitude of lateral oscillation to membrane chord
$\mathcal{J}$	$\frac{2\eta}{S}$ = non-dimensional spanwise parameter
η	spanwise parameter
μ	$\frac{2\gamma}{\rho_a S}$ = mass ratio parameter

ν	$\frac{2y}{s}$ = non-dimensional spanwise coordinate
ξ	$\frac{x}{\ell}$ = non-dimensional streamwise coordinate
ρ_a	mass density of air in free stream
ρ_s	mass density of membrane
σ_n	Eigenvalue, see equation 6, Appendix A
τ	$\frac{Ut}{\ell}$ = non-dimensional time
ϕ	velocity potential
ω	$2\pi f$ = frequency radius per second

INTRODUCTION

The membrane flutter problem is as old as flag flutter itself. The earliest work on the problem dates back to Lord Rayleigh's (Ref. 1) investigation of the flapping of flags and sails. More recent investigations have been made by Greenspan and Goldman (Ref. 2), Jordon (Ref. 3), Miles (Ref. 4), Hedgepath (Ref. 5), Thoma (Ref. 6), and Ashley and Zartarian (Ref. 7). The theoretical problem is more difficult than it first appears, and in certain cases the seemingly simple membrane problem requires more effort to solve than the corresponding plate problem (Ref. 8). Since a theoretical solution to the flutter of a finite membrane had not yet been obtained, an experimental investigation was carried out to observe some of the physical features of the phenomena.

The tests were conducted in the GALCIT* Merrill Wind Tunnel which has a maximum operating speed of approximately 160 miles per hour. The rectangular vented test section measures 42 inches wide, 36 inches high, and has a usable length of about four feet.

Rectangular slender membranes were the only models used in the flutter tests. (A slender membrane, as used here, means a planar body with a low aspect ratio, and negligible bending stiffness). This particular geometry of membrane was chosen because it appeared that the experimental results might be compared with the deductions of the simple slender wing theory.

---

* Guggenheim Aeronautical Laboratory, California Institute of Technology.

Moving pictures were taken of the fluttering membranes to illustrate and clarify the types of motion that occurred. The experiment was also designed to provide information on the frequency and maximum amplitude of flutter, and the combination of parameters which define the regions of flutter.

MODEL AND INSTRUMENTATION

The membranes were made of a Mylar Polyester Film* which proved superior to most metal, cloth or paper materials due to its greater toughness, excellent uniformity, and availability in several close tolerance thicknesses. Tests were made on membranes with a common length of 28 inches, spans of 5 and 6 inches, and thicknesses of 0.001, 0.003, and 0.0075 of an inch.

All of the membranes formed a small aspect ratio deformable wing with its leading edge taped behind a NACA 0018 wing section spanning the tunnel width. This was done to ensure a uniform flow of air over both sides of the membrane, and to eliminate the possibility of a separated flow caused by a sharp leading edge. The trailing edge of the membrane was fastened to a small rod mounted on bearings which allowed a horizontal but not vertical movement as flutter occurred. This moveable rear support was used to help maintain a constant membrane tension N_x (i.e. one which would be independent of the flutter amplitude). The tension load in the membrane was applied through a whiffle tree connected to the trailing edge support. Different tension levels then could be applied with a damped spring system or with free hanging weights. Installation of a model in the test section is shown in Figures 1, 2, and 3. An alternate attachment was developed to shorten the length of the rear supporting rod. This was done to increase the rod rigidity and reduce its drag (see Figures 7 and 8). The wing section was mounted at each end through a point

---

* Mylar Polyester Film is manufactured by E. I. DuPont De Nemours and Co., Inc., Film Dept., Wilmington, Delaware.

located at its center of gravity. Alignment of the wing and membrane was then obtained by applying a large tension load, at the whiffle tree, which snapped the wing, free to rotate, into the proper position where it was locked.

Since the flow direction changed with tunnel velocity it was necessary to rotate the wing membrane combination relative to the tunnel test section to obtain zero angle of attack at all velocities. This was accomplished by the handle on the gear pinion at the rear of the test section shown in Figure 3. The complete system was also counterbalanced so it could be stopped and locked at any position in which it was set by the handle. An airfoil angle of attack was indicated by a manometer which measured the static pressure differential, at a chordwise point, between the upper and lower surfaces of the symmetric wing.

The test section dynamic pressure was measured from two static rings built in the tunnel wall and connected to a micromanometer. The true dynamic pressure was then obtained from this recorded data with the aid of a calibration curve of the tunnel. No blockage correction was used since it was found to be less than 0.1 per cent based on the model/test section area ratio.

The frequency of the membrane vibration and amplitude of a point on its edge were measured with the aid of an optical oscillograph which was made for low frequency measurements. A schematic view of the instrument and its principle of operation are shown in Figures 4 and 5. A pencil of light was reflected into a lens system by the flattened and polished head of a straight steel pin taped to the edge of the membrane. An image of this pin was then focused by the lens

system onto photo-sensitive paper rolled on a rotating drum. As the pin moved with the fluttering membrane in the light field a trace was recorded on the moving paper. The speed of the paper could be varied for different spacings of the trace. Figure 6 illustrates some traces of amplitude time response at the 75 per cent chord of the membrane during flutter. A further discussion of these traces is given in the "Test Results" section.

TEST PROCEDURE

The significant parameters which could be varied in the wind tunnel test were the dynamic pressure, membrane thickness (i.e. mass per unit area), span, length, and membrane tension. The following variations in geometric parameters were tested; 0.001, 0.003, and 0.0075 inch in thicknesses, two span widths of 5 and 6 inches and one length of 28 inches. Membrane tensions ranged from 0 to 20 pounds per foot while corresponding dynamic pressures ranged from 0 to 56 pounds per square foot. Tensile stress in the membranes was less than 1000 pounds per square inch. Mylar film's yield strength is around 7000 - 8000 pounds per square inch. Only one material was used for these tests since preliminary investigations indicated that the Mylar Polyester Film made a good durable light weight membrane. (Mylar has a specific gravity of 1.39).

The procedure used to establish a stability boundary was as follows: After a membrane was installed and a given tension load applied, the tunnel velocity was increased until the first flutter was visually observed. The tunnel velocity was increased further until an upper bound was reached where the flutter was damped out and the membrane remained undeflected with no noticeable flutter. The tunnel velocity was then decreased until flutter again occurred and then stopped. In this manner the first stability boundary was approached from both increasing and decreasing wind speeds.

A variation on the above procedure was to increase the tunnel speed beyond the equilibrium zone and observe the second type flutter

that occurred. Investigations were made on the width of the equilibrium zone separating the two types of flutter and the effect of approaching this zone from the second flutter regime.

The frequency of flutter and amplitude of a given point on the membrane were determined by using the optical oscillograph described in the "Model and Instrumentation" section.

TEST RESULTS

Two types of flutter were found for rectangular slender membranes similar to the model shown in Figures 1 and 2. The first to appear as the wind speed was increased from zero, with a fixed tension level in the membrane, was a small amplitude flutter having a shallow wave form which traveled in the direction of the airstream. As the wind speed was further increased, a point was reached at which this first type of flutter appeared to be damped out, leaving the membrane in a flat highly unstable position. The membrane would stay in this flat state for a very narrow range of wind speed. A slight increase in speed above this value would cause the membrane to jump into a larger amplitude traveling wave motion, while a decrease in speed would take the membrane back into the first flutter zone.

Figures 7 and 8, taken from movie films of the motion, illustrate this first and second type flutter respectively. (The tuft spacing in the figures is approximately two inches between rows). The traveling wave nature of the motions can be seen as well as the differences in amplitude, wave length, and wave speed. No measurements were made on the lengths of the traveling waves, but for a given membrane tension and span the length of waves in the second type flutter appeared to be smaller than those of the first type flutter. The width of the equilibrium zone was quite narrow and difficult to measure, so no accurate estimates were obtained on the zone dimensions. The experimental data shown in Figure 10 define only where the first type flutter was damped out; the second type flutter occurred slightly to the other side of this line.

During both types of motion the wave amplitude grew as it traveled toward the trailing edge of the membrane, and reached a maximum near the 75 - 85 per cent chord. This amplitude growth was more prominent, however, in the second type of flutter.

The first stability boundary was found to be invariant under the direction of approach. It was not possible in the experiment, however, to reach the narrow equilibrium zone from above; it seemed to disappear when approached from the large amplitude flutter regime.

The trailing edge condition, whether free to move horizontally or completely restrained, seems to have no effect on the first type of flutter. This is probably due to the small amplitude of motion. For this reason the restraining of the trailing edge from horizontal movement will not change the character or position of the first stability boundary or the equilibrium zone. The amplitude of the second type flutter was, as could be expected, smaller when the trailing edge was restrained from horizontal movement.

In Figure 6 is shown the behavior of an amplitude time response at the 75 per cent chord of the membrane. A discrete progression is made in velocity, for a constant N_x/S of 36 lb/ft^2, from the first through the second stability boundary. In Figure 10 this represents the straight line progression as shown by the dotted arrow. The top four traces represent the membrane during its first type flutter; while the fifth trace was taken with the membrane in the narrow equilibrium zone. The last two traces illustrate the amplitude response found immediately upon entering the second flutter regime. If the recording tape were

traveling the speed of the wave the traces would be representative of the true wave shape. Since this did not occur the traces represent a distorted picture of the wave.

At the onset of the first type flutter (see top trace), the motion is harmonic and a single frequency exists. As the wind speed increases the form of wave is perturbed slightly as shown by the second trace. Further increase in wind speed causes an unusual shape to occur on the side of the fundamental wave form (see trace 3). It appears as though a smaller wave were riding on the side of the larger one. Shown in trace 4, at a still slightly higher wind speed, is an apparent break-up of the fundamental wave form. A break-up of wave pattern with increasing air speed has also been observed by Jordan (Ref. 3) in an earlier report.

Figure 12 shows the frequency and reduced frequency ranges that occur during a well established first type flutter (i.e. about midway between the first and second stability boundaries). The characteristic length in the reduced frequency is the membrane chord.

Shown in Figures 9 and 10 are the two types of boundaries as defined by the experimental data. The parameters used to determine the first flutter boundary (Figure 9) are the membrane tension N_x, the span S, and the free stream dynamic pressure q. This first boundary, defined by

$$\frac{N_x}{Sq} = 0.988 \approx 1 \qquad (1)$$

is independent of the mass of the membrane. Thus $\frac{N_x}{Sq} < 1$ is a requirement for the observation of flutter on the membrane.

The second boundary or equilibrium zone is plotted against the same parameters which determined the first flutter boundary (see Figure 10). The experimental data here indicate a dependence of the equilibrium zone on the membrane mass. A suggested form for this second boundary is

$$\frac{N_x}{Sq} = 1 - f(\mu) \qquad (2)$$

$$f(\mu) > 0 \text{ for any } \mu > 0$$

where μ is the membrane mass ratio parameter. No explicit form was obtained for the function $f(\mu)$.

Figure 11 represents a summary of the membrane stability boundaries as obtained from the experimental study. Table I contains the experimental data that defines these boundaries.

Utilizing equation 1 a comparison can be made between the wave speed of the membrane in a vacuum and the first critical wind speed causing flutter.

$C_o = \sqrt{\frac{N_x}{\gamma}}$ = wave speed of a membrane in a vacuum.

$q = \frac{N_x}{S}$ = critical dynamic pressure first causing flutter.

$$\left(\frac{C_o}{U}\right)_{cr} = \sqrt{\frac{\rho_a}{\gamma}\,\frac{S}{Z}} = \sqrt{\frac{\rho_a}{\rho_s}\,\frac{S}{Zt}} = 1/\sqrt{\mu} \qquad (3)$$

Shown in Figure 13 is a plot of $(C_o/U)_{cr}$ as a function of the mass ratio parameter μ and the membrane thickness t. From this plot it can be seen that the critical wind speed causing flutter may be larger, equal to, or smaller than the wave speed of the membrane in a vacuum.

The effect of the turbulent wake of the wing section on the membrane flutter and equilibrium boundaries is not known. Reference 9, however, indicates that the frequencies found in the wake of a thin wing are many times higher than the flutter frequencies observed in this experiment.

REFERENCES

1. Rayleigh, Lord (John William Strutt): On the Instability of Jets. Proc. of London Math. Soc., 10, 1 (1878) 4-12 Scientific Papers, Vol. 1, p. 361. See also Lamb, H.: Hydrodynamics. 6th Edition, Dover Publications, p. 374.

2. Greenspan, J. and Goldman, R.: Flutter of Thin Panels at Subsonic and Supersonic Speeds. Office of Scientific Research, United States Air Force Contract No. AF 18(603)-76, OSR Technical Report No. 57-65 (Martin Aircraft Co.), November 1957.

3. Jordan, P. F.: The Physical Nature of Panel Flutter. Aero Digest, February 1956, pp. 34-38.

4. Miles, J. W.: On the Aerodynamic Instability of Thin Panels. Journal of Aero. Sci., Vol. 23, No. 8, August 1956, pp. 771-780.

5. Hedgepeth, J. M.: On the Flutter of Panels at High Mach Numbers. Journal of Aero. Sci. (Readers Forum), Vol. 23, No. 6, June 1956, pp. 609-610.

6. Thoma, D.: Why Does the Flag Flutter? Cornell Aero. Lab. Translation, 1949 (Translated from Mitteilungen des Hydraulischen Instituts der Technischen, Hochschule, Muenchen, No. 9, pp. 30-34, 1939).

7. Ashley, H. and Zartarian, G.: Piston Theory - A New Aerodynamic Tool for the Aeroelastician. Journal of Aero. Sci., Vol. 23, No. 12, December 1956, pp. 1109-1118.

8. Fung, Y. C.: On Two-Dimensional Panel Flutter. Journal of Aero. Sci., Vol. 25, No. 3, March 1958, pp. 145-160.

9. Cambell, G. S.: Turbulence in the Wake of a Thin Airfoil at Low Speeds. NACA TM 1427, January 1957.

10. Miles, J. W.: Unsteady Supersonic Flow. University of California at Los Angeles Monograph, March 1955.

11. Garrick, I. E.: Some Research on High Speed Flutter, Appendix B. Anglo-American Aeronautical Conference, Brighton, 1951, pp. 442-444.

12. Miles, J. W.: On Non-Steady Motion of Slender Bodies. Aero. Quarterly, Vol. 2, Part III, November 1950, pp. 183-194.

13. Kac, M.: On Some Connections Between Probability Theory and Differential and Integral Equations. Second Berkeley Symposium on Mathematical Statistics and Probability, University of California Press, 1951, pp. 189-215.

14. Kac, M. and Pollard, H.: On the Distribution of the Maximum of Partial Sums of Independent Random Variables. Canadian Journal of Math., Vol. 2, 1950, pp. 375-384.

15. Hildebrand, F. B.: Methods of Applied Mathematics. Prentice-Hall Inc., New York, 1952.

16. Hardy, G.: Divergent Series. Oxford at the Clarendon Press, 1949, pp. 3-5, Appendix I, pp. 349-352.

APPENDIX A

Theoretical Formulation of the Slender Membrane Flutter Problem

The following is an obvious formulation of the slender membrane flutter problem for the model shown in Figure 14. The equation of motion and appropriate boundary conditions assuming small deflections are:

$$P_a - \gamma \frac{\partial^2 h}{\partial t^2} + N_x \frac{\partial^2 h}{\partial x^2} = 0 \qquad (1)$$

$$h(0, y, t) = h(\ell, y, t) = 0$$

where $h(x, y, t)$ is the lateral deflection of the membrane, $P_a(x, y, t)$ the lateral load per unit area due to the aerodynamic pressures, γ its mass per unit area, and N_x its tension per unit width.

The aerodynamic pressures on the membrane are determined from a solution of the following slender wing problem:

$$\phi_{yy} + \phi_{zz} = 0$$

$$\left.\frac{\partial \phi}{\partial z}\right|_{z = o^+} = w = \left(\frac{\partial}{\partial t} + U \frac{\partial}{\partial x}\right) h(x, y, t) \text{ B.C. on wing}$$

$$\phi(x, y, 0, t) = 0 \quad \text{B.C. off wing} \qquad (2)$$

$$\phi(x, y, z, t) = 0 \text{ as } |y|, |z| \to \infty \text{ B.C. at } \infty$$

$$\left(\frac{P - P_\infty}{\rho_\infty}\right) = -\left(\frac{\partial \phi}{\partial t} + U \frac{\partial \phi}{\partial x}\right) \qquad \text{Note } (\rho_\infty = \rho_a)$$

This problem formulation is subject to the following parametric restrictions (Ref. 10):

$$\varsigma << 1$$

$$K = O(1)$$

$$K << (M\ )^{-2}$$

$$|M^2 - 1| << (AR)^{-2}$$

$$AR << |\varsigma|^{-1/2}$$

Its solution gives the pressure loading on the membrane in terms of the lateral deflection as

$$P = -\frac{\rho_a}{\pi} \int_{-S/2}^{S/2} L(y, \eta, S) \left(\frac{\partial}{\partial t} + U \frac{\partial}{\partial x}\right)^2 h(x, \eta, t)\, d\eta$$

where $L(y, \eta, S)$ is a well known kernel (see references 11 and 12 given by:

$$L(y, \eta, S) = -L_1(y, \eta, S) =$$

$$-L_n\left[\frac{(y-\eta)^2 + \left[\sqrt{(S/2)^2 - y^2} + \sqrt{(S/2)^2 - \eta^2}\right]^2}{(y-\eta)^2 + \left[\sqrt{(S/2)^2 - y^2} - \sqrt{(S/2)^2 - \eta^2}\right]^2}\right]$$

Noting that $P_a = -P$ the equation of motion and boundary conditions for the slender membrane take the following form:

$$- \frac{\rho_a}{\pi} \int_{-S/2}^{S/2} L_1(y, \eta, S) \left[\frac{\partial^2 h}{\partial t^2} + 2U \frac{\partial^2 h}{\partial x \partial t} + U^2 \frac{\partial^2 h}{\partial x^2} \right] d\eta$$

(3)

$$- \gamma \frac{\partial^2 h}{\partial t^2} + N_x \frac{\partial^2 h}{\partial x^2} = 0$$

$h(0, y, t) = h(\ell, y, t) = 0$

Introducing the dimensionless variables:

$$H = \frac{h}{\ell} \qquad \mathcal{S} = \frac{2\eta}{S} \qquad K = \frac{\omega \ell}{U}$$

$$\xi = \frac{x}{\ell} \qquad \tau = \frac{Ut}{\ell}$$

$$\nu = \frac{2y}{S} \qquad \mu = \frac{2\gamma}{\rho_a S}$$

into the equation of motion 3 gives:

$$- \frac{1}{\pi} \int_{-1}^{1} L_1(\nu, \mathcal{S}) \left[\frac{\partial^2 H}{\partial \tau^2} + 2 \frac{\partial^2 H}{\partial \xi \partial \tau} + \frac{\partial^2 H}{\partial \xi^2} \right] d\mathcal{S} - \mu \frac{\partial^2 H}{\partial \tau^2} + \frac{N_x}{Sq} \frac{\partial^2 H}{\partial \xi^2} = 0$$

(4)

with boundary conditions

$$H(0, \nu, \tau) = H(1, \nu, \tau) = 0$$

The kernel $L_1(\nu, \mathcal{S})$ reduces to:

$$L_1(\nu, \varsigma) = \ln \left[\frac{1 - \nu\varsigma + (1 - \nu^2)(1 - \varsigma^2)}{1 - \nu\varsigma - (1 - \nu^2)(1 - \varsigma^2)} \right]$$

Assuming the following form of solution

$$H(\xi, \nu, \tau) = H_n(\xi, \tau)\, g_n(\nu)$$

the equation of motion becomes:

$$-\frac{1}{\pi}\left[\frac{\partial^2 H_n}{\partial \tau^2} + 2\frac{\partial^2 H_n}{\partial \xi \partial \tau} + \frac{\partial^2 H_n}{\partial \xi^2}\right] \int_{-1}^{1} L_1(\nu, \varsigma)\, g_n(\varsigma)\, d\varsigma +$$

$$\left[-\mu \frac{\partial^2 H_n}{\partial \tau^2} + \frac{N_x}{Sq} \frac{\partial^2 H_n}{\partial \xi^2}\right] g_n(\nu) = 0 \qquad (5)$$

If the pressure distribution across the span of the membrane is assumed to be directly proportional to the spanwise displacement $g_n(\nu)$, the system of chordwise modes will be uncoupled from the spanwise modes and the equation of motion 5 reduced to partial differential equations with constant coefficients. Further this unknown displacement function $g_n(\nu)$ may be obtained by solving the following Fredholm integral equation.

$$\int_{-1}^{1} L_1(\nu, \varsigma)\, g_n(\varsigma)\, d\varsigma = \frac{1}{\sigma_n}\, g_n(\nu) \qquad (6)^*$$

The eigenvalues in equation 6 are ordered so that σ_1 equals the minimum one in absolute value. The singular kernel $L_1(\nu, \varsigma)$ is real, symmetric, positive definite, and quadratically integrable, i.e.

$$\int_{-1}^{1} \int_{-1}^{1} L_1^2(\nu, \varsigma)\, d\nu \quad d\varsigma < \infty$$

Thus the existing eigenvalues are all positive and denumerable, while the corresponding eigenfunctions are continuous, orthogonal, and form a complete set. The eigenfunctions also vanish at the end points (-1, 1) (i.e. the wing tips). The integral equation 6, however, does not seem solvable in terms of known functions**. Fortunately further analysis requires only a knowledge of the eigenvalues σ_n***. In the subsequent investigation, therefore, the unknown eigenfunctions $g_n(\nu)$ are used to represent the spanwise mode shapes of the membrane flutter to within a rigid body translation H_o of the spanwise element (see Section A-A

---

* It is of interest to note that this eigenvalue problem is identical to one that has arisen in Probability Theory - see for example Reference 13, equation 8.15 and 8.16 and Reference 14.

** ibid.

*** It has been shown in Reference 13 that $\sigma_n \sim n$.

Figure 14). Under this assumption the integral differential equation of motion 5 is reduced to:

$$\left(\mu + \frac{1}{\sigma_n \pi}\right) \frac{\partial^2 H_n}{\partial \tau^2} + \left(- \frac{N_x}{Sq} + \frac{1}{\sigma_n \pi}\right) \frac{\partial^2 H_n}{\partial \xi^2} + \frac{2}{\sigma_n \pi} \frac{\partial^2 H_n}{\partial \xi \partial \tau} = 0 \quad n=1, 2, \ldots \tag{7}$$

with boundary conditions.

$$H_n(0, \tau) = H_n(1, \tau) = 0$$

All n equations of motions are qualitatively the same since they differ only in their constant coefficients. It is thus sufficient to obtain and discuss only the solution of the nth equation. Further the equations are all of the Euler type given by:

$$a \frac{\partial^2 H_n}{\partial \tau^2} + 2b \frac{\partial^2 H_n}{\partial \xi \partial \tau} + c \frac{\partial^2 H_n}{\partial \xi^2} = 0 \tag{8}$$

and may take one of three forms as defined by their coefficients.

$$\begin{aligned} b^2 - ac &> 0 \quad \text{hyperbolic} \\ b^2 - ac &= 0 \quad \text{parabolic} \\ b^2 - ac &< 0 \quad \text{elliptic} \end{aligned} \tag{9}$$

where

$$a = \left(\mu + \frac{1}{\sigma_n \pi}\right)$$

$$b = \frac{1}{\sigma_n \pi} \tag{10}$$

$$c = \left(-\frac{N_x}{Sq} + \frac{1}{\sigma_n \pi}\right)$$

The motion at the critical flutter condition may be considered as harmonic and thus given by:

$$H(\xi, \nu, \tau) = H_n(\xi)\, g_n(\nu)\, e^{iK\tau} \tag{11}$$

Solutions of the form:

$$H_n(\xi)\, e^{iK\tau} \tag{12}$$

are then assumed for the n partial differential equations of motion.

Substituting 12 into 7 leads to the eigenvalue problem

$$A H_n(\xi) - K^2 H_n(\xi) = 0$$

$$H_n(0) = H_n(1) = 0 \tag{13}$$

where $H_n(\xi)$ is the eigenfunction and K^2 the eigenvalue of the differential operator A given by:

$$A = \frac{1}{a}\left[c\,\frac{d^2}{d\xi^2} + i\,2K\,b\,\frac{d}{d\xi}\right]$$

The mth eigenfunction and associated eigenvalue of the operator A will be designated as H_{mn} and K_m respectively. Since for each spanwise mode n there are associated m chordwise modes.

The eigenfunctions $H_{nm}(\xi)$ are of the form

$$H_{nm}(\xi) = B\,e^{\Omega\xi}$$

with the following characteristic equation for Ω

$$c\,\Omega^2 + 2\,iKb\,\Omega - K^2 a = 0$$

which has the following two roots

$$\Omega_{1,2} = K\frac{b}{c}\left[-i \pm \sqrt{-1 + \frac{ac}{b^2}}\right] \qquad (14)$$

It is convenient at this point to parallel the two solutions to 8 which are classified as hyperbolic or elliptic. In the hyperbolic zone

$$1 - \frac{ac}{b^2} > 0$$

and the roots $\Omega_{1,2}$ take the form

$$\Omega_{1,2} = iK\frac{b}{c}\left[-1 \pm \sqrt{1 - \frac{ac}{b^2}}\right] = ik\alpha\left[-1 \pm \beta\right] \qquad (15)$$

α, β real

while in the elliptic zone

$$1 - \frac{ac}{b^2} < 0$$

giving

$$\Omega_{1,2} = K\frac{b}{c}\left[-i \pm \sqrt{-1 + \frac{ac}{b^2}} \right] = K\alpha\left[-i \pm \bar{\beta} \right] \qquad (16)$$

$\alpha, \bar{\beta}$ real

The eigenfunctions thus become:

$$H_{nm}(\xi) = e^{-iK\alpha\xi}\left[B_1 e^{iK\alpha\beta\xi} + B_2 e^{-iK\alpha\beta\xi}\right] \text{(hyperbolic)} \qquad (17a)$$

$$H_{nm}(\xi) = e^{-iK\alpha\xi}\left[B_1 e^{K\alpha\bar{\beta}\xi} + B_2 e^{-K\alpha\bar{\beta}\xi}\right] \text{(elliptic)} \qquad (17b)$$

Satisfying the boundary condition $H_{nm} = 0$ at the leading edge gives:

$$H_{nm} = 2i B_1 e^{-iK\alpha\xi} \sin(K\alpha\beta\xi) \qquad \text{(hyperbolic)} \qquad (18a)$$

$$H_{nm} = 2 B_1 e^{-iK\alpha\xi} \sinh(K\alpha\bar{\beta}\xi) \qquad \text{(elliptic)} \qquad (18b)$$

The trailing edge boundary condition $H_n(1) = 0$ yields the eigenvalues:

$$K = \pm \frac{m\pi}{\alpha\beta} \qquad m = 0, 1, 2, 3, \ldots \qquad \text{(hyperbolic)} \qquad (19a)$$

$$K = \pm i\frac{m\pi}{\alpha\bar{\beta}} \qquad m = 0, 1, 2, 3, \ldots \qquad \text{(elliptic)} \qquad (19b)$$

and the corresponding eigenfunctions

$$H_{nm}(\xi) = \pm 2iB_1 e^{\mp (i \frac{m\pi}{\beta} \xi)} \sin m\pi\xi \qquad \text{(hyperbolic)} \quad (20a)$$

$$H_{nm}(\xi) = \pm 2iB_1 e^{\pm (\frac{m\pi}{\beta}\xi)} \sin m\pi\xi \qquad \text{(elliptic)} \quad (20b)$$

The final solutions to the equation of motion 5 may be written in the form:

$$H(\xi, \nu, \tau) = \pm Be^{+ i \frac{m\pi}{\beta}(\xi - \frac{1}{\alpha}\tau)} \sin m\pi\xi \; g_n(\nu) \quad \text{(hyperbolic)} \quad (21a)$$

$$H(\xi, \nu, \tau) = \pm Be^{\pm \frac{m\pi}{\beta}(\xi - \frac{1}{\alpha}\tau)} \sin m\pi\xi \; g_n(\nu) \quad \text{(elliptic)} \quad (21b)$$

where

$$\frac{1}{\alpha} = \frac{c}{b} = \frac{C}{U} = \frac{\text{wave speed}}{\text{air speed}} = \sigma_n\pi \left[\frac{N_x}{Sq} + \frac{1}{\sigma_n\pi} \right]$$

$$\bar{\beta} = \sqrt{-1 + \frac{ac}{b^2}}$$

$$\beta = \sqrt{1 - \frac{ac}{b^2}}$$

The solution 21a is valid when

$$b^2 - ac > 0$$

or

$$\frac{1}{\sigma_n\pi} \left[1 - \frac{\frac{1}{\sigma_n\pi}}{+\frac{1}{\sigma_n\pi}} \right] < \frac{N_x}{Sq} < \infty$$

and represents a modulated traveling wave on the membrane which moves upstream ($-\xi$ direction) or downstream ($+\xi$ direction) as α is negative or positive respectively. The coefficient $c = \left(-\frac{N_x}{Sq} + \frac{1}{\sigma_n \pi}\right)$ is the quantity that controls the wave direction. When $q \longrightarrow 0$ (i.e. at the lower wind speeds)

$$\frac{N_x}{Sq} > \frac{1}{\sigma_n \pi}, \quad \frac{1}{\alpha} < 0$$

and the traveling wave moves against the airstream. The waves cease to propagate against the airstream and move with it at the critical speed where the coefficient c vanishes (i.e. at

$$\frac{N_x}{Sq} = \frac{1}{\sigma_n \pi} = \text{constant}$$

The largest value of the constant $\left(\frac{1}{\sigma_n \pi}\right)$ represents the lowest possible wind speed, for a given membrane tension and span, at which waves start propagating in the direction of the airstream. This largest value occurs when

$$\sigma_n = \sigma_1$$

(i.e. for the minimum eigenvalue of the integral equation 6). An approximation to this first eigenvalue (see Appendix B) shows

$$\frac{N_x}{Sq} \approx 1.81 \qquad (22)$$

as the critical condition for waves to first start propagating with the airstream. If the coefficient c of equation 8 is considered as an effective tension, the restoring force of the membrane is:

$$\text{RESTORING FORCE} \approx \left(-\frac{N_x}{Sq} + \frac{1}{\sigma_n \pi} \right) \frac{\partial^2 H_n}{\partial \xi^2} \tag{23}$$

The vanishing of the effective restoring force in the membrane is thus the condition causing waves to propagate with the airstream.

At the higher wind speeds, i.e. when

$$b^2 - ac < 0$$

or

$$\frac{N_x}{Sq} < \frac{1}{\sigma_n \pi} \left[1 - \frac{\frac{1}{\sigma_n \pi}}{\mu + \frac{1}{\sigma_n \pi}} \right]$$

the solution 21b is valid. This represents a divergent motion in time.

Figure 15 illustrates the boundaries of the motions associated with the nth spanwise mode. The motions associated with the other n-1 spanwise modes are identical but each mode has its own characteristic boundaries which are determined by its respective eigenvalue σ_n.

The foregoing analysis failed to predict a divergent oscillation in time which is associated with flutter. Instead propagating waves of neutral stability were found which traveled first against and then with the airstream as the wind velocity was increased from zero. Thus the question arises as to which of the waves, if any, will be unstable and

grow to a visible size and which will be damped out and thus not observed. It must be concluded, therefore, that the above formulation using linear equations and slender wing theory, but without other approximations, failed to explain the experimental features of the problem.

APPENDIX B

Bounds on the Minimum Eigenvalue

Although the integral equation

$$g_n(\nu) - \sigma_n \int_{-1}^{1} L_1(\nu, \varsigma)\, g_n(\varsigma)\, d\varsigma = 0 \tag{1}$$

$$L_1 = \ln \left[\frac{1 - \nu\varsigma + \sqrt{(1-\nu^2)(1-\varsigma^2)}}{1 - \nu\varsigma - \sqrt{(1-\nu^2)(1-\varsigma^2)}} \right]$$

has not been solved in terms of known functions it is possible to obtain a bound on its minimum eigenvalue.

A lower bound may be obtained from 15:

$$|\sigma_1| \geq \frac{1}{\sqrt{\int_{-1}^{1} \int_{-1}^{1} L_1^2(\nu, \varsigma)\, d\nu\, d\varsigma}} \tag{2}$$

The equality sign holds if and only if the product $g_n(\nu)\, g_n(\varsigma)$ is a constant multiple of $L_1(\nu, \varsigma)$.

Taking

$$\int_{-1}^{1} L_1^2(\nu, \varsigma)\, d\varsigma = \int_{-1}^{1} u\, dv$$

$$u = L_1(\nu, \varsigma)$$

$$du = \frac{2\sqrt{1-\nu^2}}{(\nu - \varsigma)\sqrt{1-\varsigma^2}}$$

$$dv = L_1(\nu, \varsigma)\, d\varsigma$$

$$v = \int_0^{\varsigma} L_1(\nu, \varsigma)\, d\varsigma$$

$$v = -(\nu - \varsigma) L_1(\nu, \varsigma) + \nu L_1(\nu, 0) - 2n\pi \sqrt{1 - \nu^2} + 2\sqrt{1 - \nu^2} \arcsin \varsigma$$

an integration by parts may be performed giving

$$\int_{-1}^{1} L_1^2(\nu, \varsigma)\, d\varsigma = 2\sqrt{1 - \nu^2} \int_{-1}^{1} \frac{L_1(\nu, \varsigma)\, d\varsigma}{\sqrt{1 - \varsigma^2}} - 4(1 - \nu^2) \int_{-1}^{1} \frac{\arcsin \varsigma\, d\varsigma}{(\nu - \varsigma)\sqrt{1 - \varsigma^2}}$$

or

$$\int_{-1}^{1} L_1^2(\nu, \varsigma)\, d\varsigma = -8(1 - \nu^2) \int_{-1}^{1} \frac{\arcsin \varsigma\, d\varsigma}{(\nu - \varsigma)\sqrt{1 - \varsigma^2}}$$

The above definite integral may be evaluated by making the transformation:

$$\nu = \cos \theta$$

$$\varsigma = \cos \psi$$

It then becomes

$$\int_{-1}^{1} \frac{\arcsin \varsigma\, d\varsigma}{(\nu - \varsigma)\sqrt{1 - \varsigma^2}} \longrightarrow \int_0^{\pi} \frac{\psi\, d\psi}{\cos \psi - \cos \theta}$$

Hardy (Ref. 16) illustrates the use of the divergent series

$$\frac{1}{\cos\varphi - \cos\theta} = 2 \sum_{n=1}^{\infty} \frac{\sin n\theta}{\sin\theta} \cos n\varphi$$

for evaluating certain definite integrals.

An evaluation of the above integral by this method yields

$$\int_0^{\pi} \frac{\varphi \, d\varphi}{\cos\varphi - \cos\theta} = -\frac{4}{\sin\theta} \sum_{n=1,\,3,\,\ldots}^{\infty} \frac{\sin n\theta}{n^2}$$

and

$$\int_{-1}^{1} L_1^2(\nu, \varsigma)\, d\varsigma = 32 \sqrt{1-\nu^2} \sum_{n=1,\,3,\,..}^{\infty} \frac{\sin n(\arccos\nu)}{n^2}$$

Integrating over the domain again with respect to ν gives

$$\int_{-1}^{1} \int_{-1}^{1} L_1^2(\nu, \varsigma)\, d\nu \, d\varsigma = 32 \int_{-1}^{1} \sqrt{1-\nu^2} \sum_{n=1,\,3,\,..}^{\infty} \frac{\sin n(\arccos\nu)}{n^2} d\nu$$

The integral on the right may be evaluated by applying the transformation

$$\nu = \cos\theta$$

$$\varsigma = \cos\varphi$$

which results in:

$$32\int_{-1}^{1}\sqrt{1-\nu^2}\sum_{n=1,3,..}^{\infty}\frac{\sin n(\arccos\nu)}{n^2}d\nu = 32\int_{0}^{\pi}\sum_{n=1,3,..}^{\infty}\frac{\sin n\theta\sin^2\theta}{n^2}d\theta$$

but

$$32\int_{0}^{\pi}\sum_{n=1,3,..}^{\infty}\frac{\sin n\theta\sin^2\theta}{n^2}d\theta = 128\sum_{n=1,3,..}^{\infty}\frac{1}{n^3(4-n^2)}$$

so the above reduces to

$$\int_{-1}^{1}\int_{-1}^{1}L_1^2(\nu,\varsigma)d\nu\,d\varsigma = 128\sum_{n=1,3,..}^{\infty}\frac{1}{n^3(4-n^2)} \qquad (3)$$

Since the sum of the above series to three significant figures is:

$$\sum_{n=1,3,..}^{\infty}\frac{1}{n^3(4-n^2)} = 0.326$$

equation 3 has the following numerical value correct to the same accuracy.

$$\int_{-1}^{1}\int_{-1}^{1}L_1^2(\nu,\varsigma)d\nu\,d\varsigma = 41.7$$

Thus the lower bound for the minimum eigenvalue becomes

$$\sigma_1 \geqq 0.155 \qquad (4)$$

Further estimates on the minimum eigenvalue may be obtained from the following (Ref. 15):

$$\sigma_1 = \frac{\int_{-1}^{1} y^{(n)}(z)\,dz}{\int_{-1}^{1} f^{(n)}(z)\,dz} \tag{5a}$$

$$\sigma_1 = \frac{\int_{-1}^{1} y^{(n)}(z)\, f^{(n)}(z)\,dz}{\int_{-1}^{1} \left[f^{(n)}(z)\right]^2\,dz} \tag{5b}$$

where

$$f^n(z) = \int_{-1}^{1} L_1(z, s)\, y^n(s)\,ds$$

and $y^n(s)$ for $n = 1$ is an arbitrary function which should not be orthognal to $g_1(s)$.

Since equation 5b is, in general, more accurate than equation 5a (see above reference) an upper bound on σ_1 may be obtained if the following holds true:

$$0.155 < \sigma_1 \text{ (from 5b)} < \sigma_1 \text{ (from 5a)}$$

Assuming the general form:

$$y^1(\xi) = \frac{\sin n(\arccos \xi)}{\sqrt{1 - \xi^2}}$$

gives

$$f^1(\nu) = \frac{2\pi}{n} \sin n(\arccos \nu)$$

as a first approximation to the eigenfunction.

An approximation to the minimum eigenvalue as obtained from 5a for:

$$y^1(\xi) = \frac{\sin(\arccos \xi)}{\sqrt{1 - \xi^2}} = 1$$

$$f^1(\nu) = 2\pi \sin(\arccos \nu)$$

is

$$\sigma_1 \approx 0.203$$

while a first approximation from 5b is

$$\sigma_1 \approx 0.188$$

Since 5b yields the more accurate results, the upper bound becomes:

$$\sigma_1 < 0.196$$

The minimum eigenvalue is thus bounded by:

$$0.155 < \sigma_1 < 0.196 \qquad (6)$$

An approximation to the minimum eigenvalue will be taken as

$$\sigma_1 \approx 0.176 \qquad (7)$$

TABLE I

CRITICAL FLUTTER SPEEDS

ℓ = 2.36 ft, t = in, q = lb/ft^2, N_x = lb/ft, S = ft

t	S	N_x	$\frac{N_x}{S}$	q_1	q_2
		2	4	4.6	5.5
		3	6	6.6	7.6
		4	8	8.4	9.6
		5	10	10.4	12.1
		6	12	12.5	14.0
.001	1/2	7	14	14.6	16.8
		8	16	16.7	18.7
		9	18	18.5	21.1
		10	20	20.9	23.7
		11	22	23.3	27.1
		12	24	25.3	28.5

TABLE I (cont'd)

CRITICAL FLUTTER SPEEDS

ℓ = 2.36 ft, t = in, q = lb/ft^2, N_x = lb/ft, S = ft

t	S	N_x	$\frac{N_x}{S}$	q_1	q_2
		1	2	2.7	3.5
		2	4	4.7	5.7
		3	6	6.8	8.1
		4	8	8.5	10.7
		5	10	10.7	12.9
		6	12	12.6	15.5
.003	1/2	8	16	16.8	20.1
		10	20	20.8	25.1
		12	24	24.8	29.8
		14	28	29.0	33.8
		16	32	32.9	38.3
		18	36	37.4	42.8

TABLE I (cont'd)

CRITICAL FLUTTER SPEEDS

ℓ = 2.36 ft, t = in, q = lb/ft^2, N_x = lb/ft, S = ft

t	S	N_x	$\frac{N_x}{S}$	q_1	q_2
		3	6	7.0	8.3
		4	8	8.8	10.8
		6	12	13.3	15.8
		8	16	16.6	20.4
		10	20	21.5	25.3
.0075	1/2	12	24	25.6	30.5
		14	28	29.1	35.0
		16	32	33.4	39.3
		18	36	37.1	43.9
		20	40	40.8	48.0
		4.8	11.5	13.1	14.9
		9.6	23.1	24.7	29.2
		10.8	25.9	27.0	32.0
.0075	5/12	12.0	28.8	29.8	34.9
		13.2	31.7	33.2	38.8
		14.4	34.6	35.7	42.3
		15.6	37.4	37.8	44.9
		16.8	40.3	41.9	48.0

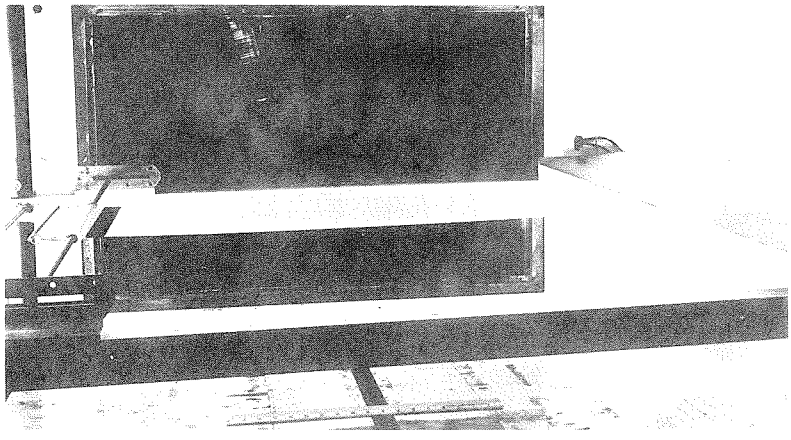

Fig. 1

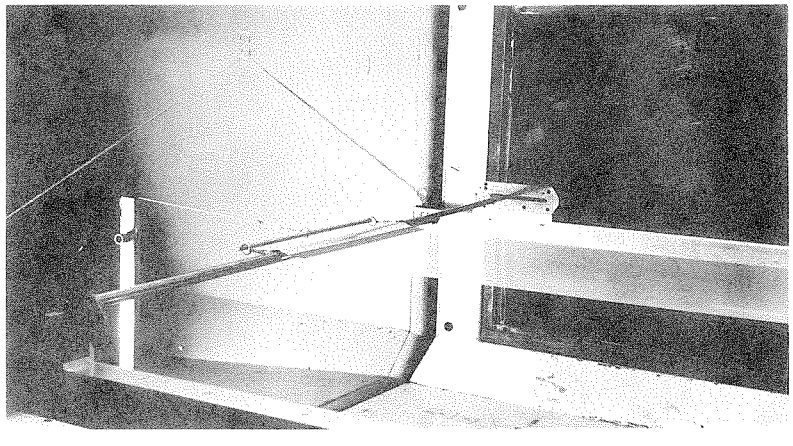

Fig. 2

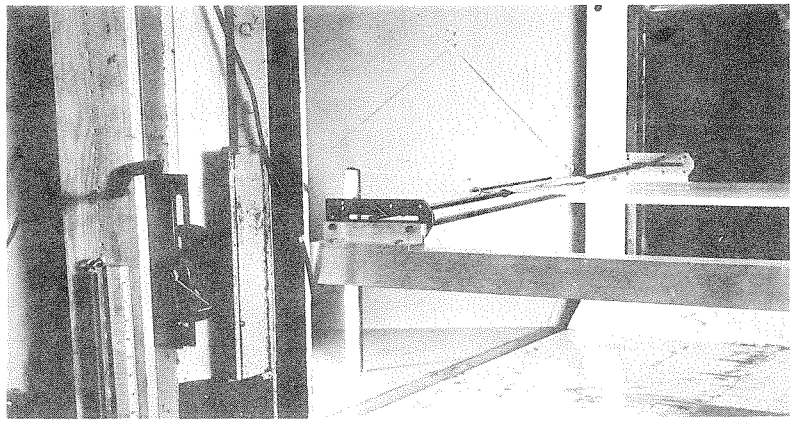

Fig. 3

Model and Installation

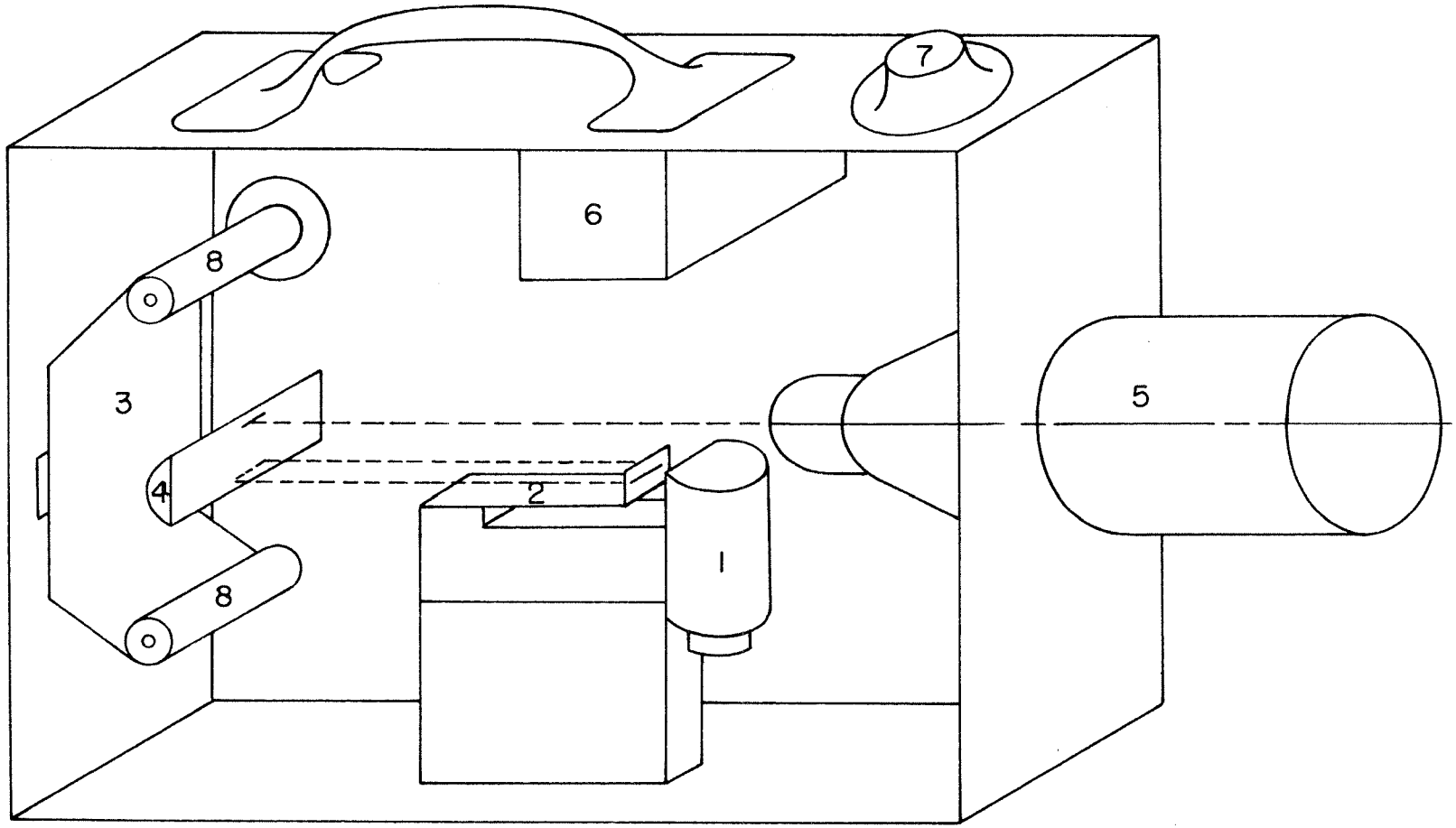

1. Timing Light
2. Timing Reed
3. Photo-Sensitive Paper
4. Cylindrical Lens
5. Optical Lens System
6. D.C. Motor
7. Speed Control
8. Rotating Drums

FIG. 4 – OPTICAL OSCILLOGRAPH

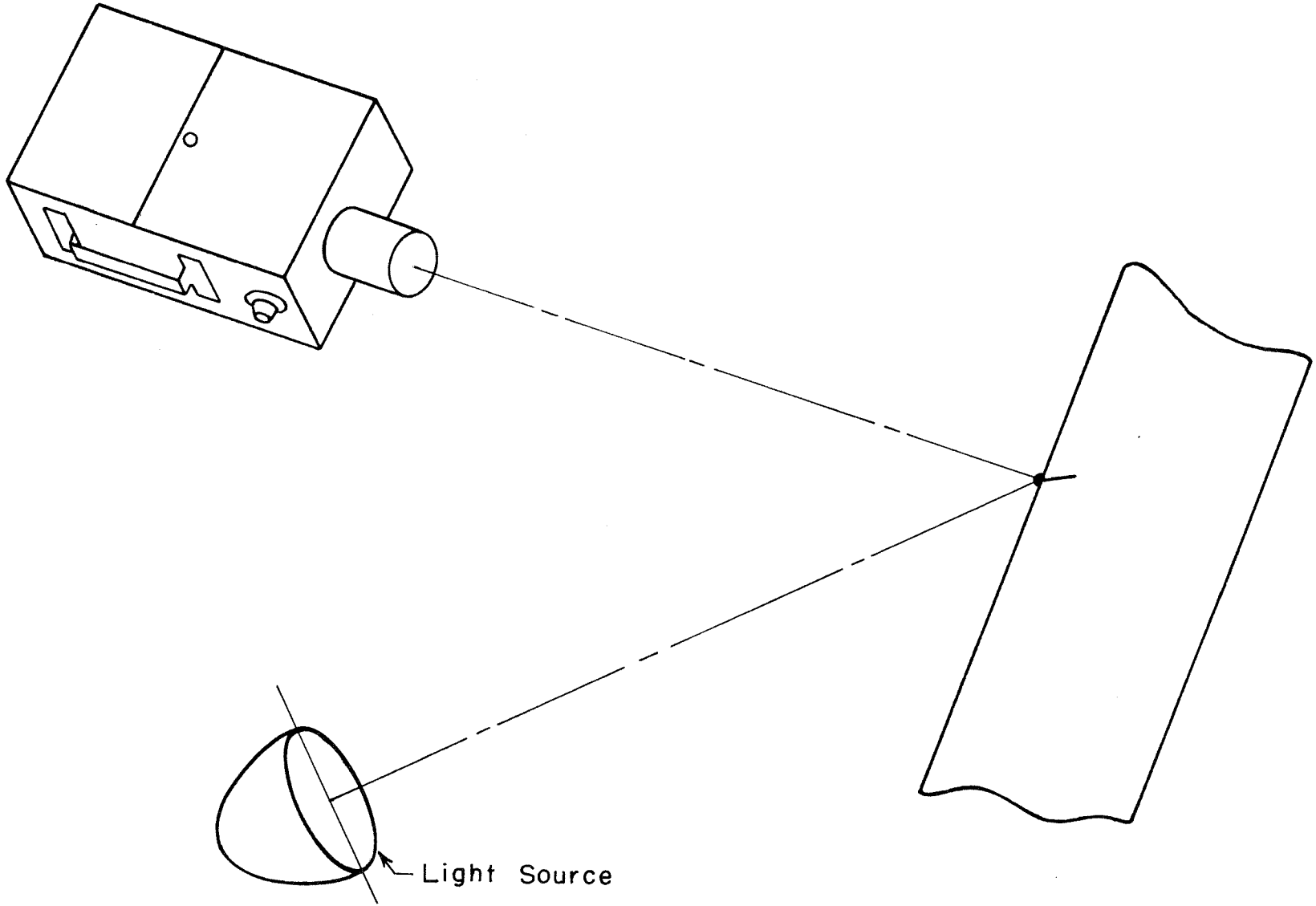

FIG. 5 - OPTICAL OSCILLOGRAPH AND MODEL

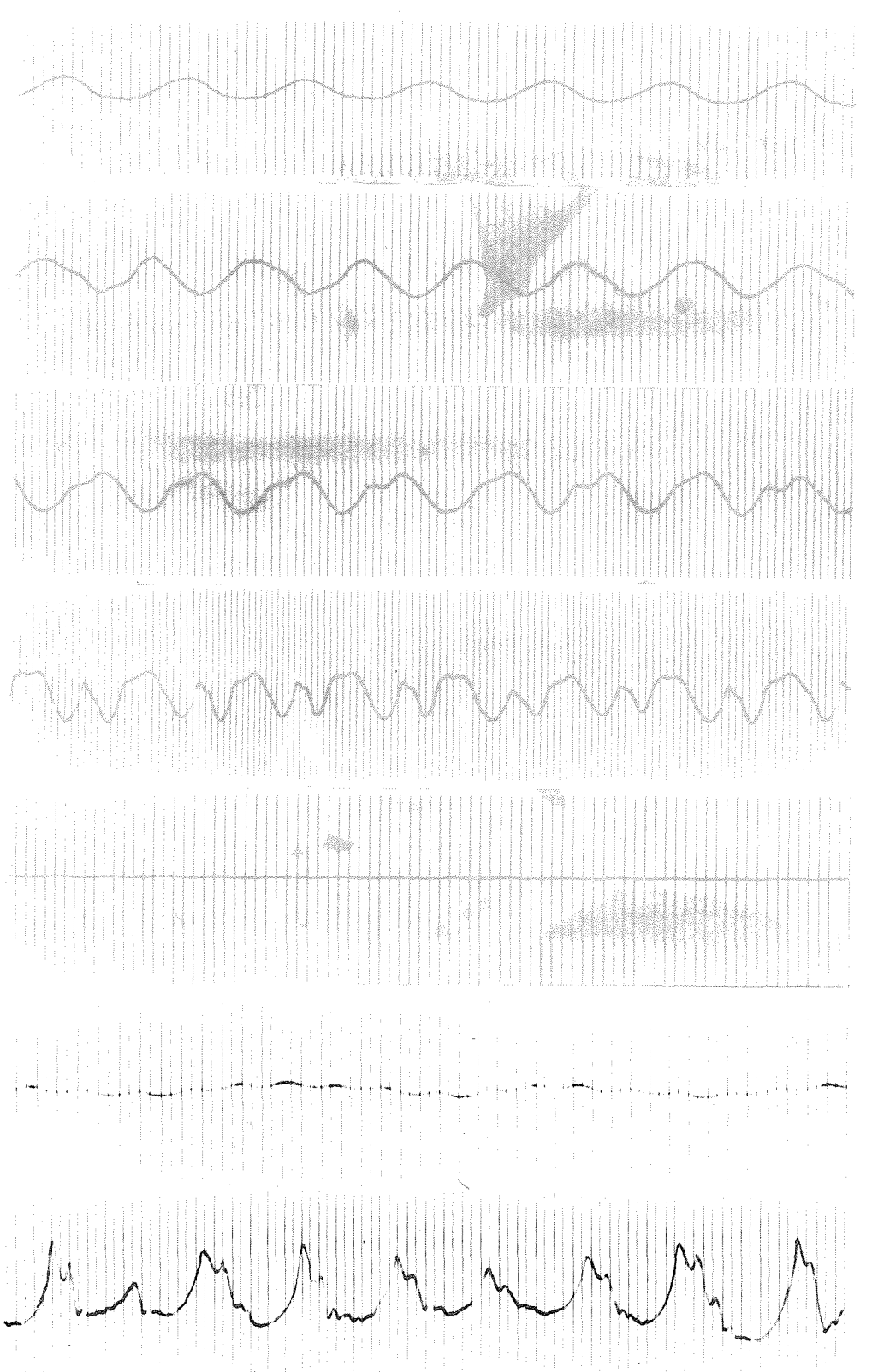

Fig. 6 - Amplitude Time Response - 75 o/o Chord
Time Scale 0.01 Sec., Amplitude Scale 1/4, S = 1/2 Ft.

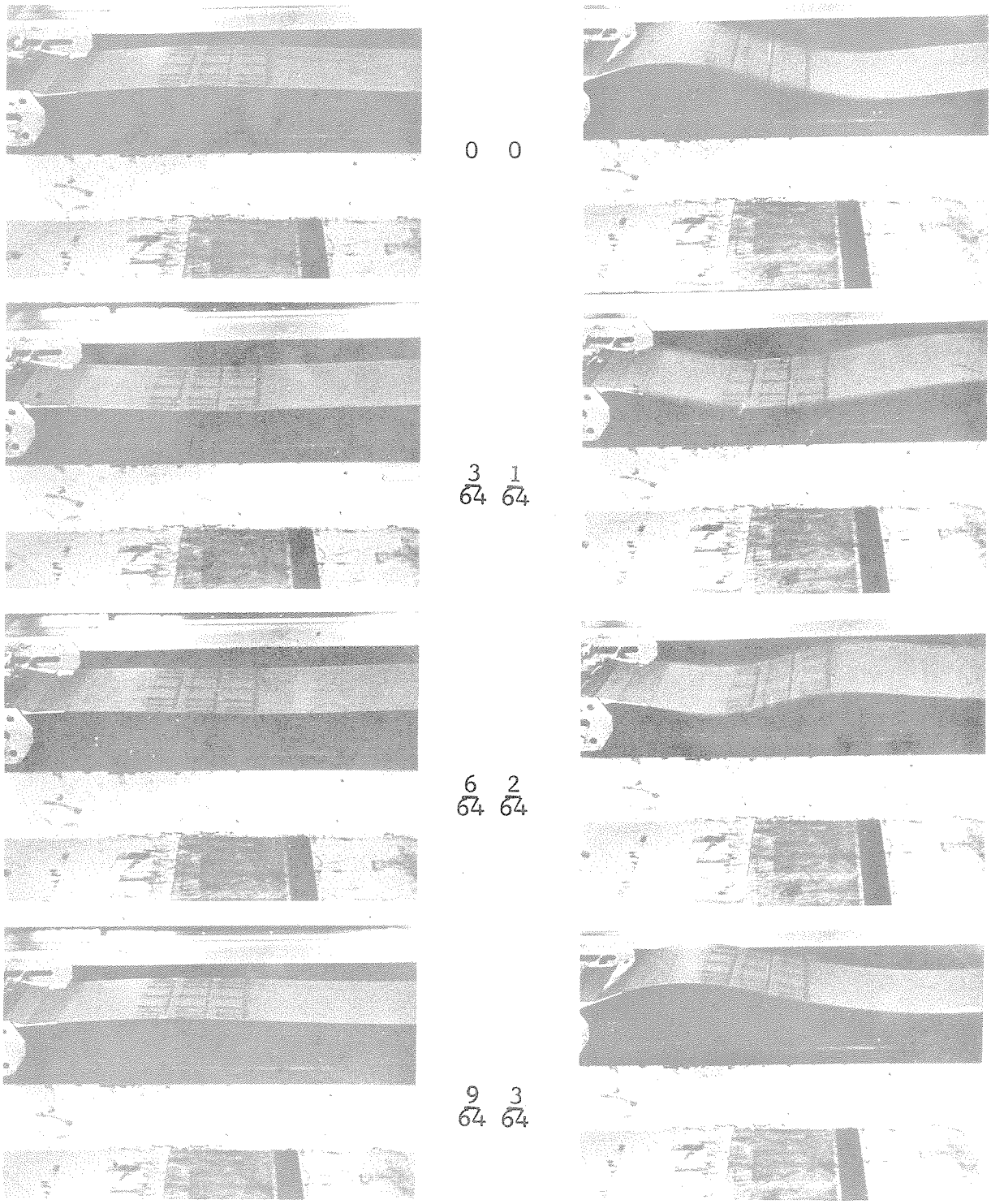

Fig. 7 - First Type Flutter

Fig. 8 - Second Type Flutter

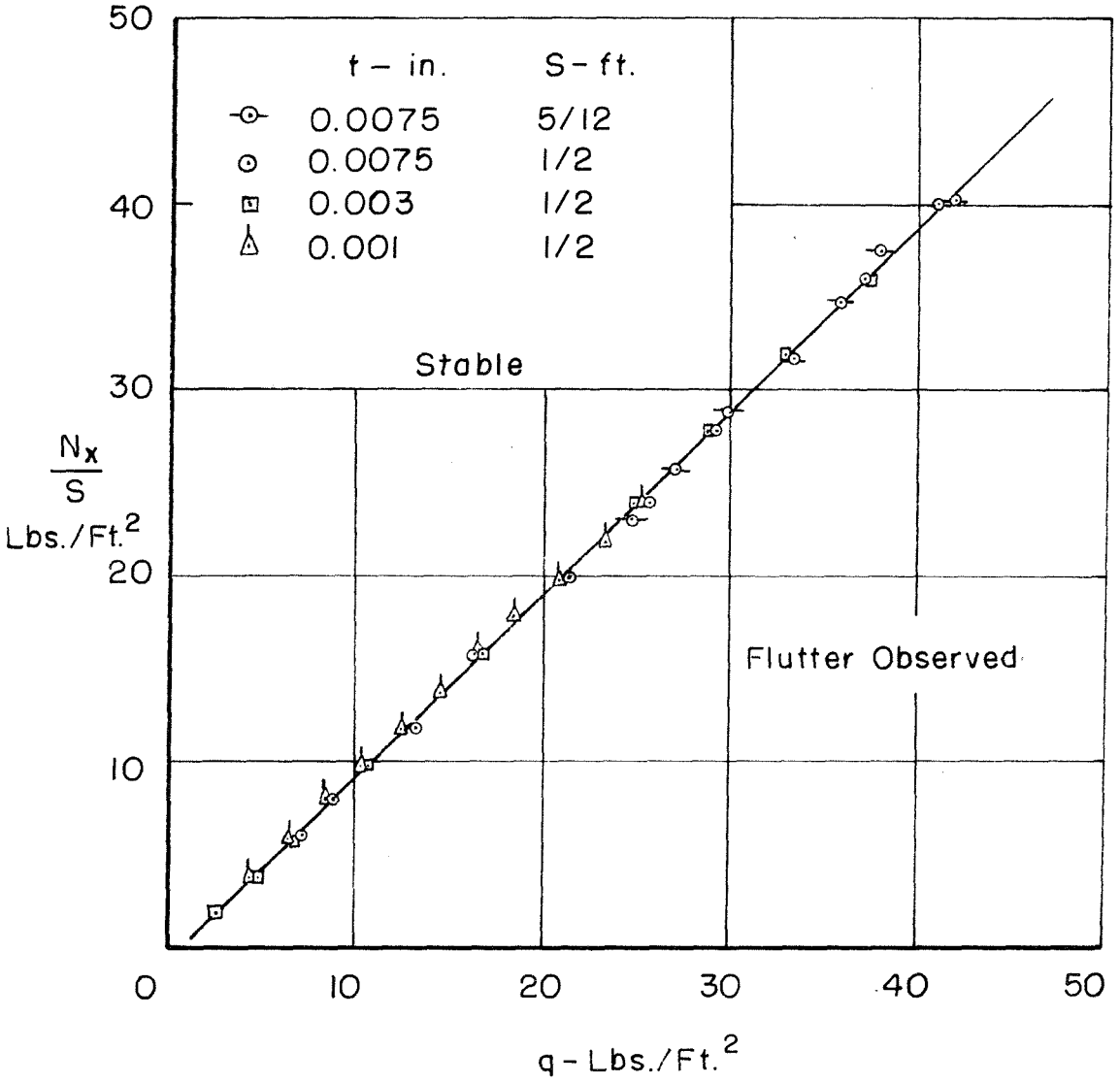

FIG. 9 – FIRST STABILITY BOUNDARY

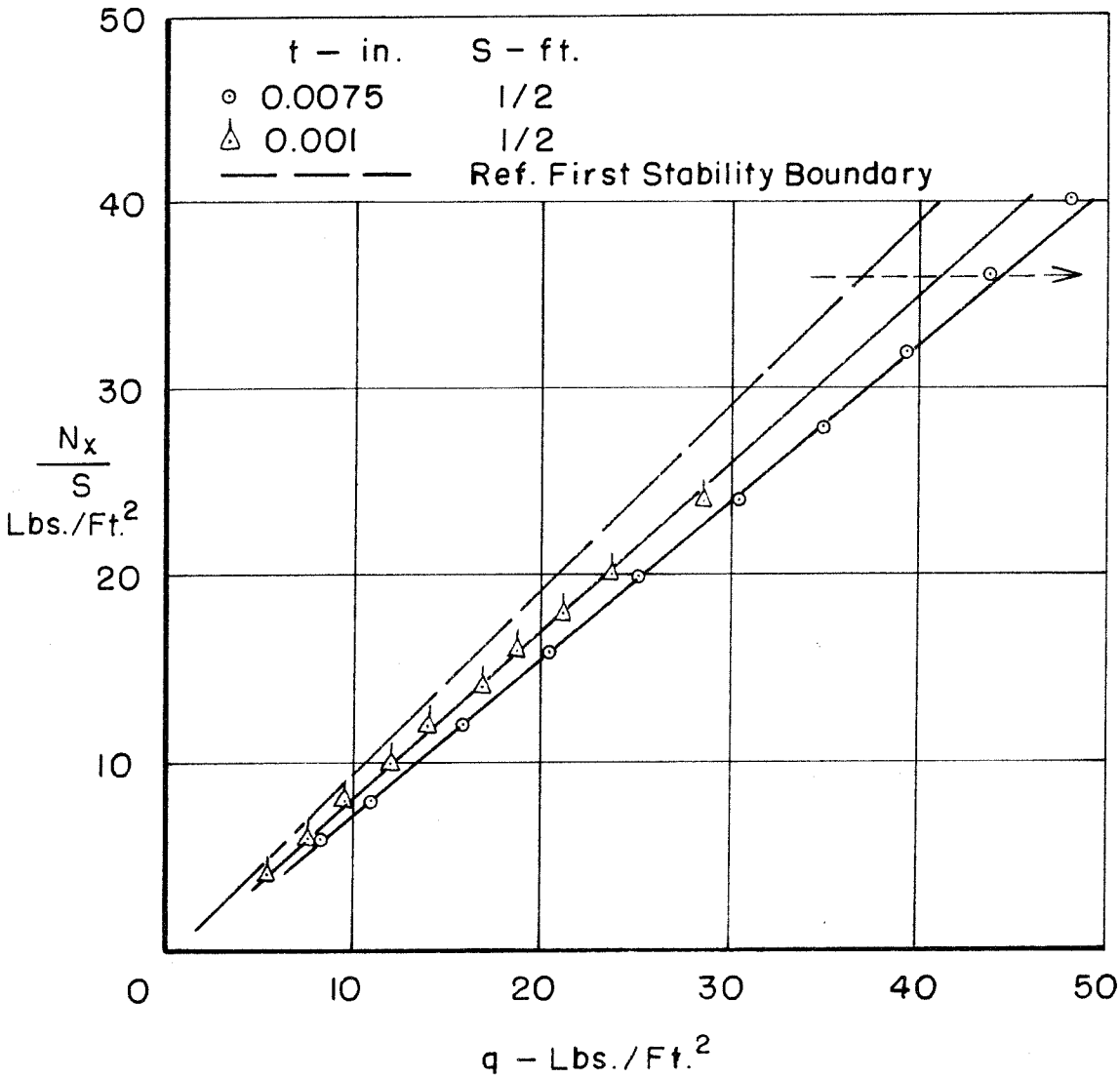

FIG. 10 – EQUILIBRIUM BOUNDARIES

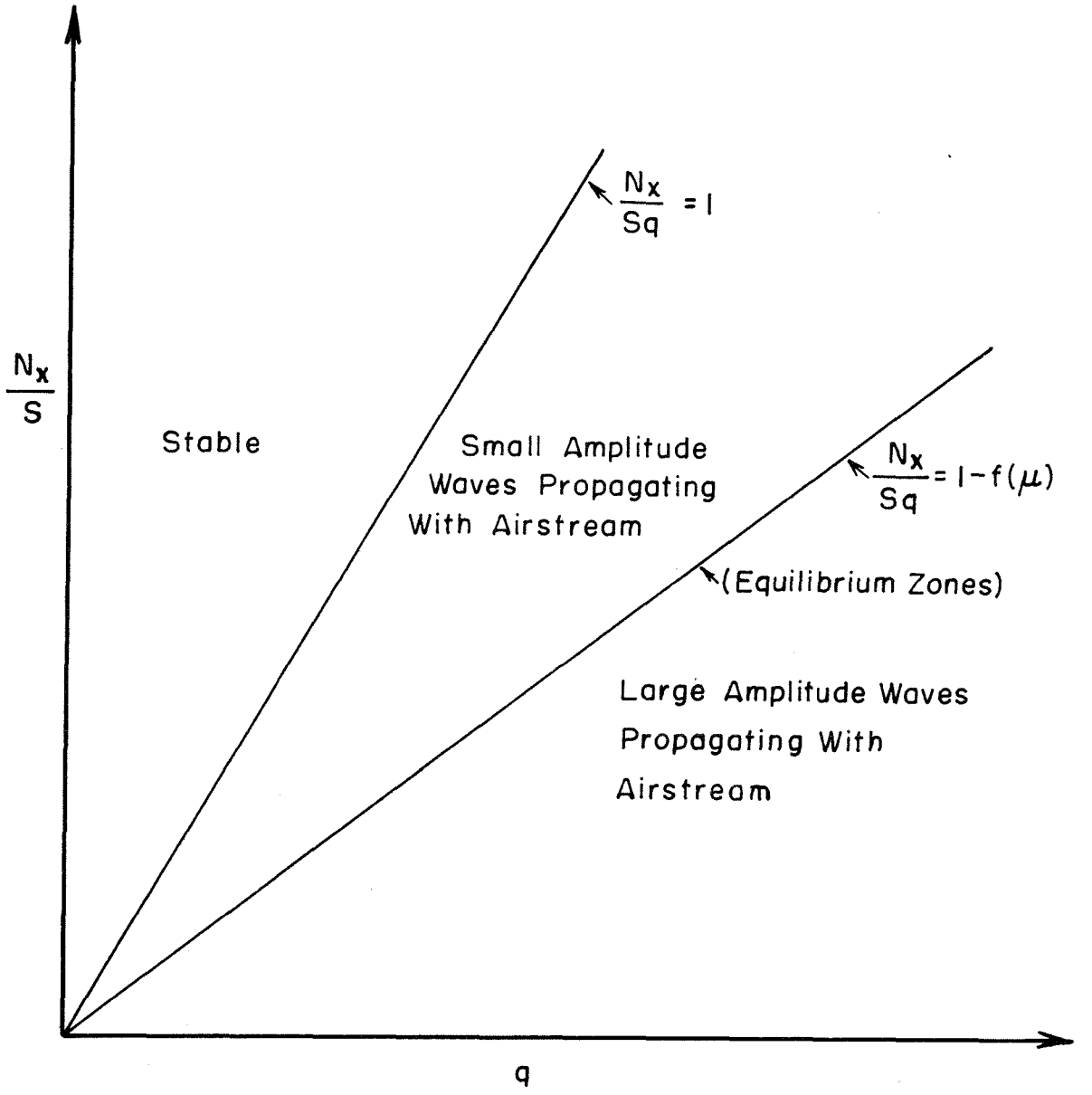

FIG. 11 – EXPERIMENTAL STUDY OF STABILITY BOUNDARIES

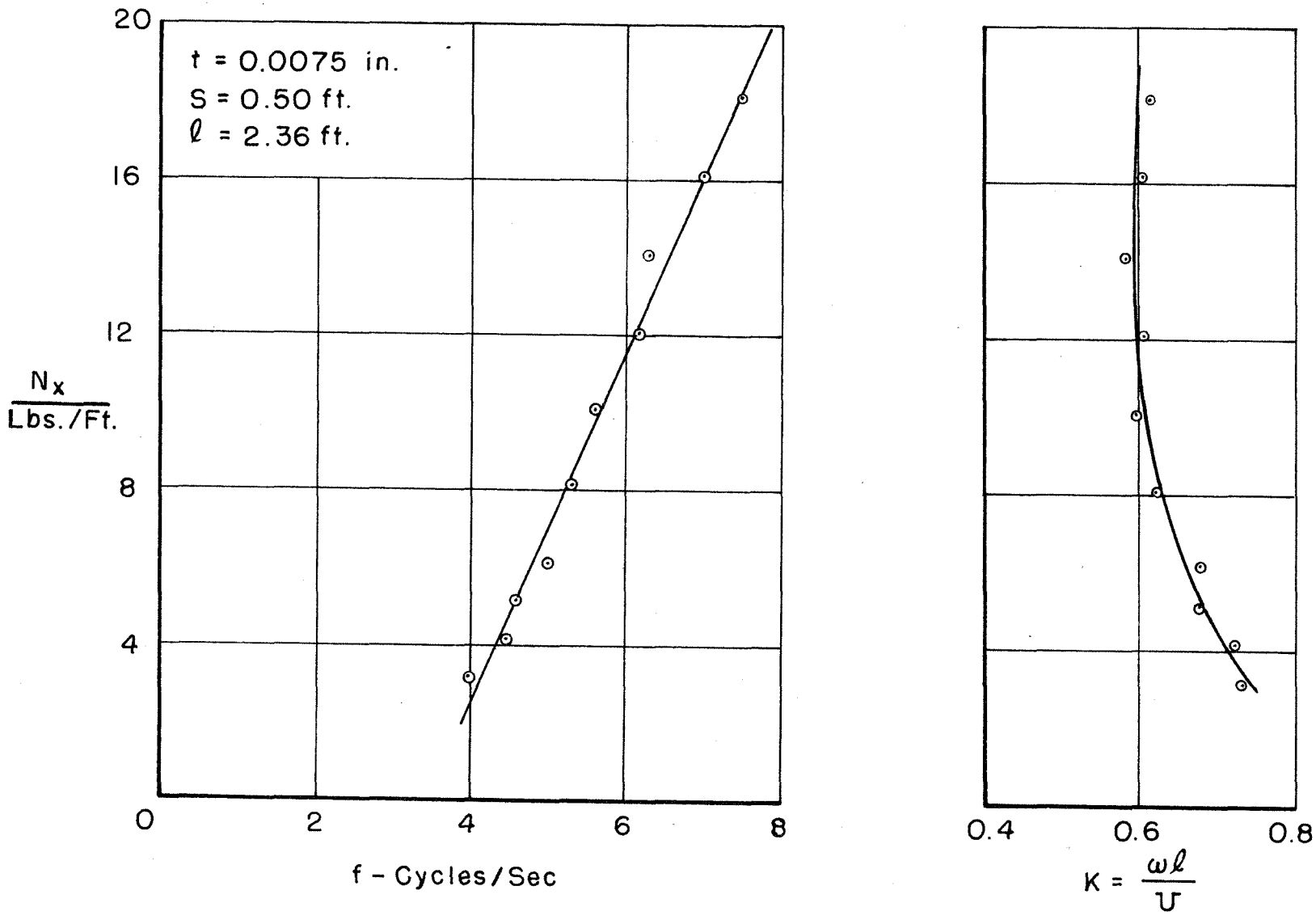

FIG. 12 - FREQUENCY VARIATION DURING FIRST TYPE FLUTTER

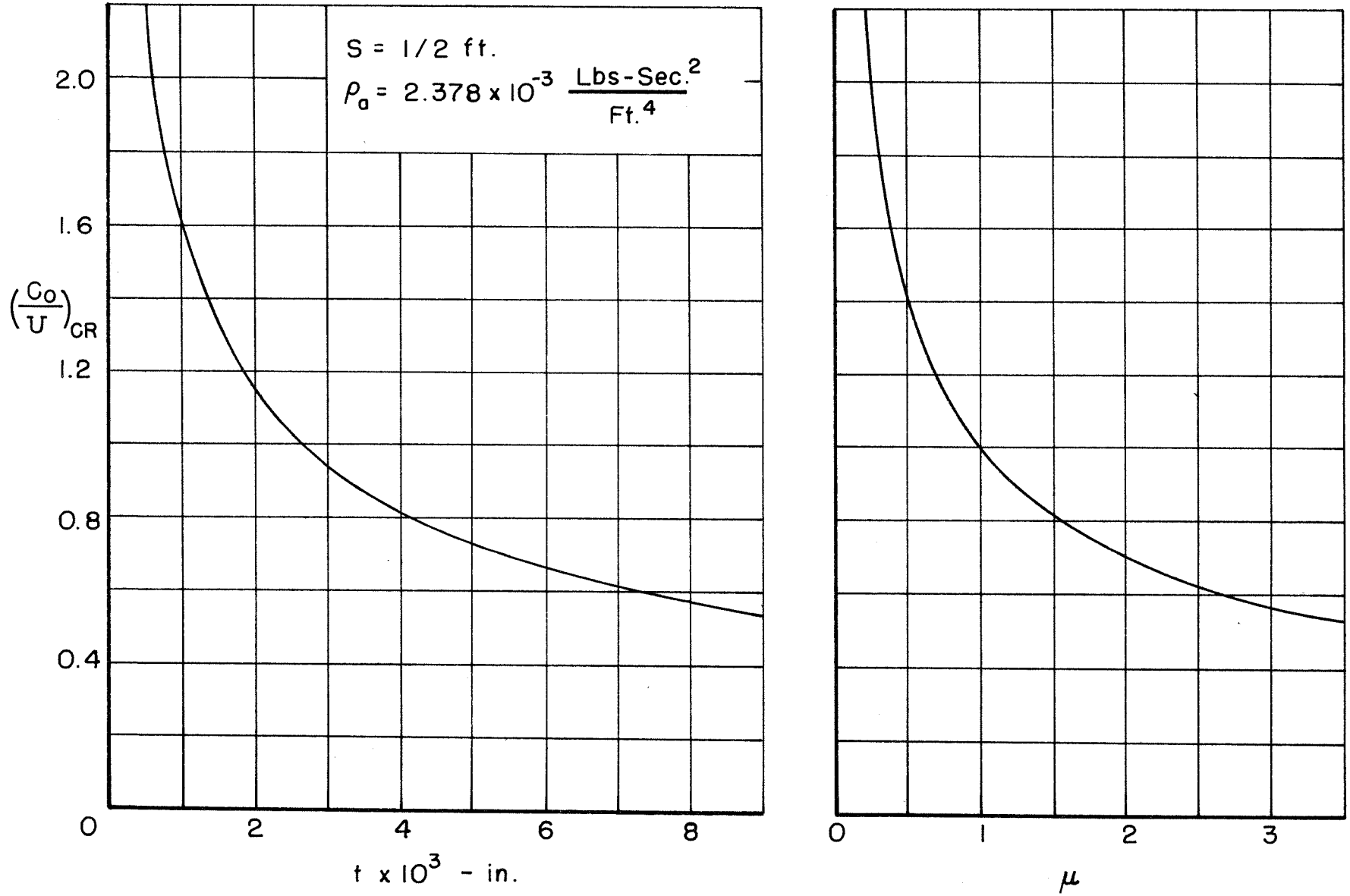
S = 1/2 ft.
$\rho_a = 2.378 \times 10^{-3}$ Lbs-Sec.^{2} / Ft.^{4}
2.0
1.6
1.2
0.8
0.4
0
$\left(\frac{C_o}{U}\right)_{CR}$
2
4
6
8
t x 10^3 - in.
0
1
2
3
μ

FIG. 13

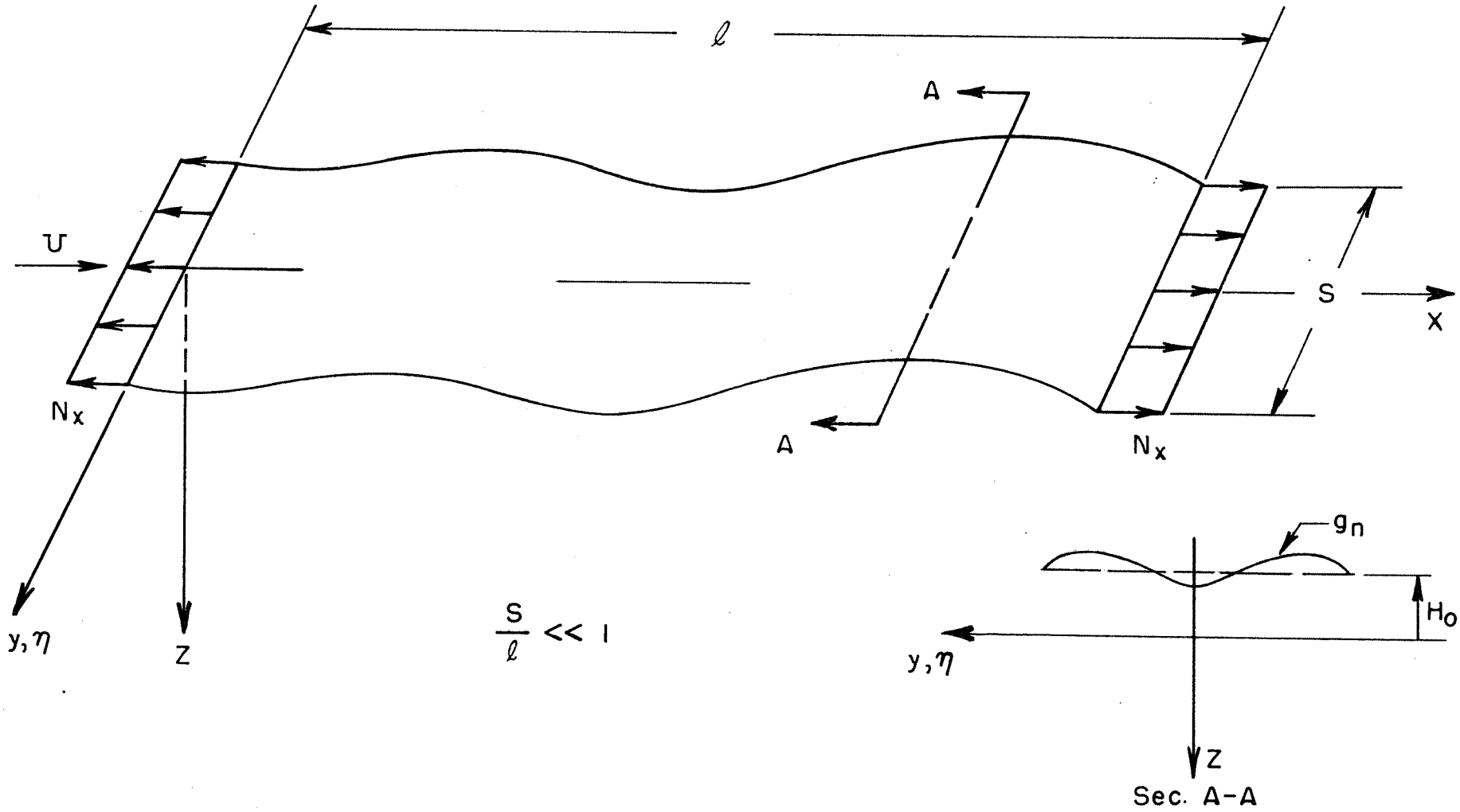

FIG. 14 - THEORETICAL MODEL AND COORDINATE SYSTEM

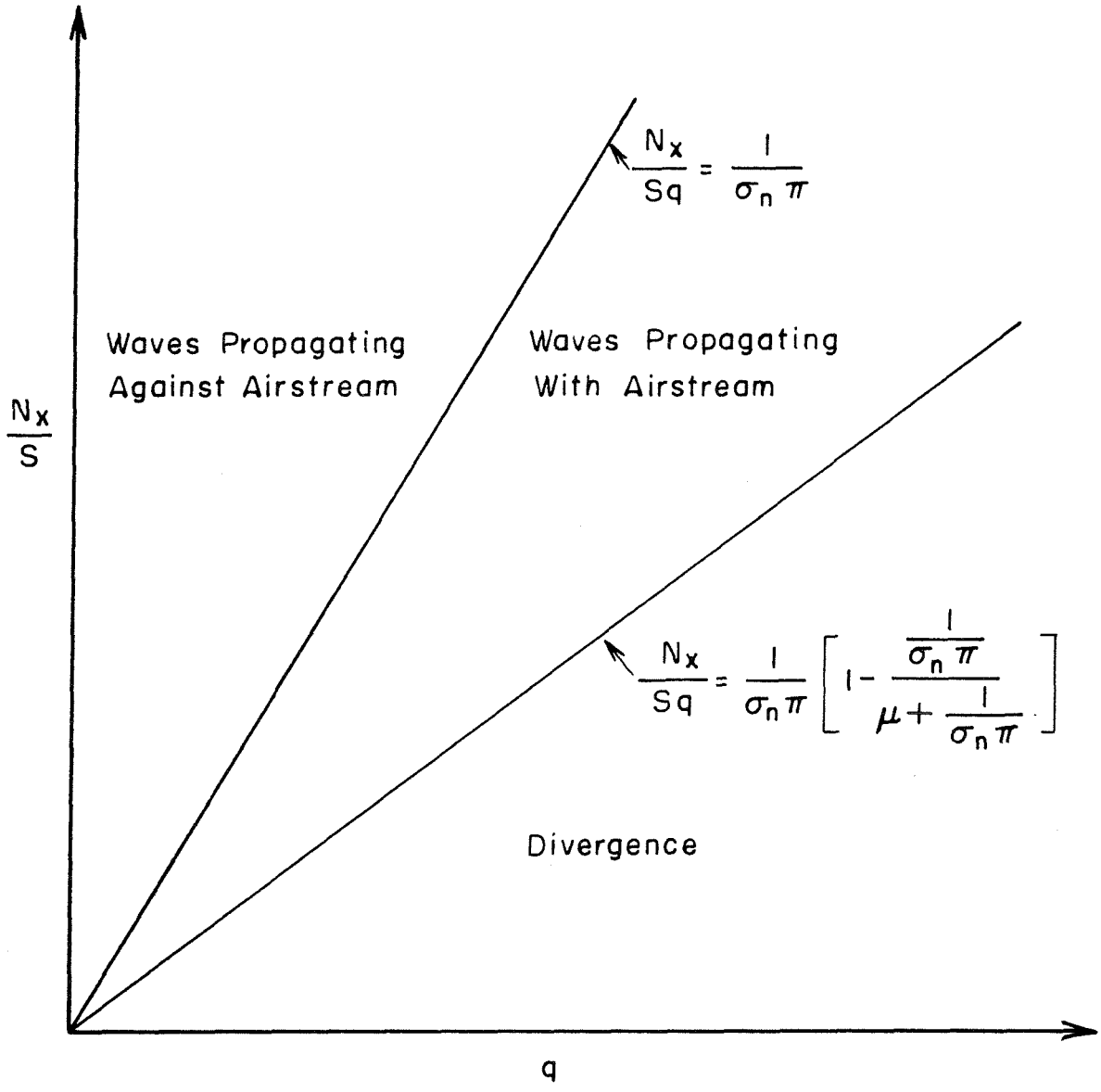

FIG. 15 - STABILITY BOUNDARIES ASSOCIATED WITH THE n^{th} SPANWISE MODE

PART II

THE STABILITY OF A GRID OF PANELS IN A SUPERSONIC FLOW

ABSTRACT

A theoretical investigation has been made on the stability of a grid of panels in a supersonic flow. The problem is formulated by considering this structure as a limiting case of a more general configuration composed of a ring of panels (i.e. an axially stiffened cylindrical shell) whose outer surface is exposed to a supersonic flow parallel to its axis. It is shown that the stability analysis of this more general configuration can be reduced to the analysis of an "equivalent" single panel using the circulant matrix idea. The reduction procedure, applicable to most cyclic configurations, allows for all types of inter-element (panel) coupling and is subject to the sole restriction that the dynamic phenomenon be satisfactorily described by linear theory.

It is shown that at least five different multi-panel configurations can be obtained from this general problem by taking the appropriate limiting process. The stability (flutter) analysis of one of these limiting cases is discussed for high Mach number flows where only an elastic coupling exists between neighboring panels.

TABLE OF CONTENTS

LIST OF FIGURES

LIST OF SYMBOLS

a	$\lim_{R \to \infty} R\alpha_1$ plate length - Figure 1b
A	coefficient - see Table II
$\bar{A}$	coefficient - see Table II
b	$\lim_{R \to \infty} R\beta_1$ plate width - Figure 1b
B	coefficient - see Table II
c	$h/\sqrt{12}\,R$
C	coefficient - see Table II
D_{mn}	$\left[(m^2 + \lambda^2 n^2)^4 + \epsilon m^4\right] / (m^2 + \lambda^2 n^2)^2$
E	modulus of elasticity in tension and compression
f	known function - see Table I
g	known function - see Table I
h	plate thickness
$\underset{\sim}{H}$	matrix
i	integer
j	integer - used in Appendix A as $\sqrt{-1}$
k_o	fundamental solution - see page 81
k_1	fundamental solution - see page 81
K_{ij}	kernels of the integral equations 16 and 17 - see page 80
$\underset{\sim}{K}$	matrix
L	cylinder length
L_n	Spence function - see footnote Table I
$\mathcal{L}$	aerodynamic operator

m	integer
$M_{\eta}^{(i)}$	bending moment per unit length of the ith shell segment acting about an axis parallel to the ξ axis - see Figure 2
n	integer
N	$Eh^3/12(1 - \nu^2)$ flexural rigidity of the shell or plate
P	concentrated load normal to the shell surface
$\underset{\sim}{P}$	matrix
q	Fourier coefficient and dynamic pressure parameter
R	radius of curvature of the cylindrical shell
t_m	$2m\pi/\lambda$
U	speed of flow at infinity
u, v, w	longitudinal, circumferential, and radial components of deflection - positive sense shown in Figure 2a
W	generalized radial deflection - see Table III
x, y	curvilinear coordinates located on the middle surface of the shell in the axial and circumferential directions respectively
Z	distributed loading normal to the shell surface
α	$= \frac{x}{R}$, dimensionless axial coordinate
α'	α/β_1
α_1	shell length - dimensionless
β	$= \frac{y}{R}$, dimensionless circumferential coordinate
β_1	stringer spacing - dimensionless - see Figure 1a
γ	$C/B + \sqrt{(C/B)^2 - 1}$
δ_{ij}	Kronecker delta

Δ forward difference operator

∇^2 $\left(\frac{\partial^2}{\partial \alpha^2} + \frac{\partial^2}{\partial \beta^2}\right)$

ϵ $12(1 - \nu^2)R^2 \alpha_1^4 / \pi^4 h^2 = \frac{12(1 - \nu^2)}{\pi^4} \left(\frac{L}{R}\right)^4 \left(\frac{R}{h}\right)^2$

η special value of β where an edge moment is applied

H special value of β where a concentrated load is applied

Θ_i Jacobi Theta Functions

λ α_1 / β_1

$\bar{\lambda}$ $1/\lambda$

μ $\frac{\rho_s h}{\rho_o R \alpha_1}$ mass ratio parameter

ν Poisson's ratio

ξ special values of α when an edge moment is applied

ξ' ξ / β_1

Ξ special value of α when a concentrated load is applied

$\Pi_n(\alpha', \xi')$ $\int_0^\infty \frac{\cos t(\alpha' - \xi')}{D(t, n)} dt$

σ phase angle - positive constant

ρ_o mass density of air in free stream

ρ_s mass density of panel or shell

Ω $\frac{4}{\pi^4} \frac{2qa^3}{N\sqrt{M^2 - 1}}$ dynamic pressure parameter

INTRODUCTION

Lane (Ref. 1) made an important contribution to the theory of compressor blades flutter by showing that the system mode shapes of an n-bladed system can be obtained in terms of n single equivalent blades. This result was subject to the sole restriction that the phenomenon be satisfactorily described by linear theory, and that the fluttering elements have a finite number of degrees of freedom. Stated differently it was shown that the flutter analysis of a cyclic* arrangement characterized by a large number of identical fluttering blades could be reduced, with no loss of generality whatsoever, to the analysis of a "single equivalent blade".

Fung (Ref. 2) in an unpublished report has made an important extension to Lane's principal result by demonstrating that it is readily applicable to such apparently different problems as the panel flutter of the skin panels of a circular semimonocoque fuselage.

In the present paper Fung's reduction procedure will be employed to formulate the panel flutter problem of a finite axially stiffened cylindrical shell whose outer surface is exposed to a supersonic airstream parallel to its axis. It is necessary, of course, to assume that the shell geometry is cyclic (i.e. all panels are identical), and that the flutter phenomenon can be satisfactorily described by linear theory.

---

* A "cyclic" arrangement is a term used here to signify the usual compressor or turbine blade configuration wherein the last or nth blade is adjacent to the first blade.

An approximate method of solution of the above problem is outlined for the case where the curvature parameter ϵ approaches zero. This particular case corresponds to a grid of panels with many bays in the spanwise direction (Figure 1b).

FORMULATION OF THE FLUTTER PROBLEM

The equation of motion of a single fluttering skin panel can be written in the form:

$$w(x, y) = \Omega \iint K(x, y; x_o, y_o)\, w(x_o, y_o)\, dx_o\, dy_o \qquad (1)$$

where x, y are curvilinear coordinates on the surface and the integration interval extends over the entire panel surface. Furthermore $\mathrm{Re}\left[w(x, y) e^{j\omega t} \right]$ is the displacement at a point (x, y). Ω is a real valued dynamic pressure parameter playing the role of the eigenvalue, and $K(x, y; x_o, y_o)$ is a complex valued function depending upon Mach number, reduced frequency etc. It will be convenient to think of the kernel K as the product of an elastic influence function* times the sum of an aerodynamic and inertial operator which operate on the deflection w to yield a lateral loading normal to the panel surface. (see reference 3 for the details regarding the derivation of such an equation).

To determine the value of the parameter Ω that defines the flutter boundary the solution of equation 1 is sought for ω real. The panel is then neutrally stable and harmonic oscillation is possible. The side of this neutrally stable boundary which gives a negative imaginary part for ω is the side of oscillatory divergence (i.e. flutter). The nature of the kernel in equation 1, however, is such that the solution $w(x, y)$ and Ω are in general complex and hence the proper combination of physical parameters in K must be chosen in order to locate a

---

* An elastic influence function gives the lateral deflection w of the panel at a point (x, y) due to the action of a concentrated unit load at the point (x_o, y_o).

real valued eigenvalue. The lack of an existence theorem for such a real valued eigenvalue is the basic theoretical difficulty of the flutter problem.

Disregard for the moment the theoretical problems involved in the solution of the flutter problem and consider the stiffened cylindrical shell shown in Figure 1a. The orthotropic stiffening, consisting of two end rings and n axially longerons, is such that it divides the shell surface into a cyclic arrangement of n identical panels. Fung writes the equation of motion for this system in the same form as equation 1 by considering w as a column matrix of n elements, and K as a square matrix of n^2 elements. The jth component of the column matrix represents the deflection form of the jth panel, and the element a_{ij} in the $n \times n$ square matrix represents the effect of the jth panel on the ith panel. In physical terms the element a_{ij} represents the elastic and aerodynamic coupling* that occurs between the ith and jth panels for a structure of this type. By analogy to the single panel case the kernel K may now be thought of as the product of a matrix of elastic influence functions times the sum of an aerodynamic and an inertial operator which operate on the vector w to yield a lateral loading normal to the shell surface. The inertial operator takes the form of an identity matrix times the scalar operator $\rho_s h \frac{\partial^2}{\partial t^2}$; the elastic and/or aerodynamic matrices, however, are of diagonal form only if the elastic and/or aerodynamic coupling vanish.

---

* Since for small oscillations of the shell the inertial loading is proportional only to the local acceleration of the skin, it is not a coupling element in the problem.

The equation of motion of this system can be written in a more compact form (Ref. 2) by introducing the so called composition product of $\underset{\sim}{K}$ and w defined as:

$$\underset{\sim}{K} * w = \int\int K(x, y; x_o, y_o)\, w(x_o, y_o)\, dx_o\, dy_o$$

In addition the unitary element $\underset{\sim}{I}$ is introduced which has the following property

$$\underset{\sim}{I} * f = f * \underset{\sim}{I} = f$$

where f is any function compatible with the composition product definition.

Equation 1 may now be written as the matrix equation:

$$\underset{\sim}{H} * w = 0 \qquad (2)$$

where

$$\underset{\sim}{H} = (\underset{\sim}{I} - \Omega\underset{\sim}{K}).$$

In view of the fact that a cyclic system has no preferred element (panel) it is apparent that the coupling effect of the nth element (panel) on the first must be the same as the effect of the first element (panel) on the second and so on. This result holds true under all forms of inter-element (panel) coupling as long as the system is cyclic and linear. The matrix $\underset{\sim}{H}$ in the general equation of motion

$$\begin{Bmatrix} H_{11} & H_{12} & \cdots & H_{1n} \\ H_{21} & H_{22} & \cdots & H_{2n} \\ \cdots & \cdots & \cdots & \cdots \\ H_{n1} & \cdots & \cdots & H_{nn} \end{Bmatrix} * \begin{Bmatrix} w_1 \\ w_2 \\ . \\ w_n \end{Bmatrix} = 0$$

therefore reduces to the circulant form

$$\begin{Bmatrix} H_1 & H_2 & \cdots & H_n \\ H_n & H_1 & \cdots & H_{n-1} \\ \cdots & \cdots & \cdots & \cdots \\ H_2 & H_3 & \cdots & H_1 \end{Bmatrix} * \begin{Bmatrix} w_1 \\ w_2 \\ . \\ w_n \end{Bmatrix} = 0$$

as a consequence of the cyclic geometry of the panel arrangement. There are in addition only n independent elements in this matrix; H_i represents the total effect of the s panel on the $(s+1-i)$-th panel.

It was shown in reference 2 that the flutter analysis of this system could be considerably simplified. The reduction process is as follows:

Consider the $\underset{\sim}{PI}$ matrix where

$$\underset{\sim}{P} = \begin{Bmatrix} 1 & \omega_o^{-1} & \omega_o^{-2} & & \omega_o^{-n+1} \\ 1 & \omega_1^{-1} & \omega_1^{-2} & & \\ . & . & & & \\ . & . & & & \\ . & . & & & \\ 1 & \omega_{n-1}^{-1} & \omega_{n-1}^{-2} & & \omega_{n-1}^{-n+1} \end{Bmatrix}$$

$$\omega_\rho = e^{2\pi j(\rho/n)} \qquad (\rho = 0, 1, 2, \ldots, n-1)$$

$$j = \sqrt{-1}$$

and $\underset{\sim}{I}$ is the unitary element introduced above. In the $\underset{\sim}{PI}$ matrix every element in $\underset{\sim}{P}$ is multiplied by the unitary element $\underset{\sim}{I}$. By actual multiplication it can be seen that

$$\underset{\sim}{PI}*(\underset{\sim}{H}*w) = (\underset{\sim}{PI}*\underset{\sim}{H})*w \tag{3}$$

and that

$$\underset{\sim}{PI}*\underset{\sim}{H} = \underset{\sim}{B}*\underset{\sim}{PI} \tag{4}$$

where $\underset{\sim}{B}(x, y; x_o, y_o)$ is a diagonal matrix of which the ith element on the principle diagonal is

$$B_i(x, y; x_o, y_o) = H_1(x, y; x_o, y_o) + \omega_i^{-1} H_n(x, y; x_o, y_o) + \omega_i^{-2} H_{n-1}(x, y; x_o, y_o)$$

$$+ \ldots\ldots + \omega_i^{-n+1} H_2(x, y; x_o, y_o)$$

$(i = 0, 1, \ldots., n-1)$

On combining equations 2, 3, and 4, and letting

$$\underset{\sim}{P}I^* w = p$$

one obtains

$$\underset{\sim}{P}I^*(\underset{\sim}{H}^* w) = \underset{\sim}{B}^* p = 0 \qquad (5)$$

The eigenvalue problems 2 and 5 are completely equivalent.

By transforming the variables $w_1, w_2, \ldots..$ into

$$p_o = w_1 + w_2 + w_3 + \ldots.$$

$$p_1 = w_1 + w_2/\omega_1 + w_3/\omega_1^2 + \ldots \qquad (6)$$

$$p_2 = w_1 + w_2/\omega_2 + w_3/\omega_2^2 + \ldots$$

etc., the original eigenvalue problem of n coupled panels is reduced into solving individually the n uncoupled problems of "equivalent single panels":

$$B_i^* p_i = 0 \qquad (i = 0, 1, 2, \ldots.., n-1) \qquad (7)$$

If a pair of eigenvalues and the corresponding eigenvector p were found, the flutter mode of the panels are at once given by

$$w = \underset{\sim}{P}^{-1} p$$

i.e. by

$$\begin{aligned} w_1 &= p_o + \omega_1 p_1 + \omega_1^2 p_2 + \dots \\ w_2 &= p_o + \omega_2 p_1 + \omega_2^2 p_2 + \dots \end{aligned} \tag{8}$$

etc.

The interpretation of the flutter mode is very simple. For example, suppose that

$$p_k \neq 0$$

at the minimum flutter speed, whereas all other p's vanish. Equations 8 then show that the panel deflections $w_1(x, y)$, $w_2(x, y)$, ... of successive panels are identical in shape and magnitude but differ by a constant phase shift σ_k, i.e. each panel lags in phase behind the preceding panel by an angle $2\pi k/n$, the same as in Lane's case of finite degrees of freedom. More complicated flutter modes might also occur which are analogous to those discussed in reference 1.

An examination of the transformed problem 7 written in the form

$$B(\sigma_i)^* p_i = 0 \qquad \sigma_i = 2\pi i/n$$

$$B(\sigma_i) = H_1 + H_2 e^{j\sigma_i} + H_n e^{-j\sigma_i} + H_3 e^{j2\sigma_i} + H_{n-1} e^{-j2\sigma_i} \dots \tag{9}$$

shows that the flutter solution of the ith equivalent panel actually corresponds to the situation in which the original flutter problem is solved for one panel when this panel is under a very special form of influence from all other panels; namely all other panels oscillate with the same panel

mode, the same magnitude of occurrence of this panel mode, and with a phase shift angle σ_i (as yet undetermined) between adjacent panels. This result, therefore, makes it possible to think in terms of the original physical problem when solving the simpler equivalent panel problem. It is important to realize that this result is valid when all panels of the original problem flutter at the same frequency but with different modes and also different phase shift between different panels, as well as when all panels flutter in the same mode shape but differ by a constant phase shift between different panels. (i, e. all interpanel interference is correctly accounted for).

The operator $B(\sigma_i)$ in equation 9 resembles a finite complex Fourier series in the undetermined phase angle σ_i. The physical nature of the original flutter problem, in addition, guarantees that the coefficients (i. e. the H's) of the higher harmonic terms will diminish quite rapidly. That is to say the influence of the neighboring panels becomes quite small with increasing distance. Thus a tremendous simplification suggests itself for cyclic configurations with a large number of panels (Ref. 1). The operation of solving the above n eigenvalue problems is replaced by a minimization process with respect to an interpanel phase angle σ. In other words a general complex eigenvalue problem

$$B(\sigma)^* p = 0 \tag{10}$$

$$B(\sigma) = H_1 + H_2 e^{j\sigma} + H_n e^{-j\sigma} + H_3 e^{j2\sigma} + H_{n-1} e^{-2j\sigma} + \ldots$$

is considered wherein the i discrete values of the n roots of unity are replaced by a parameter σ which is temporarily assumed to be a continuous variable between 0 and 2π. The finite Fourier series can then be replaced by an infinite series which in some cases will be summable in closed form to a relatively simple continuous function of σ. This new eigenvalue problem is then solved for a small (relative to n) number of values of the parameter σ. A plot of the minimum eigenvalues obtained verses the phase angle is drawn as a smooth curve. The final $\sigma_{\nu_{CR.}}$ and $\Omega_{\nu_{CR.}}$ are then obtained from this plot by picking the admissible value σ_ν closest to the minimum point on the curve; i.e. by taking

$$\sigma_\nu = 2\pi\nu/n$$

with ν restricted to be a positive integer less than n. It should be pointed out that the choice of σ_ν must be such that the resulting flutter mode allowes each panel to be "in phase with itself" as it certainly must be in actuality.

A justification of this minimization process can be made from a physical point of view. Briefly it seems reasonable to believe that a ring panel system with n panels, where n is large, will exhibit a critical flutter velocity U and frequency ω which differs only slightly from a system with identical panels, identically supported, but $n+1$ in number. Thus the critical frequency and eigenvalue parameter Ω, which may be thought of as a critical velocity, should vary smoothly with σ. This in turn implies that the minimization process and the replacement of the minimizing angle σ, by its nearest admissible

value σ_ν should be a valid means of determining the critical flutter velocity and associated frequency.

The original flutter problem may thus be analyzed, in all generality, in terms of a single "equivalent" panel. The critical conditions for flutter corresponding simply to the admissible interpanel phase angle σ_ν yielding the minimum eigenvalue Ω_ν, and to the frequency and panel mode associated therewith.

It is to be emphasized that all forms of elastic and aerodynamic coupling have been accounted for in the above formulation, and that the results are quite general within the realm of linear theory.

Although the formulation of the flutter problem allows for both types of interpanel coupling, their simultaneous treatment offers some complications. Thus it is at this point that another important simplification suggests itself. Under certain flight conditions*, roughly speaking when the shell is flying at so called "hypersonic" velocities, the aerodynamic coupling vanishes and the local air loads are a function only of the local downwash. The shell therefore retains only its elastic coupling and the flutter problem is further simplified.

Under these conditions the aerodynamic matrix takes on a form similar to the inertial matrix and the eigenvalue problem 10 reduces to

$$B(\sigma)*p_\sigma = p_\sigma(x, y) - \Omega \iint \left[K'(x, y; x_o, y_o)\right]\left[\mathcal{L} + \rho_s \omega^2 h\right] p_\sigma(x_o, y_o)\, dx_o\, dy_o$$

with

$$K' = K'_1 + K'_2 e^{j\sigma} + K'_n e^{-j\sigma} + K'_3 e^{j2\sigma} + K'_{n-1} e^{-j2\sigma} + \ldots$$

---

* See section on Aerodynamic Pressure Loads.

and the elements K_i' defined as follows:

K_2' = The influence function yielding the deflection surface of the first panel when a concentrated load is applied at any point on the second panel. Due to the cyclic property of the structure it also equals the deflection surface of the nth panel when a concentrated load is applied in the same relative position on the first panel.

K_n' = The influence function yielding the deflection surface of the first panel when a concentrated load is applied at any point on the nth panel. Due to the cyclic property it equals the deflection surface of the second panel when a concentrated load is placed in the same relative position on the first panel.

By referring to Figure 2a it becomes apparent that all the elements K_i' will be known once the Green's function of the stiffened shell is determined. For example, if a concentrated load were applied to the first panel (denoted by the number zero in Figure 2a) K_n' and K_2' would be given by the deflection surfaces of the panels labeled 1 and -1 respectively. K_{n-1}' and K_3' would be given by the deflection surface of the panels labeled 2 and -2 respectively etc. It is easily seen from this physical picture that the structural matrix is not symmetric i.e.

$$K_2' \neq K_n'$$

etc.

The function K', appearing in the flutter problem, may be thought of as a generalized elastic influence function yielding the lateral deflection surface of the equivalent panel (denoted by the number zero) when this panel is under a very special form of influence from all other panels (see Figure 5). The concentrated loads in this case are normal to the shell surface and occupy the same position relative to each panel.

AERODYNAMIC PRESSURE LOADS

The unsteady aerodynamic pressures acting on the outer surface of the shell arise through the interaction of the shell surface motion and the airstream. This motion differs from that which occurs in conventional wing flutter in that it involves only local deformation of the aerodynamic surfaces; rigid body motions of the shell are not allowed. Furthermore only infinitesimal elastic deformations in the neighborhood of an equilibrium state will be considered in the stability analysis. In the following, therefore, the unsteady flow problem will be regarded as a small perturbation on a local steady flow.

In supersonic flight the unsteady aerodynamic pressure acting at a point on the shell will in general be influenced by the motion of the shell at other points. This aerodynamic coupling, however, complicates the flutter analysis and a further simplification is introduced to eliminate this problem. For $M >> 1$ the compression and expansion waves caused by disturbances on the shell surface make small angles with the undisturbed flow. It follows that gradients transverse to the flight direction are large compared with those parallel to it. These facts suggest Hayes' (Ref. 4) hypersonic approximation that any plane slab of fluid initially perpendicular to the undisturbed flow may be assumed to remain so as it is swept downstream. The slab thus moves in its own plane under the laws of one-dimensional unsteady motion for the case of initially planar bodies*. The pressure generated by the motion of the body is related to the local normal component of fluid velocity in the same way that these quantities are related at the face of a piston

---

* This unsteady motion will be two-dimensional for non-planar bodies.

moving in a one-dimensional channel. The net simplification results from the fact that the local pressure is a function only of the local downwash and no aerodynamic coupling occurs.

The above piston analogy was introduced by Lighthill (Ref. 5) and later utilized by Ashley and Zartarian (Ref. 6) in certain aeroelastic problems. They concluded that the approximation should be valid when the local piston velocity does not exceed the local speed of sound in the undisturbed fluid i.e. when

$$M\left[\left|\frac{\partial w}{\partial x}\right|_{max} + |w|_{max}\, k\right] < 1$$

where M is the local Mach number of the flow, $\left|\frac{\partial w}{\partial x}\right|_{max}$ is the maximum inclination of the shell surface to the airstream, $|w|_{max}$ the maximum displacement of the shell, and k the reduced frequency or a measure of the unsteadiness of the flow. When the magnitude of the surface disturbances are such that this condition is satisfied the local unsteady pressure is given by

$$p = -\rho a \left(U \frac{\partial w}{\partial x} + \frac{\partial w}{\partial t}\right) \approx -\frac{\rho U^2}{\sqrt{M^2 - 1}} \left(\frac{\partial w}{\partial x} + \frac{1}{U} \frac{\partial w}{\partial t}\right) \qquad (11)$$

with x taken as the coordinate parallel to the free stream direction.

Now for the stability analysis of the grid of panels at high Mach numbers ($M \geq 2$) the lateral pressure loading on the structure will be adequately described by static piston theory or as it is more commonly called the simple Ackeret theory given by

$$p = -\frac{2q}{\sqrt{M^2 - 1}} \frac{\partial w}{\partial x} .$$

Houbolt (Ref. 7) and Hedgepeth (Ref. 8) have shown for flat three-dimensional panels in the above Mach number range that there is no appreciable difference in the flutter boundaries predicted with Ackeret theory as compared to those predicted by linear piston theory or even a more accurate three-dimensional theory if

$$\sqrt{M^2 - 1}\ \bar{\lambda} \geq 1 .$$

The results discussed above are based on the assumption of an approximately plane surface, even though Hayes' approximation is equally valid for non-planar bodies. Some general considerations regarding hypersonic unsteady flow past non-planar bodies have been advanced by Eggers (Ref. 9). In the absence of more detailed studies one can only conjecture that equation 11 with ρ and a calculated from the undisturbed steady flow, should prove adequate for unsteady motions involving local deformations of finite length shells if (Ref. 10)

$$\frac{M}{L/2R} >> 1 \qquad k << 1$$

Thus for non-planar shell structures flying at high Mach numbers the eigenvalue problem 10 with the time factor removed reduces to the form

$$B(\sigma)^* p_\sigma = p_\sigma - \Omega \iint \left[K(x, y; x_o, y_o) \right] \left[-\frac{2q}{\sqrt{M^2-1}} \left(\frac{\partial}{\partial x} + \frac{\omega}{U} \right) + \rho_s \omega^2 h \right] p_\sigma \, dx_o \, dy_o . \tag{12}$$

THE GREEN'S FUNCTION FOR THE RADIAL DISPLACEMENT OF A FINITE AXIALLY STIFFENED CYLINDRICAL SHELL

General Remarks

Now that the formal reduction of the flutter problem is complete it will be convenient to renumber the panels as shown in Figure 2.

The utilization of the reduction process in the actual flutter analysis requires the knowledge of the Green's function yielding the radial displacement component at any point on the stiffened shell due to a concentrated radial load acting on one of the panels. In this section such a function is derived and the results extended to five limiting cases of shell structures. The solution is based upon the assumption that the differential equations of equilibrium of the shell are adequately described by the well known Donnell equations (Ref. 11), and that the complete stiffened shell can be assembled from freely supported shell segments. This in turn implies that the stiffeners do not bend in the radial direction nor offer rotational resistance to the shell.

In Appendix A the results of this section have been used along with the principle of superposition to compute the elastic influence function required for the flutter analysis.

Problem Formulation

A cylindrical shell of radius R and length $R\,\alpha_1$ supported by stiffening rings along its two ends and by straight longitudinal stiffeners equally spaced along the circumference forms a continuous stiffened shell*. When one of the panels of such a shell structure is subjected to

---

* The exact boundary conditions will be defined later.

a concentrated radial load its deformation pattern will induce deflections in its neighboring panels which will in turn influence their neighbors etc. The longitudinal stiffeners, however, tend to damp out this influence and at a sufficient number of spans away from the loaded panel no appreciable deflections will be observed. The bending of each span of such a loaded shell can be readily investigated by combining a solution for a freely supported cylindrical shell segment under a concentrated unit load with a solution for a similar shell segment bent by a concentrated unit moment. Thus the Green's function for the complete stiffened shell may be built up from these two fundamental solutions. This approach requires only that the complete shell be assembled from cylindrical shell segments whose displacement boundary conditions have been properly matched along the longitudinal stiffeners.

In the following analysis the axial coordinate x and the circumferential coordinate y of a point on the middle surface of the cylindrical shell will be denoted by the non-dimensional coordinates α and β where

$$\alpha = \frac{x}{R}, \quad \beta = \frac{y}{R}.$$

The ith panel of the cylinder is described by α in the interval $(0 \leq \alpha \leq \alpha_1)$ and β in the interval $(\beta^{(i)} \leq \beta \leq \beta^{(i+1)})$.

Let the components of elastic displacement of a point on the middle surface of the shell be denoted by $u^{(i)}$, $v^{(i)}$, and $w^{(i)}$. The inplane displacement components in the axial and circumferential

directions are $u^{(i)}$ and $v^{(i)}$ respectively while the radial deflection component is $w^{(i)}$ (see Figure 2a for positive sense). A complete set of boundary conditions for the ith shell segment that are appropriate to the panel flutter problem is the freely supported condition along the two end rings.

$$w^{(i)}(0, \beta^{(i)}) = 0 \qquad w^{(i)}(\alpha_1, \beta^{(i)}) = 0$$

$$\frac{\partial^2 w^{(i)}}{\partial \alpha^2}(0, \beta^{(i)}) = 0 \qquad \frac{\partial^2 w^{(i)}}{\partial \alpha^2}(\alpha_1, \beta^{(i)}) = 0$$

$$v^{(i)}(0, \beta^{(i)}) = 0 \qquad v^{(i)}(\alpha_1, \beta^{(i)}) = 0$$

$$\frac{\partial u^{(i)}}{\partial \alpha}(0, \beta^{(i)}) = 0 \qquad \frac{\partial u^{(i)}}{\partial \alpha}(\alpha_1, \beta^{(i)}) = 0$$

and the following "matching conditions" along the longitudinal stiffeners

$$w^{(i+1)}(\alpha, 0) = w^{(i)}(\alpha, \beta_1) = 0 \qquad \text{(a)}$$

$$u^{(i+1)}(\alpha, 0) = u^{(i)}(\alpha, \beta_1) = 0 \qquad \text{(b)} \qquad (13)$$

$$v^{(i+1)}(\alpha, 0) = v^{(i)}(\alpha, \beta_1) = 0 \qquad \text{(c)}$$

$$\frac{\partial w^{(i+1)}(\alpha, 0)}{\partial \beta^{(i+1)}} = \frac{\partial w^{(i)}(\alpha, \beta_1)}{\partial \beta^{(i)}} \qquad \text{(d)}$$

The freely supported condition along the two end rings will be realistic for rings that are rigid in their own plane but deform easily out of their plane.

The following analysis can be considerably simplified if the matching condition 13c is replaced by

$$\frac{\partial v^{(i+1)}(\alpha, 0)}{\partial \beta^{(i+1)}} = \frac{\partial v^{(i)}(\alpha, \beta_1)}{\partial \beta^{(i)}} = 0. \tag{14}$$

The physical meaning of the condition 14 is that the midplane stress component σ_y vanishes along the edges $(\alpha, 0)$ and (α, β_1). Free extensions in v must therefore occur at these edges to satisfy this zero stress condition. Obviously a rather special type of stiffener panel attachment would be required to insure such free inplane extensions. In view of the simplification that is possible in the analysis, however, the condition 13c will be replaced by the condition 14. For the limiting case of a grid of flat panels u and v are identically zero on the longitudinal stiffeners and the solution will be exact.

The simplest formulation of the problem is one which utilizes an integral representation for the radial deflection component. This method has been successfully employed by several authors in rather complex shell problems related to both stability and deflection analysis (Refs. 12 and 13). It was found that in several cases this approach was more favorable than the direct integration of the differential equations. Proceeding in this manner the radial deflection component of the ith panel of the shell due to a concentrated radial load acting on the 0th panel at (Ξ, H) may be represented by (for notation see Figure 2)

$$w^{(i)}(\alpha, \beta^{(i)}; \Xi, H^{(i)}) = \int_0^1 M_\eta^{(i-1)}(\xi)\, k_1(\alpha, \beta^{(i)}; \xi, 0)\, d\xi$$

$$- \int_0^1 M_\eta^{(i)}(\xi) k_1(\alpha, \beta^{(i)}; \xi, \beta_1) d\xi + \delta_{io}\, k_o(\alpha, \beta^{(i)}; \Xi, H^{(i)}). \qquad (15)$$

The function $k_o(\alpha, \beta^{(i)}; \Xi, H^{(i)})$ denotes the deflection of a freely supported shell segment due to a concentrated unit load acting at $(\Xi, H^{(i)})$ while the kernels $k_1(\alpha, \beta^{(i)}; \xi, 0)$ and $k_1(\alpha, \beta^{(i)}; \xi, \beta_1)$ denote the deflections of a freely supported shell segment due to a concentrated unit moment acting at a point $(\xi, 0)$ and (ξ, β_1) of its edges respectively. The Kronecker delta symbol δ_{io} is defined as

$$\delta_{ij} = 0 \qquad i \neq j$$

$$\delta_{ii} = 1 .$$

$M_\eta^{(i)}(\xi)$ are the unknown edge moments along the longitudinal stiffeners caused by a concentrated load on the 0th panel.

Since the fundamental solutions k_o and k_1 (i.e. the kernels in equation 15) satisfy the condition of freely supported edges the matching conditions 13a, 13b, and 14 are automatically satisfied. The final matching condition 13d is satisfied by properly selecting the unknown moments $M_\eta^{(i)}(\xi)$ so that the radial slope is continuous across the supports. In view of equation 15 this matching condition at the ith support may be written for $i \neq 0$ or -1 as

$$\int_0^1 \left(M_\eta^{(i+1)}(\xi) \frac{\partial k_1(\alpha, 0; \xi, \beta_1)}{\partial \beta^{(i+1)}} - M_\eta^{(i)}(\xi) \left[\frac{\partial k_1(\alpha, 0; \xi, 0)}{\partial \beta^{(i+1)}} + \frac{\partial k_1(\alpha, \beta_1; \xi, \beta_1)}{\partial \beta^{(i)}} \right] \right.$$

$$\left. + M_\eta^{(i-1)}(\xi) \frac{\partial k_1(\alpha, \beta_1; \xi, 0)}{\partial \beta^{(i)}} \right) d\xi = 0$$

or

$$\int_0^1 \left(M_\eta^{(i+1)}(\xi) K_{13}(\alpha, \xi) - M_\eta^{(i)}(\xi) \left[K_{11}(\alpha, \xi) + K_{33}(\alpha, \xi) \right] + M_\eta^{(i-1)}(\xi) K_{31}(\alpha, \xi) \right) d\xi = 0$$

According to the Maxwell reciprocal theorem the kernels in the integral equation are symmetric

$$K_{ij}(\alpha, \beta; \xi, \eta) = K_{ji}(\xi, \eta; \alpha, \beta)$$

and the above equation may be written as

$$\int_0^1 \left(M_\eta^{(i+1)}(\xi) K_{13}(\alpha, \xi) - 2M_\eta^{(i)}(\xi) K_{11}(\alpha, \xi) + M_\eta^{(i-1)}(\xi) K_{13}(\alpha, \xi) \right) d\xi = 0$$

or

$$\int_0^1 \left(K_{13}(\alpha, \xi) \Delta_i^2 + 2 \left[K_{13}(\alpha, \xi) - K_{11}(\alpha, \xi) \right] \Delta_i + 2 \left[K_{13}(\alpha, \xi) - K_{11}(\alpha, \xi) \right] \right) M_\eta(\xi) d\xi$$

(16)

where $\underset{i}{\Delta}$ is the forward difference operator defined by

$$\underset{i}{\Delta} M_{\eta}^{(i)}(\xi) = M_{\eta}^{(i+1)}(\xi) - M_{\eta}^{(i)}(\xi) .$$

Similarly continuity across the 0th and -1st supports respectively gives

$$f(\alpha ; \Xi, H) + \int_{o}^{1} \left(M_{\eta}^{(-1)} K_{13} - 2M_{\eta}^{(o)} K_{11} + M_{\eta}^{(1)} K_{13} \right) d\xi = 0 \qquad (17)$$

$$g(\alpha ; \Xi, H) - \int_{o}^{1} \left(M_{\eta}^{(-2)} K_{13} - 2M_{\eta}^{(-1)} K_{11} + M_{\eta}^{(o)} K_{13} \right) d\xi = 0$$

where

$$f(\alpha ; \Xi, H) = \left[\frac{\partial k_{o}(\alpha, \beta^{(o)}; \Xi, H)}{\partial \beta^{(o)}} \right]_{\beta^{(o)} = \beta_1}$$

$$g(\alpha ; \Xi, H) = \left[\frac{\partial k_{o}(\alpha, \beta^{(o)}; \Xi, H)}{\partial \beta^{(o)}} \right]_{\beta^{(o)} = 0}$$

Equation 16 represents a recurrence relation between any three adjacent support moments $M_{\eta}^{(i)}(\xi)$ of the stiffened shell for $i \neq 0$ or -1. It is uncoupled from the system of equations 17 and can be solved independently of them. Its solution yields a relation between the moments at the axial supports $1 \leq i < -1$ and the two applied moments

$M_\eta^{(o)}(\xi)$ and $M_\eta^{(-1)}(\xi)$ caused by the concentrated load on the 0th panel (see Figure 3b). Equations 17, on the other hand, govern the solution of the problem illustrated in Figure 3a.

The first of the two conditions that must be imposed on the solution of equation 16 to make it unique is the physical requirement that the support moments diminish with increasing number of spans away from the loaded panel; this may be stated as

$$\|M_\eta^{(i)}(\xi)\| < \|M_\eta^{(i-1)}(\xi)\| \tag{18}$$

where the norm of the moments is given by

$$M_\eta^{(i)}(\xi) = \int_o^\beta 1 \int_o^\alpha 1 \int_o^\alpha 1 \left[M_\eta^{(i)}(\xi;\Xi, H) \right]^2 d\xi \, d\Xi \, dH.$$

Solutions of the system of equations 16 and 17 will be sought for the case in which the number of panels n tends to infinity. The condition 18 implies

$$\|M_\eta^{(i)}(\xi)\| \longrightarrow 0 \quad \text{as} \quad i \to \pm \infty$$

and that the moments at the right supports will be considered as only a function of $M_\eta^{(o)}(\xi)$ and those at the left supoorts only a function of $M_\eta^{(-1)}(\xi)$. The two unknown support moments $M_\eta^{(o)}(\xi)$ and $M_\eta^{(-1)}(\xi)$ may be solved from the system of simultaneous equations 17 once the solution to the recurrence equation 16 has been obtained.

Under the above side conditions the solution of the system of equations 16 and 17 uniquely determine all of the unknown support moments $M^{(i)}(\xi)$ and hence by equation 15 the required Green's function of the stiffened shell.

Kernels of the Integral Equations

To solve the system of equations 16 and 17 it is necessary to know the functions $f(\alpha;\Xi,H)$, $g(\alpha;\Xi,H)$ and the kernels $K_{ij}(\alpha,\xi)$ that are derived from the fundamental solutions k_o and k_1 in the following manner:

$$
\begin{aligned}
f(\alpha;\Xi,H) &= \frac{\partial k_o(\alpha,\beta_1;\Xi,H)}{\partial \beta^{(o)}} \\
g(\alpha;\Xi,H) &= \frac{\partial k_o(\alpha,0;\Xi,H)}{\partial \beta^{(o)}} \\
K_{13}(\alpha,\xi) &= \frac{\partial k_1(\alpha,0;\xi,\beta_1)}{\partial \beta^{(i+1)}} \\
K_{11}(\alpha,\xi) &= \frac{\partial k_1(\alpha,0;\xi,0)}{\partial \beta^{(i+1)}}
\end{aligned}
\qquad (19)
$$

The fundamental solutions are defined as follows:

$k_o(\alpha, \beta ; \Xi, H)$ = The radial deflection of a point (α, β) due to a concentrated unit load on a freely supported shell segment at a point (Ξ, H) normal to the shell surface.

$k_1(\alpha, \beta ; \xi, \eta)$ = The radial deflection at a point (α, β) due to a concentrated unit moment on a freely supported shell segment at a point (ξ, η) and acting about an axis parallel to the ξ axis. For positive sense see Figure 2.

Furthermore

$$k_1(\alpha, \beta ; \xi, \eta) = \lim_{\substack{P\delta \to 1 \\ \delta \to 0}} \frac{P\delta \left[k_o(\alpha, \beta ; \xi, \eta + \delta) - k_o(\alpha, \beta ; \xi, \eta) \right]}{\delta}$$

or in the limit

$$k_1(\alpha, \beta ; \xi, \eta) = \frac{\partial k_o(\alpha, \beta ; \xi, \eta)}{\partial \eta} \tag{20}$$

Thus it is sufficient to discuss the fundamental solution $k_o(\alpha, \beta ; \xi, \eta)$.

The Donnell equation governing the radial deflection component may be written in the form (Ref. 13)

$$\nabla^8 F(\alpha, \beta) + \frac{1 - \nu^2}{c^2} \frac{\partial^4 F(\alpha, \beta)}{\partial \alpha^4} = \frac{R^4}{N} Z(\alpha, \beta) \tag{21}$$

where

$w(\alpha,\beta)$ = $\nabla^4 F(\alpha,\beta)$ = radial component of displacement

$F(\alpha,\beta)$ = stress function

$Z(\alpha,\beta)$ = load normal to the shell surface

$$N = \frac{Eh^3}{12(1-\nu^2)} = \text{flexural rigidity of the shell}$$

$$c^2 = \frac{h^2}{12R^2}$$

A solution of equation 21 for the case when the external load $Z(\alpha,\beta)$ is a concentrated force normal to the shell and located at (Ξ, H) is (Ref. 13)

$$k_o(\alpha,\beta;\Xi,H) = \frac{4R^2\alpha_1^3}{\pi^4 N\beta_1}\sum_{m=1}^{\infty}\sum_{n=1}^{\infty}\frac{\sin\frac{m\pi}{\alpha_1}\alpha\,\sin\frac{n\pi}{\beta_1}\beta\,\sin\frac{m\pi}{\alpha_1}\Xi\,\sin\frac{n\pi}{\beta_1}H}{D_{mn}}$$

where

$$\frac{1}{D_{mn}} = \frac{(m^2+\lambda^2n^2)^2}{(m^2+\lambda^2n^2)^4+\epsilon m^4} = \frac{1}{(m^2+\lambda^2n^2)^2} - \frac{\epsilon m^4}{(m^2+\lambda^2n^2)^2\left[(m^2+\lambda^2n^2)^2+\epsilon m^4\right]}$$

$$\lambda = \frac{\alpha_1}{\beta_1} = \frac{1}{\bar{\lambda}}$$

$$\epsilon = \frac{12(1-\nu^2)R^2\alpha_1^4}{\pi^4 h^2} = \frac{12(1-\nu^2)}{\pi^4}\left(\frac{L}{R}\right)^4\left(\frac{R}{h}\right)^2$$

The functions $f(\alpha;\Xi,H)$, $g(\alpha;\Xi,H)$ and $K_{ij}(\alpha,\xi)$, given by equations 19 and 20, are listed in Table I under "original case". The first three functions of equation 19 are represented by series that are convergent at every point in the interval under consideration. The series representing the function $K_{11}(\alpha,\xi)$ is convergent everywhere except at $\alpha = \xi$ where it has a logarithmic singularity and is divergent (Ref. 13). For one may write $K_{11}(\alpha,\xi)$ in the form

$$K_{11}(\alpha,\xi) = \frac{4R^2\alpha_1^3}{\pi^2 N\beta_1^3}\left[\sum_{m=1}^{\infty}\sum_{n=1}^{\infty}\frac{n^2 \sin\frac{m\pi}{\alpha_1}\alpha \sin\frac{m\pi}{\alpha_1}\xi}{(m^2+\lambda^2n^2)^2}\right.$$

$$\left. -\epsilon\sum_{m=1}^{\infty}\sum_{n=1}^{\infty}\frac{n^2m^4 \sin\frac{m\pi}{\alpha_1}\alpha \sin\frac{m\pi}{\alpha_1}\xi}{(m^2+\lambda^2n^2)^2\left[(m^2+\lambda^2n^2)^4+\epsilon m^4\right]}\right]$$

or by using the relation

$$\frac{4}{\pi^2 N}\sum_{m=1}^{\infty}\sum_{n=1}^{\infty}\frac{n^2 \sin\frac{m\pi}{\alpha_1}\alpha \sin\frac{m\pi}{\alpha_1}\xi}{(m^2+\lambda^2n^2)^2} = \frac{1}{2\pi N}\frac{\partial}{\partial\bar{\lambda}}\left(\bar{\lambda}\,\mathrm{Ln}\left[\frac{\Theta_1(\alpha-\xi;\bar{\lambda})}{\Theta_1(\alpha+\xi;\bar{\lambda})}\right]\right)$$

in the form

$$K_{11} = \frac{R^2}{2\pi N}\left\{ \frac{\partial}{\partial \bar{\lambda}} \left(\bar{\lambda} \operatorname{Ln}\left[\frac{\theta_1(\alpha - \xi; \bar{\lambda})}{\theta_1(\alpha + \xi; \bar{\lambda})} \right] \right) \right.$$

$$\left. 8\frac{\lambda^3}{\pi}\epsilon \sum_{m=1}^{\infty}\sum_{n=1}^{\infty} \frac{n^2 m^4 \sin\frac{m\pi}{\alpha_1}\alpha \sin\frac{m\pi}{\alpha_1}\xi}{(m^2 + \lambda^2 n^2)^2\left[(m^2 + \lambda^2 n^2)^4 + \epsilon m^4\right]} \right\}$$

This splitting up operation is characterized by the fact that the first series contains the logarithmic singularity and does not depend upon the radius of curvature of the shell while the second series converges everywhere in the interval and vanished for a flat plate. The nature of the kernel $K_{11}(\alpha, \xi)$ thus implies that the system of integral equations 16 and 17 are singular.

Limiting Cases

The system of equations 16 and 17 not only solve the problem illustrated in Figure 3 but also contain the following special cases shown in Figure 4.

(a) Axially stiffened semi-infinite cylinder

(b) Axially stiffened infinite cylinder

(c) Rib stiffened infinite plate strip

(d) Rib stiffened semi-infinite plate

(e) Rib stiffened infinite plate

Cases (a) and (b), for example, are obtained from the original problem by a special limiting process* in which the aspect ratio parameter $\lambda = \alpha_1/\beta_1$ tends to infinity with the origin of the coordinates on the finite shell segments as shown below.

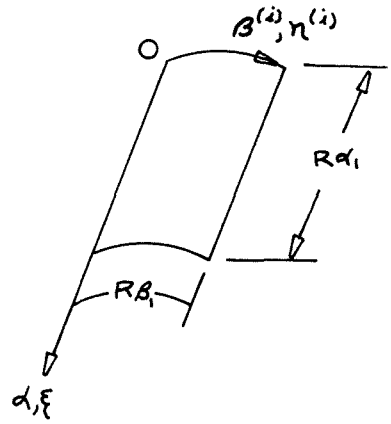

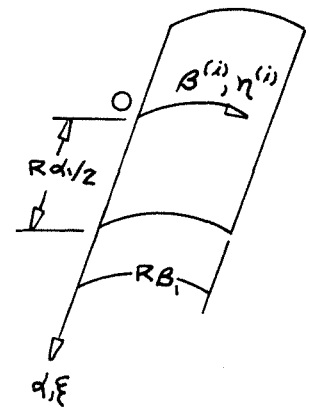

case (a) = $\lim_{\substack{\lambda \to \infty \\ \alpha_1 \to \infty}}$

case (b) = $\lim_{\substack{\lambda \to \infty \\ \alpha_1 \to \infty}}$

The corresponding infinite series is then interpreted in the sense of a Riemann sum and hence replaced by an appropriate infinite integral.

This method will now be illustrated by considering the special case (b). Shifting the origin of the coordinates to the middle of the left hand side of the shell segment and taking the limit as $\lambda \to \infty$ gives the following system of equations which govern the solution of the problem shown in Figure 4b.

---

* This limiting process is similar to the one applied by Quinlan in relation to problems associated with flat plates (see Ref. 14).

$$\int_{-\infty}^{\infty} \left(M_{\eta}^{(i+1)} K'_{13} - 2M_{\eta}^{(i)} K'_{11} + M_{\eta}^{(i-1)} K'_{13} \right) d\xi = 0$$

$$f' + \int_{-\infty}^{\infty} \left(M_{\eta}^{(-1)} K'_{13} - 2M_{\eta}^{(o)} K'_{11} + M_{\eta}^{(1)} K'_{13} \right) d\xi = 0$$

$$g' - \int_{-\infty}^{\infty} \left(M_{\eta}^{(-2)} K'_{13} - 2M_{\eta}^{(-1)} K'_{11} + M_{\eta}^{(o)} K'_{13} \right) d\xi = 0$$

The appropriate functions f', g', and K'_{ij} are obtained from the "original case" (Table I) by the special limiting process. Due to the similar form of all these functions it will be sufficient to carry out this limiting operation only on the fundamental function $k_o(\alpha, \beta; \xi, \eta)$. By interchanging the order of summation and making the appropriate coordinate transformation $k_o(\alpha, \beta; \xi, \eta)$ may be written in the form

$$k_o = \frac{4R^2 \alpha_1^3}{\pi^4 N \beta_1} \sum_{n=1}^{\infty} \sin \frac{n\pi}{\beta_1}\beta \sin \frac{n\pi}{\beta_1}\eta \left[\sum_{m=1}^{\infty} \frac{\sin\left(\frac{m\pi}{\alpha_1}\alpha + \frac{m\pi}{2}\right)\sin\left(\frac{m\pi}{\alpha_1}\xi + \frac{m\pi}{2}\right)}{D_{mn}} \right]$$

Since

$$\sin\left(\frac{m\pi}{\alpha_1}\alpha + \frac{m\pi}{2}\right) \sin\left(\frac{m\pi}{\alpha_1}\xi + \frac{m\pi}{2}\right)$$

$$= \cos\frac{m\pi}{\alpha_1}\alpha \cos\frac{m\pi}{\alpha_1}\xi \qquad m \text{ odd}$$

$$= \sin\frac{m\pi}{\alpha_1}\alpha \sin\frac{m\pi}{\alpha_1}\xi \qquad m \text{ even}$$

the sum over m may be split into an even and an odd term

$$\frac{2\lambda^3}{\pi^3}\sum_{m=1}^{\infty}\frac{\sin\left(\frac{m\pi}{\alpha_1}\alpha + \frac{m\pi}{2}\right)\sin\left(\frac{m\pi}{\alpha_1}\xi + \frac{m\pi}{2}\right)}{D_{mn}} =$$

$$\frac{2\lambda^3}{\pi^3}\sum_{m=1}^{\infty}\frac{\sin\frac{2m\pi}{\alpha_1}\alpha \sin\frac{2m\pi}{\alpha_1}\xi}{D_{2mn}} + \frac{2\lambda^3}{\pi^3}\sum_{m=1}^{\infty}\frac{\cos(2m-1)\frac{\pi}{\alpha_1}\alpha \cos(2m-1)\frac{\pi}{\alpha_1}\xi}{D_{2m-1\,n}}$$

Now let

$$\alpha' = \frac{\alpha}{\beta_1}, \quad \xi' = \frac{\xi}{\beta_1}$$

and in the first series set

$$t_m = \frac{2m\pi}{\lambda}, \quad \Delta t_m = \frac{2\pi}{\lambda}$$

while in the second series set

$$t_m = \frac{(2m-1)\pi}{\lambda}, \quad \Delta t_m = \frac{2\pi}{\lambda}$$

The two series then take the form

$$\sum_{m=1}^{\infty} \frac{\sin t_m \alpha' \sin t_m \xi' \Delta t_m}{D(t_m, n)} + \sum_{m=1}^{\infty} \frac{\cos t_m \alpha' \cos t_m \xi' \Delta t_m}{D(t_m, n)}$$

where

$$\frac{1}{D(t_m, n)} = \frac{(t_m^2 + n^2\pi^2)^2}{(t_m^2 + n^2\pi^2)^4 + \bar{\epsilon} t_m^4}$$

$$\bar{\epsilon} = \frac{12(1-\nu^2)R^2\beta_1^4}{h^2}$$

$k'_o(\alpha, \beta; \xi, \eta)$ may now be written as

$$k'_o(\alpha, \beta; \xi, \eta) = \frac{2(R\beta_1)^2}{\pi N} \sum_{n=1}^{\infty} \sin\frac{n\pi}{\beta_1}\beta \sin\frac{n\pi}{\beta_1}\eta \left[\lim_{\lambda\to\infty} \sum_{m=1}^{\infty} \frac{\sin t_m \alpha' \sin t_m \xi' \Delta t_m}{D(t_m, n)} \right.$$

$$\left. + \lim_{\lambda\to\infty} \sum_{m=1}^{\infty} \frac{\cos t_m \alpha' \cos t_m \xi' \Delta t_m}{D(t_m, n)} \right]$$

The limit of the above sums is Riemann's definition of the infinite integral when $1/D(t, n)$ is a function of bounded variation in t in any finite range, and the resulting integral is convergent. Since these conditions are satisfied the function $k_o(\alpha, \beta; \xi, \eta)$ may be written as

$$k_o(\alpha',\beta;\xi',\eta)=\frac{2(R\beta_1)^2}{\pi N}\sum_{n=1}^{\infty}\sin\frac{n\pi}{\beta_1}\beta\sin\frac{n\pi}{\beta_1}\eta\left[\int_0^{\infty}\frac{\sin t\alpha'\sin t\xi' dt}{D(t,n)}+\int_0^{\infty}\frac{\cos t\alpha'\cos t\xi' dt}{D(t,n)}\right]$$

or by combining the two convergent integrals as

$$k_o(\alpha',\beta;\xi',\eta)=\frac{2(R\beta_1)^2}{\pi N}\sum_{n=1}^{\infty}\sin\frac{n\pi}{\beta_1}\beta\sin\frac{n\pi}{\beta_1}\eta\left[\int_0^{\infty}\frac{\cos t(\alpha'-\xi')dt}{D(t,n)}\right]$$

This last integral has been evaluated in closed form and will be referred to as $\Pi_n(\alpha',\xi')$ in the remainder of the report (Ref. 15)*. The known functions to be used in the solution of the equations for case (b) are given in Table I.

Case (c) is obtained from the original problem by letting $R\to\infty$ and by observing that

$$\lim_{R\to\infty}\ (M_{\eta\ \text{shell}})\ R = M_{\eta\ \text{plate}}$$

$$\lim_{R\to\infty}\ \left(\frac{f_{\text{shell}}}{R}\right) = f_{\text{plate}}$$

$$\lim_{R\to\infty}\ \left(\frac{g_{\text{shell}}}{R}\right) = g_{\text{plate}}$$

---

* There is some question as to the accuracy of the Donnell equations when the cylinder length is infinite, or in fact when $L/R>10$. Therefore if accurate results are required for deflections in these limiting cases the more exact Morley or the Flugge equations should be employed. The results will be identical to the above form if $D(t,n)$ is defined in the appropriate manner. The corresponding integral has been evaluated in reference 16 for the Morley equations and in reference 17 for the Flugge equations.

$$R\alpha_1 \longrightarrow a \qquad R\alpha_{shell} \longrightarrow \alpha_{plate}$$

$$R\beta_1 \longrightarrow b \qquad R\beta_{shell} \longrightarrow \beta_{plate}$$

$$\epsilon \longrightarrow 0 \qquad \text{etc.}$$

The special cases (d) and (e) are obtained from (c) in the same manner as cases (a) and (b) were derived from the original problem. Table I summarizes the known functions obtained for the different cases shown in Figure 4.

There is one additional case of interest worth mentioning that occurs for configurations (b) and (e) when the transverse loading on the shell does not vary along its length. Replacing the concentrated load at (Ξ, H) by a line load at $\beta^{(o)} = H$ of constant magnitude and infinite length in the ξ direction yields moments at the supports which are constants, and the governing equations for (e) take the form

$$M_\eta^{(i+1)} + 4M_\eta^{(i)} + M_\eta^{(i-1)} = 0$$

$$-\frac{\eta(b^2-\eta^2)}{2Nb^2} + M_\eta^{(-1)} + M_\eta^{(o)}(2+\sqrt{3}) = 0 \qquad (22)$$

$$\frac{(b-\eta)\,b^2-(b-\eta)^2}{2Nb^2} + M_\eta^{(-1)}(2+\sqrt{3}) + M_\eta^{(o)} = 0$$

since

$$\int_{-\infty}^{\infty} K_{11}(\alpha, \xi)\, d\xi = \frac{2}{3}\pi b, \quad \int_{-\infty}^{\infty} K_{12}(\alpha, \xi)\, d\xi = -\frac{\pi}{3} b, \quad M_{\eta}^{(1)} = (-2+\sqrt{3}) M_{\eta}^{(0)}$$

This particular case is similar to that of a concentrated load on an infinite beam with equidistant supports (Ref. 18). The analogue to case (b) would be that of a concentrated load on a curved beam with equidistant supports.

Solution of the System of Integral Equations

The direct solution of the integral equations can be avoided by replacing the integral-difference equation 16 and the system of two Fredholm integral equations 17 by a difference equation and two algebraic equations respectively. This is accomplished by assuming that the moments along the supports may be expressed in the form

$$M_{\eta}^{(i)}(\xi) = \sum_{m=1}^{\infty} q_m^{(i)} \sin \frac{m\pi}{\alpha_1} \xi ,$$

and by substituting this expression into the system of equations 16 and 17. After carrying out the indicated integrations and noting the occurring orthogonality property the following system of equations are obtained for the unknown Fourier coefficients:

$$\frac{2R^2\lambda^4\beta_1}{\pi^2 N}\sum_{m=1}^{\infty}\sin\frac{m\pi}{\alpha_1}\alpha\left[q_m^{(i+1)}B_m - 2q_m^{(i)}C_m + q_m^{(i-1)}B_m\right] = 0$$

$$\frac{2R^2\lambda^4\beta_1}{\pi^2 N}\sum_{m=1}^{\infty}\sin\frac{m\pi}{\alpha_1}\alpha\left[q_m^{(-1)}B_m - q_m^{(0)}\left(2C_m - \gamma_m B_m\right) + A_m(\Xi, H)\right] = 0 \qquad (23)$$

$$\frac{2R^2\lambda^4\beta_1}{\pi^2 N}\sum_{m=1}^{\infty}\sin\frac{m\pi}{\alpha_1}\alpha\left[q_m^{(-1)}\left(2C_m - \gamma_m B_m\right) - q_m^{(0)}B_m + A(\Xi, H)\right] = 0$$

where A, $\bar{A}$, B, and C are given by Table II, and

$$M_\eta^{(1)}(\xi) = \sum_{m=1}^{\infty}\gamma_m q_m^{(0)}\sin\frac{m\pi}{\alpha_1}\xi, \quad M_\eta^{(-2)}(\xi) = \sum_{m=1}^{\infty}\gamma_m q_m^{(-1)}\sin\frac{m\pi}{\alpha_1}\xi$$

γ_m is determined from the solution of the difference equation for the Fourier coefficients. Since continuity of the slope must exist for $0 \le \alpha \le \alpha_1$ the following equations are obtained from 23 for each value of m.

$$q_m^{(i+1)}B_m - 2q_m^{(i)}C_m + q_m^{(i-1)}B_m = 0$$

$$q_m^{(-1)}B_m - q_m^{(0)}\left(2C_m - \gamma_m B_m\right) + A_m(\Xi, H) = 0 \qquad (24)$$

$$q_m^{(-1)}\left(2C_m - \gamma_m B_m\right) - q_m^{(0)}B_m + \bar{A}_m(\Xi, H) = 0$$

These results may be extended directly to the case shown in Figure 4a by the special limiting process described earlier. The analogue of the Fourier sine series expansion for the moments is given by

$$M_{\eta}^{(i)}(\xi) = \int_{o}^{\infty} q^{(i)}(t) \sin t\,\xi' \, dt$$

where

$$q^{(i)}(t) = \lim_{\lambda \to \infty} \left(\frac{\lambda}{\pi} q_m^{(i)}\right)$$

The function $q(t)$ must, of course, satisfy the hypothesis of the Fourier Integral Theorem i. e.

$$\int_{o}^{\infty} \left|q^{(i)}(t)\right| \, dt < \infty$$

and $q^{(i)}(t)$ must be a function of bounded variation in $[0, \infty)$. The analogue to the system of equations 23 is then for $q^{(i)}(t)$ continuous on $[0, \infty)$

$$\frac{2R^2\beta_1\pi^2}{N}\int_{o}^{\infty} \sin t\alpha' \left[q^{(i-1)}(t)B(t) - 2q^{(i)}(t)C(t) + q^{(i-1)}(t)B(t)\right] dt = 0$$

$$\frac{2R^2\beta_1\pi^2}{N}\int_{o}^{\infty} \sin t\alpha' \left[q^{(-1)}(t)B(t) - q^{(o)}(t)\left|2C(t) - \gamma(t)B(t)\right| + A(\Xi', H, t)\right] dt = 0 \qquad (25)$$

$$\frac{2R^2\beta_1\pi^2}{N}\int_{o}^{\infty} \sin t\alpha' \left[q^{(-1)}(t)\left|2C(t) - \gamma(t)B(t)\right| + q^{(o)}(t)B(t) + \bar{A}(\Xi', H, t)\right] dt = 0$$

where A, $\bar{A}$, B, and C are given by Table II case (b), and

$$M_\eta^{(1)}(\xi') = \int_0^\infty \gamma(t) q^{(0)}(t) \sin t\xi' \, dt, \quad M_\eta^{(-2)}(\xi') = \int_0^\infty \gamma(t) q^{(-1)}(t) \sin t\xi' \, dt.$$

The method of extending the system of equations 24 to the case (a) is now obvious. In fact the system of equations for the moment coefficients of all the special cases shown in Figure 4 can be written in the form:

$$\begin{aligned} q^{(i+1)}B - 2q^{(i)}C + q^{(i-1)}B &= 0 \\ q^{(-1)}B - q^{(0)}(2C - \gamma B) + A &= 0 \\ q^{(-1)}(2C - \gamma B) - q^{(0)}B + \bar{A} &= 0 \end{aligned} \tag{26}$$

where A, $\bar{A}$, B, and C are given by Table II. The solution of this system is

$$\begin{aligned} q^{(0)} &= -\frac{\bar{A}B - A(2C - \gamma B)}{(2C - \gamma B)^2 - B^2} = \frac{\bar{A}B - A\left[C - \sqrt{C^2 - B^2}\right]}{2\sqrt{C^2-B^2}\left[C - \sqrt{C^2-B^2}\right]} \\ q^{(-1)} &= \frac{AB - \bar{A}(2C - \gamma B)}{(2C - \gamma B)^2 - B^2} = -\frac{AB - \bar{A}\left[C - \sqrt{C^2-B^2}\right]}{2\sqrt{C^2-B^2}\left[C - \sqrt{C^2-B^2}\right]} \\ q^{(i)} &= \left[\gamma\right]^i q^{(0)} \qquad i \geq 0 \\ q^{(-1)} &= \left[\gamma\right]^{i-1} q^{(-1)} \qquad i \geq 1 \end{aligned} \tag{27}$$

where

$$\gamma = C/B + \sqrt{(C/B)^2 - 1}, \qquad |C/B| > 1, \; -1 < \gamma < 0$$

The support moments for the original problem and the special cases shown in Figure 4 can be determined from equation 27 with the aid of Table II and the following expressions.

Case	Expression for the Moment
original	$\sum_{1}^{\infty} q_m^{(i)} \sin \frac{m\pi}{\alpha_1} \xi$
(a)	$\int_0^{\infty} q^{(i)}(t) \sin t\,\xi' \, dt$
(b)	$\int_0^{\infty} q^{(i)}(t) \cos t(\xi' - \Xi') \, dt$
(c)	$\sum_{1}^{\infty} q_m^{(i)} \sin \frac{m\pi}{a} \xi$
(d)	$\int_0^{\infty} q^{(i)}(t) \sin t\,\xi/b \, dt$
(e)	$\int_0^{\infty} q^{(i)}(t) \cos t\,(\xi' - \Xi') \, dt$

(28)

The required Green's functions are then obtained from a generalized equation 15 written in the form

$$w^{(i)}(\alpha, \beta^{(i)}; \Xi, H^{(i)}) = W^{(i)}(\alpha, \beta^{(i)}) + \delta_{io} k_o(\alpha, \beta^{(i)}; \Xi, H^{(i)}) \quad (29)$$

where $W^{(i)}(\alpha, \beta^{(i)})$ and k_o are given by Table III.

FLUTTER ANALYSIS

In this section an approximate method of solution is discussed for the flutter problem of an infinite strip plate supported by equally spaced cross members (Figure 1b).

Writing the equation of motion 12 in dimensionless form and retaining only the simple Ackeret expression for the aerodynamic pressure loads yields the "equivalent" eigenvalue problem

$$p_\sigma(\alpha'', \beta'') = \Omega_\sigma \int_0^1 \int_0^1 K'(\alpha'', \beta''; \Xi'', H''; \sigma) \left[\mu k^2 \sqrt{M^2-1}\, p(\Xi'', H'') - \frac{\partial p(\Xi'', H'')}{\partial \Xi''} \right] d\Xi'' dH'' \quad (30)$$

where the kernel K' is obtained from equation A.1 for case (c) and the eigenvalue Ω_σ and dimensionless coordinates are defined as*

$$\Omega_\sigma = \frac{4}{\pi^4} \frac{2q a^3}{N\sqrt{M^2-1}} \qquad \alpha'' = \alpha/a \quad \beta'' = \beta/b \quad \Xi'' = \Xi/a \quad H'' = H/b$$

The stability analysis involves the problem of finding the smallest value of the parameter Ω_σ that causes the reduced frequency k to first take on a negative imaginary part.

In the following analysis Galerkin's approximate method of solving differential and integral equations (Ref. 19) is applied to the homogeneous

* In the remainder of this section the double primes will be omitted for convenience in writing.

flutter equation 30 to illustrate a method for determining the minimum Ω_σ. The procedure is to write the assumed flutter mode or deflection shape as a linear combination of independent functions in the series form

$$p_\sigma(\alpha,\beta) = \mathrm{Re}\left[\sum_{r=1}^{M}\sum_{s=1}^{N} A_{rs}\,\varphi_r(\alpha)\,\psi_s(\beta,\sigma)\right] \tag{31}$$

valid in the region $0 \le \alpha \le 1$, $0 \le \beta \le 1$. The functions $\varphi_r(\alpha)$ and $\psi_s(\beta,\sigma)$ must be continuous, integrable and continuously differentiable in the interval of interest. They should in addition, satisfy the geometric boundary conditions imposed on the deflection surface*. Substituting equation 31 into equation 30 results in an error function $\varepsilon(\alpha,\beta,\sigma)$ as follows

$$\varepsilon(\alpha,\beta,\sigma) = \sum_{r=1}^{M}\sum_{s=1}^{N} A_{rs}\left[\varphi_r(\alpha)\,\psi_s(\beta,\sigma)\right.$$

(32)

$$\left. -\Omega_\sigma\int_0^1\int_0^1 K'(\alpha,\beta;\Xi,H)\left[\mu k^2\sqrt{M^2-1} - \frac{\partial}{\partial\Xi}\right]\varphi_r(\Xi)\,\psi_s(H,\sigma)\,d\Xi\,dH\right)$$

According to the Galerkin method $\varepsilon(\alpha,\beta,\sigma)$ should be orthogonal to $\varphi_r(\alpha)\,\psi_s(\beta,\sigma)$ ($r = 1, 2, \ldots M$; $s = 1, 2, \ldots N$), that is the

---

* In the integral formulation of the flutter problem for the "equivalent" panel the boundary forces are included as part of the system. The functions $\varphi_r(\alpha)$ and $\psi_s(\beta,\sigma)$, therefore, need not satisfy these natural or force boundary conditions.

average value with respect to the weighting function $\varphi_r(\alpha)\,\psi_s(\beta,\sigma)$ is zero.

$$\int_0^1 \int_0^1 \varepsilon(\alpha,\beta,\sigma)\,\varphi_r(\alpha)\,\psi_s(\beta,\sigma)\,d\alpha\,d\beta = 0 \qquad (33)$$

Substituting equation 32 into 33 gives

$$0 = \sum_{r=1}^{M}\sum_{s=1}^{N} A_{rs}\left\{\int_0^1\int_0^1 \varphi_r(\alpha)\psi_s(\beta,\sigma)\,\varphi_v(\alpha)\psi_\mu(\beta,\sigma)\,d\alpha\,d\beta - \right.$$

$$\left. \Omega_\sigma \int_0^1\int_0^1 \varphi_v(\alpha)\psi_\mu(\beta,\sigma)\left[\int_0^1\int_0^1 K'(\mu k^2\sqrt{M^2-1} - \frac{\partial}{\partial\Xi})\varphi_r(\Xi)\psi_s(H,\sigma)\,d\Xi\,dH\right]d\alpha\,d\beta\right\}$$

This constitutes an eigenvalue problem of the form

$$\left[\underset{\sim}{A} - \Omega_\sigma \underset{\sim}{B}(k)\right] x = 0 \qquad (34)$$

where the vector x is composed of the unknown coefficients A_{rs} and the matrix $\underset{\sim}{B}$ is a function of the unknown reduced flutter frequency k. Since the onset of flutter is determined by investigating the imaginary part of this reduced frequency parameter as the dynamic pressure changes, it will be convenient to rearrange the equation 34 in the form

$$\left[\underset{\sim}{A}(\Omega_\sigma) - k^2 \underset{\sim}{B}\right] x = 0 \qquad (35)$$

The reduced frequency now plays the role of the eigenvalue while Ω_σ is considered only as a real valued dynamic pressure parameter. For most regular functions $\Phi_r(\alpha)$ and $\Psi_s(\beta,\sigma)$ the matrix $\underset{\sim}{B}$ will be non-singular and equation 35 can be transformed into

$$\left[\underset{\sim}{B}^{-1}\ \underset{\sim}{A} - k^2\ \underset{\sim}{I}\right] x = 0 \qquad (36)$$

The elements of the matrix $B^{-1}A$ are all real since Ω_σ is defined to be a real valued parameter. In addition the off diagonal terms, representing the aerodynamic forces, satisfy the relation (Ref. 20)

$$C_{mn} = (-1)^{n+m} C_{nm}.$$

Since the complex eigenvalues must occur in conjugate pairs, flutter ensues once k^2 becomes complex. For Ω_σ small the eigenvalues or characteristic frequencies k^2 will be real*. As Ω_σ increases, however, two eigenvalues will coalesce into a pair of complex conjegate roots. The stability analysis thus reduces to an iteration procedure applied to equation 36 for determining the lowest value of Ω_σ that first causes two eigenvalues to coalesce.

Franklin (Ref. 21) has developed a numerical method for computing eigenvalues for matrix problems of the form 36. This method has

---

* This is a consequence of retaining only the simple Ackeret theory which neglects aerodynamic damping.

been programmed by the California Institute of Technology Computing Center for the Datatron 220 digital computer. A few sample calculations that have been carried out show that the flutter boundaries can be obtained numerically by using this routine to follow the eigenvalues up to coalescence as the parameter Ω_σ is increased.

In conclusion a few remarks will be made concerning the proper choice of the assumed flutter modes. For the problem at hand probably the most suitable chordwise (streamwise) functions $\varphi_r(\alpha)$ that satisfy the required boundary conditions are

$$\varphi_r(\alpha) = \sin r\pi\alpha. \qquad (r = 1, 2, \ldots) \qquad (37)$$

It is always necessary to retain the first two modes $r = 1$ and $r = 2$. Past experience with the Galerkin method (Ref. 8) has also shown that best convergence is obtained when an even number of these modes are used consecutively in the analysis. The choice of spanwise functions $\psi_s(\beta, \sigma)$ should be such that they satisfy the following

$$0 < \sigma \leq \pi \qquad \psi_s(\beta_1', \sigma) = \psi_s(0, \sigma) = 0$$

$$\sigma \longrightarrow 0 \qquad \begin{cases} \psi_s(\beta_1', 0) = \psi_s(0, 0) = 0 \\ \dfrac{\partial \psi_s}{\partial \beta}(\beta_1', 0) = \dfrac{\partial \psi_s}{\partial \beta}(0, 0) = 0 \end{cases}$$

A suggested function $\psi_s(\beta, \sigma)$ that satisfies these conditions is

$$\psi_s(\beta,\sigma) = \frac{\sigma}{\pi} \sin s\pi\bar{\beta} + \left|1 - \frac{\sigma}{\pi}\right| \left[\frac{1}{s} \sin s\pi\bar{\beta} + \frac{1}{s+2} \sin (s+2)\pi\bar{\beta}\right] \qquad (38)$$

Experience has again shown that $s = 1$ is the most important mode to retain, at least for the configurations involving flat single panels. If it is desirable to use a higher number of these modes they should be chosen in such a way that the envelope of the motion across the span is symmetric with respect to the center line of the panel. (i.e. there should be no preferred spanwise direction.)

It may be possible to find other mode shapes that converge at a faster rate but these have been suggested because they satisfy certain orthogonality properties with respect to the kernel of the integral equation 30. The choice of $\psi_s(\beta, \sigma)$ also allows for the possibility of a phase shift across the span for $0 < \sigma < \pi$ when only the term $s = 1$ is retained. Preliminary calculations indicate that very little phase shift across the span occurs for the case $\sigma = 0$ or $\sigma = \pi$.

Figure 6 illustrates some of the results obtained from the initial computer studies for the problem of interest. In this study a four mode analysis was employed using the functions 37 for $r = 1, 2$ and the functions 38 for $s = 1, 3$. The investigations were confined to the neighborhood of $\sigma = \pi$ since a local minimum was found to occur here, and the assumed modes could be simplified. In addition only the interval $\sigma = 0 \rightarrow \pi$ is shown since the curve is symmetric with respect to $\sigma = \pi$. The results for $\sigma = 0$, which can be obtained from

investigating the stability of a single panel clamped on the two streamwise edges, are also shown on the plot. These preliminary investigations suggest that $\sigma = \pi$ is an absolute as well as a local minimum. If this should prove to be the case then at the critical flutter speed all panels of the grid would flutter in exactly the same mode shape, the same magnitude of occurrence of this mode shape and with a phase shift equal to π occurring between successive panels.

A rather extensive numerical program is required to investigate the remaining features of the above problem and the stability of the stiffened shell shown in Figure 1a. For this reason the actual numerical analysis will be reserved for a future report.

REFERENCES

1. Lane, F.: System Mode Shapes in the Flutter of Compressor Blade Rows. Journal of Aero. Sci., Vol. 23, January 1956, pp. 54-66.

2. Fung, Y. C. B.: Aeroelastic Problems of a Ring of Bodies, Such as Compressor Blades, or Skin Panels on a Fuselage. Unpublished Report, California Institute of Technology, February 25, 1956.

3. Fung, Y. C. B.: On Two-Dimensional Panel Flutter. Journal of Aero. Sci., Vol. 25, No. 3, March 1958, pp. 145-160.

4. Hayes, W. D.: On Hypersonic Similitude. Quarterly of Appl. Math., Vol. 5, 1947, pp. 105-106.

5. Lighthill, M. J.: Oscillating Airfoils at High Mach Number. Journal of Aero. Sci., Vol. 20, 1953, pp. 402-406.

6. Ashley, H. and Zartarian, G.: Piston Theory - A New Aerodynamic Tool for the Aeroelastician. Journal of Aero. Sci., Vol. 23, 1956, pp. 1109-1118.

7. Houboult, J. C.: A Study of Several Aerothermoelastic Problems of Aircraft Structures. Doctoral Thesis, E. T. H., Zurich, 1958.

8. Hedgepeth, J. M.: Flutter of Rectangular Simply Supported Panels at High Supersonic Speeds. Journal of Aero. Sci., Vol. 24, No. 8, August 1957, pp. 563-573.

9. Eggers, A. J., Jr.: On the Calculation of Flow About Objects Traveling at High Supersonic Speeds. NACA TN 2811, October 1952.

10. Miles, J. W.: Unsteady Flow at Hypersonic Speeds. Proc. of the Eleventh Symposium of the Colston Research Society, Vol. XI, University of Bristol, 1959.

11. Donnell, L. H.: Stability of Thin-Walled Tubes under Torsion. NACA TR 479, 1933.

12. Nowacki, W.: Some Stability Problems of Cylindrical Shells. Proc. of the Second Symposium of Concrete Shell Roof Construction, 1957, pp. 232-241.

13. Olesiak, Zbigniew: Discontinuous Boundary Conditions and Linear Supports in Statical Problems of Cylindrical Shells. Archiwum Mechaniki Stosowanej, Vol. 9, No. 5, 1957, pp. 549-563.

14. Quinlan, P. M.: Rectangular Plates – A New Approach. Nat'l. University of Ireland, TN 3 (USAF EOARDC TN 58-259), AD 154163, January 1958.

15. Yuan, S. W.: Thin Cylindrical Shells Subjected to Concentrated Loads. Quarterly of Appl. Math., Vol. 4, No. 1, April 1946, pp. 13-26.

16. Morley, L. S. D.: The Thin-Walled Circular Cylinder Subjected to Concentrated Radial Loads. Quarterly Journal of Mechs. and Appl. Math., Vol. 13, Part I, February 1960, pp. 24-37.

17. Yuan, S. W.: On Radial Deflections of a Cylinder Subjected to Equal and Opposite Concentrated Radial Loads – Infinitely Long Cylinders and Finite Length Cylinders with Simply Supported Ends. Journal of Appl. Mechs., Vol. 24, No. 2, June 1957, pp. 278-282.

18. Hetenyi, M.: The Infinite Beam on Equidistant Supports and Related Problems. Proc. of the Third U. S. Nat'l. Congress of Appl. Mechs., 1958, pp. 369-374.

19. Duncan, W. J.: Galerkin's Method in Mechanics and Differential Equations. ARC R and M 1798, 1937.

20. Miles, J. W.: On a Reciprocity Condition for Supersonic Flutter. Journal of Aero. Sci., Vol. 24, No. 12, December 1957, p. 920.

21. Franklin, J. N.: Computation of Eigenvalues by the Method of Iteration. Computing Center Technical Report No. 111, California Institute of Technology, October 1957.

22. Powell, E. O.: An Integral Related to the Radiation Integrals. Phil. Mag., Series 7, Vol. 35, 1943, pp. 600-607.

APPENDIX A

Influence Function for the Flutter Analysis

The elastic influence function required for the flutter analysis is derived in this section by employing the method of superposition.

In the formulation of the flutter problem it was shown that this influence function is represented by the deflection surface of the 0th panel of the stiffened shell when the shell is subjected to the special loading condition shown in Figure 5. (The concentrated loads in this case are normal to the shell surface and occupy the same position relative to each span.)

The function $W^{(i)}(\alpha, \beta^{(i)})$ given by Table III for the deflections of the ith and -ith panels of the stiffened shell due to a concentrated unit load on the 0th panel may be written in the form

$$W^{(i)}(\alpha, \beta^{(i)}) = \frac{2R^2\alpha_1^4}{\pi^3 N\beta_1^2} \sum_{m=1}^{\infty}\sum_{n=1}^{\infty}\left[\gamma_m\right]^i q_m^{(o)}\left[\frac{1-(-1)^n\gamma_m}{\gamma_m}\right]\frac{n\sin\frac{n\pi}{\beta_1}\beta^{(i)}\sin\frac{m\pi}{\alpha_1}\alpha}{D_{mn}}$$

$$W^{(-i)}(\alpha, \beta^{(-i)}) = \frac{2R^2\alpha_1^4}{\pi^3 N\beta_1^2} \sum_{m=1}^{\infty}\sum_{n=1}^{\infty}\left[\gamma_m\right]^i q_m^{(-1)}\left[\frac{\gamma_m-(-1)^n}{\gamma_m}\right]\frac{n\sin\frac{n\pi}{\beta_1}\beta^{(-i)}\sin\frac{m\pi}{\alpha_1}\alpha}{D_{mn}}$$

If the 0th panel has a concentrated load of magnitude P the corresponding deflections will be given by

$$P\,W^{(i)}(\alpha, \beta^{(i)})$$

$$P\,W^{(-i)}(\alpha, \beta^{(-i)}).$$

By superimposing the effects of the concentrated loads and employing the cyclic property of the structure the deflection of the 0th panel due to this special loading may be written for a total of $2N+1$ panels as

$$W^{(o)}(\alpha, \beta^{(o)}) + k_o(\alpha, \beta^{(o)}; \Xi, H^{(o)}) + \sum_{i=1}^{N} W^{(i)}(\alpha, \beta^{(o)}) e^{-j(i\sigma)}$$

$$+ \sum_{i=1}^{N} W^{(-i)}(\alpha, \beta^{(o)}) e^{j(i\sigma)}$$

Assuming that it is permissible to interchange the order of summation the above may be written as:

$$W^{(o)}(\alpha, \beta^{(o)}) + \frac{2R^2\alpha_1^4}{\pi^3 N \beta_1^2} \sum_{m=1}^{\infty} \sum_{n=1}^{\infty} \left[\sum_{i=1}^{N} e^{j(i\sigma)} \left[\gamma_m\right]^i q_m^{(-1)} \left(\frac{\gamma_m - (-1)^n}{\gamma_m}\right) \right.$$

$$\left. + \sum_{i=1}^{N} e^{-j(i\sigma)} \left[\gamma_m\right]^i q_m^{(o)} \left(\frac{1 - (-1)^n \gamma_m}{\gamma_m}\right) \right] \frac{n \sin\left(\frac{n\pi}{\beta_1}\right)\beta^{(o)} \sin\left(\frac{m\pi}{\alpha_1}\right)\alpha}{D_{mn}}$$

Now the series summed over i may be approximated for large N by

$$\sum_{i=1}^{N} e^{-j(i\sigma)} \left[\gamma_m\right]^i \approx \sum_{i=1}^{\infty} e^{-j(i\sigma)} \left[\gamma_m\right]^i = \frac{\gamma_m(e^{-j\sigma} - \gamma_m)}{1 - 2\gamma_m \cos\sigma + \gamma_m^2}$$

$$\sum_{i=1}^{N} e^{j(i\sigma)} \left[\gamma_m\right]^i \approx \frac{\gamma_m(e^{j\sigma} - \gamma_m)}{1 - 2\gamma_m \cos\sigma + \gamma_m^2}$$

and hence the deflection function of the 0th panel approximated by

$$k_o(\alpha, \beta^{(o)}; \Xi, H) + \frac{2R^2\alpha_1^4}{\pi^3 N \beta_1^2} \sum_{m=1}^{\infty} \sum_{n=1}^{\infty} \left[\bar{q}_m^{(-1)} - (-1)^n \bar{q}_m^{(o)} \right] \frac{n \sin(\frac{n\pi}{\beta_1}) \beta^{(o)} \sin(\frac{m\pi}{\alpha_1}) \alpha}{D_{mn}} \tag{A.1}$$

where

$$\bar{q}_m^{(-1)}(\Xi, H) = q_m^{(-1)}(\Xi, H) \frac{(1 - \gamma_m e^{-j\sigma})}{1 - 2\gamma_m \cos\sigma + \gamma_m^2}$$

$$+ q_m^{(o)}(\Xi, H) \frac{(e^{-j\sigma} - \gamma_m)}{1 - 2\gamma_m \cos\sigma + \gamma_m^2}$$

$$\bar{q}_m^{(o)}(\Xi, H) = q_m^{(-1)}(\Xi, H) \frac{(e^{j\sigma} - \gamma_m)}{1 - 2\gamma_m \cos\sigma + \gamma_m^2}$$

$$+ q_m^{(o)}(\Xi, H) \frac{(1 - \gamma_m e^{j\sigma})}{1 - 2\gamma_m \cos\sigma + \gamma_m^2}$$

The extension of these results to the other cases shown in Figure 3 follows immediately with the aid of Table III.

Equation A-1 yields the radial deflection surface of an equivalent panel bent by moments distributed along the two straight sides and concentrated load acting at the point (Ξ, H).

TABLE I

Case	$K_{11}(\alpha, \xi)$
Original	$\frac{4R^2\lambda^3}{\pi^2 N} \sum_{m=1}^{\infty}\sum_{n=1}^{\infty} \frac{n^2 \sin\frac{m\pi}{\alpha_1}\alpha \sin\frac{m\pi}{\alpha_1}\xi}{D_{mn}}$
(a)	$\frac{2R^2\pi}{N} \sum_{n=1}^{\infty} n^2 \left[\pi_n(\alpha'-\xi') - \pi_n(\alpha'+\xi')\right]$
(b)	$\frac{2R^2\pi}{N} \sum_{n=1}^{\infty} n^2 \pi_n(\alpha'-\xi')$
(c)	$\frac{1}{2\pi N}\frac{\partial}{\partial\bar{\lambda}}\left[\bar{\lambda} LN \frac{\theta_1\left[\frac{\pi}{2a}(\alpha-\xi);\bar{\lambda}\right]}{\theta_1\left[\frac{\pi}{2a}(\alpha+\xi);\bar{\lambda}\right]}\right]$
(d)	case (e) $- \frac{\mathcal{L}_1(e^{-\frac{\pi}{b}(\alpha+\xi)})}{2\pi N} + \frac{\pi}{b}(\alpha+\xi)\frac{\mathcal{L}_0(e^{\frac{\pi}{b}(\alpha+\xi)})}{2\pi N}$
(e)	$\frac{1}{2\pi N}\left[\mathcal{L}_1(e^{\pm\frac{\pi}{b}(\alpha-\xi)}) \mp \frac{\pi}{b}(\alpha-\xi)\mathcal{L}_0(e^{\pm\frac{\pi}{b}(\alpha-\xi)})\right]$

Note: $\mathcal{L}_0(Z) = -1/L_0(Z) = Z/1-Z$ $\quad \alpha > \xi$ Lower sign

$\mathcal{L}_1(Z) = -L_1(1-Z) = LN\frac{1}{1-Z}$ $\quad \alpha < \xi$ Upper sign

See Reference 22 for a table of these functions.

TABLE I (Cont'd)

Case	$K_{13}(\alpha, \xi)$
Original	$\frac{4R^2\lambda^3}{\pi^2 N} \sum_{m=1}^{\infty} \sum_{n=1}^{\infty} \frac{(-1)^n n^2 \sin \frac{m\pi}{\alpha_1}\alpha \sin \frac{m\pi}{\alpha_1}\xi}{D_{mn}}$
(a)	$\frac{2R^2\pi}{N} \sum_{n=1}^{\infty} (-1)^n n^2 \left[\pi_n(\alpha' - \xi') - \pi_n(\alpha' + \xi') \right]$
(b)	$\frac{2R^2\pi}{N} \sum_{n=1}^{\infty} (-1)^n \pi_n(\alpha' - \xi')$
(c)	$\frac{1}{2\pi N} \frac{\partial}{\partial \bar{\lambda}} \left[\bar{\lambda} LN \frac{\theta_o\left[\frac{\pi}{2a}(\alpha - \xi); \bar{\lambda}\right]}{\theta_o\left[\frac{\pi}{2a}(\alpha + \xi); \bar{\lambda}\right]} \right]$
(d)	case (e) - $\frac{\mathcal{L}_1(-e^{-\frac{\pi}{b}(\alpha+\xi)})}{2\pi N} + \frac{\pi}{b}(\alpha+\xi) \frac{\mathcal{L}_o(-e^{\frac{\pi}{b}(\alpha+\xi)})}{2\pi N}$
(e)	$\frac{1}{2\pi N} \left[\mathcal{L}_1(-e^{\pm\frac{\pi}{b}(\alpha-\xi)}) \mp \frac{\pi}{b}(\alpha-\xi) \mathcal{L}_o(-e^{\pm\frac{\pi}{b}(\alpha-\xi)}) \right]$

$\alpha > \xi$ Lower sign

$\alpha < \xi$ Upper sign

TABLE I (Cont'd)

Case	$f(\alpha;\Xi,H)$
Original	$\dfrac{4R^2\alpha_1^3}{\pi^3 N\beta_1^2}\displaystyle\sum_{m=1}^{\infty}\sum_{n=1}^{\infty}\dfrac{(-1)^n n \sin\frac{m\pi}{\alpha_1}\alpha \sin\frac{m\pi}{\alpha_1}\Xi \sin\frac{n\pi}{\beta_1}H}{D_{mn}}$
(a)	$\dfrac{2R^2\beta_1}{N}\displaystyle\sum_{n=1}^{\infty}(-1)^n n \sin\frac{n\pi}{\beta_1}H\left[\pi_n(\alpha'-\Xi')-\pi_n(\alpha'+\Xi')\right]$
(b)	$\dfrac{2R^2\beta_1}{N}\displaystyle\sum_{n=1}^{\infty}(-1)^n n \sin\frac{n\pi}{\beta_1}H\ \pi_n(\alpha'-\Xi')$
(c)	$\dfrac{b}{\pi^2 N}\displaystyle\sum_{m=1}^{\infty}\dfrac{\sin\frac{m\pi}{a}\alpha\ \sin\frac{m\pi}{a}\Xi}{m^2}\dfrac{\partial}{\partial\bar{\lambda}}\left[\dfrac{\sinh m\pi\bar{\lambda}\frac{H}{b}}{\sinh m\pi\bar{\lambda}}\right]$
(d)	$\dfrac{b}{2\pi^2 N}\displaystyle\sum_{n=1}^{\infty}(-1)^n\left(\left[1\mp\frac{n\pi}{b}(\alpha-\Xi)\right]e^{\pm\frac{n\pi}{b}(\alpha-\Xi)}-\left[1+\frac{n\pi}{b}(\alpha+\Xi)\right]e^{-\frac{n\pi}{b}(\alpha+\Xi)}\right)\dfrac{\sin\frac{n\pi}{b}H}{n^2}$
(e)	$\dfrac{b}{2\pi^2 N}\displaystyle\sum_{n=1}^{\infty}(-1)^n\left[1\mp\frac{n\pi}{b}(\alpha-\Xi)\right]e^{\pm\frac{n\pi}{b}(\alpha-\Xi)}\dfrac{\sin\frac{n\pi}{b}H}{n^2}$

TABLE I (Cont'd)

Case	$g(\alpha;\Xi,\ H)$
Original	$\dfrac{4R^2\alpha_1^3}{\pi^3 N\beta_1^2}\sum_{m=1}^{\infty}\sum_{n=1}^{\infty}\dfrac{n\sin\frac{m\pi}{\alpha_1}\alpha\ \sin\frac{n\pi}{\alpha_1}\Xi\sin\frac{n\pi}{\beta_1}H}{D_{mn}}$
(a)	$\dfrac{2R^2\beta_1}{N}\sum_{n=1}^{\infty} n\sin\frac{n\pi}{\beta_1}H\left[\pi_n(\alpha'-\Xi')-\pi_n(\alpha'+\Xi')\right]$
(b)	$\dfrac{2R^2\beta_1}{N}\sum_{n=1}^{\infty} n\sin\frac{n\pi}{\beta_1}H\ \pi_n(\alpha'-\Xi')$
(c)	$-\dfrac{b}{\pi^2 N}\sum_{m=1}^{\infty}\dfrac{\sin\frac{m\pi}{a}\alpha\sin\frac{m\pi}{a}\Xi}{m^2}\dfrac{\partial}{\partial\bar{\lambda}}\left[\dfrac{\sinh m\pi\bar{\lambda}(1-\frac{H}{b})}{\sinh m\pi\bar{\lambda}}\right]$
(d)	$\dfrac{b}{2\pi^2 N}\sum_{n=1}^{\infty}\left(\left[1\mp\frac{n\pi}{b}(\alpha-\Xi)\right]e^{\pm\frac{n\pi}{b}(\alpha-\Xi)}-\left[1+\frac{n\pi}{b}(\alpha+\Xi)\right]e^{-\frac{n\pi}{b}(\alpha+\Xi)}\right)\dfrac{\sin\frac{n\pi}{b}H}{n^2}$
(e)	$\dfrac{b}{2\pi^2 N}\sum_{n=1}^{\infty}\left[1\mp\frac{n\pi}{b}(\alpha-\Xi)\right]e^{\pm\frac{n\pi}{b}(\alpha-\Xi)}\dfrac{\sin\frac{n\pi}{b}H}{n^2}$

TABLE II

Case	A	$\overline{A}$
Original	$\frac{2}{\pi\lambda}\sin\frac{m\pi}{\alpha_1}\Xi = \sum_{n=1}^{\infty}\frac{(-1)^n n \sin\frac{n\pi}{\beta_1}H}{D_{mn}}$	$\frac{2}{\pi\lambda}\sin\frac{m\pi}{\alpha_1}\Xi = \sum_{n=1}^{\infty}\frac{n \sin\frac{n\pi}{\beta_1}H}{D_{mn}}$
(a)	$\frac{2}{\pi^2}\sin t\frac{\Xi}{\beta_1}\sum_{n=1}^{\infty}\frac{(-1)^n n \sin\frac{n\pi}{\beta_1}H}{D(t,n)}$	$\frac{2}{\pi^2}\sin t\frac{\Xi}{\beta_1}\sum_{n=1}^{\infty}\frac{n \sin\frac{n\pi}{\beta_1}H}{D(t,n)}$
(b)	$\frac{1}{\pi^2}\sum_{n=1}^{\infty}\frac{(-1)^n n \sin\frac{n\pi}{\beta_1}H}{D(t,n)}$	$\frac{1}{\pi^2}\sum_{n=1}^{\infty}\frac{n \sin\frac{n\pi}{\beta_1}H}{D(t,n)}$
(c)	$\frac{2}{\pi\lambda}\sin\frac{m\pi}{a}\Xi = \sum_{n=1}^{\infty}\frac{(-1)^n n \sin\frac{n\pi}{b}H}{(m^2+\lambda^2 n^2)^2}$	$\frac{2}{\pi\lambda}\sin\frac{m\pi}{a}\Xi = \sum_{n=1}^{\infty}\frac{n \sin\frac{n\pi}{b}H}{(m^2+\lambda^2 n^2)^2}$
(d)	$\frac{2}{\pi^2}\sin t\frac{\Xi}{b}\sum_{n=1}^{\infty}\frac{(-1)^n n \sin\frac{n\pi}{b}H}{(t^2+n^2\pi^2)^2}$	$\frac{2}{\pi^2}\sin t\frac{\Xi}{b}\sum_{n=1}^{\infty}\frac{n \sin\frac{n\pi}{b}H}{(t^2+n^2\pi^2)^2}$
(e)	$\frac{1}{\pi^2}\sum_{n=1}^{\infty}\frac{(-1)^n n \sin\frac{n\pi}{b}H}{(t^2+n^2\pi^2)^2}$	$\frac{1}{\pi^2}\sum_{n=1}^{\infty}\frac{n \sin\frac{n\pi}{b}H}{(t^2+n^2\pi^2)^2}$

TABLE II (Cont'd)

Case	B	C
Original	$\sum_{n=1}^{\infty} \frac{(-1)^n n^2}{D_{mn}}$	$\sum_{n=1}^{\infty} \frac{n^2}{D_{mn}}$
(a)	$\sum_{n=1}^{\infty} \frac{(-1)^n n^2}{D(t, n)}$	$\sum_{n=1}^{\infty} \frac{n^2}{D(t, n)}$
(b)	$\sum_{n=1}^{\infty} \frac{(-1)^n n^2}{D(t, n)}$	$\sum_{n=1}^{\infty} \frac{n^2}{D(t, n)}$
(c)	$\sum_{n=1}^{\infty} \frac{(-1)^n n^2}{(m^2 + \lambda^2 n^2)^2}$	$\sum_{n=1}^{\infty} \frac{n^2}{(m^2 + \lambda^2 n^2)^2}$
(d)	$\sum_{n=1}^{\infty} \frac{(-1)^n n^2}{(t^2 + n^2\pi^2)^2}$	$\sum_{n=1}^{\infty} \frac{n^2}{(t^2 + n^2\pi^2)^2}$
(e)	$\sum_{n=1}^{\infty} \frac{(-1)^n n^2}{(t^2 + n^2\pi^2)^2}$	$\sum_{n=1}^{\infty} \frac{n^2}{(t^2 + n^2\pi^2)^2}$

TABLE III

Case	$W^{(i)}(\alpha, \beta^{(i)})$

Original

$$\frac{2R^2\alpha_1^4}{\pi^3 N\beta_1^2}\sum_{m=1}^{\infty}\sum_{n=1}^{\infty}\frac{\left[q_m^{(i-1)}-(-1)^n q_m^{(i)}\right] n \sin\left(\frac{n\pi}{\beta_1}\right)\beta^{(i)} \sin\left(\frac{m\pi}{\alpha_1}\right)\alpha}{D_{mn}}$$

(a)

$$\frac{2R^2\beta_1^2\pi}{N}\int_0^{\infty}\left(\sum_{n=1}^{\infty}\frac{\left[q(t)^{(i-1)}-(-1)^n q^{(i)}(t)\right] n \sin\left(\frac{n\pi}{\beta_1}\right)\beta^{(i)}\sin t\alpha'}{D(t,n)}\right)dt$$

(b)

$$\frac{2R^2\beta_1^2\pi}{N}\int_0^{\infty}\left(\sum_{n=1}^{\infty}\frac{\left[q^{(i-1)}(t)-(-1)^n q^{(i)}(t)\right] n \sin\left(\frac{n\pi}{\beta_1}\right)\beta^{(i)}\cos t(\alpha'-\Xi')}{D(t,n)}\right)dt$$

(c)

$$\frac{2a^4}{\pi^3 Nb^2}\sum_{m=1}^{\infty}\sum_{n=1}^{\infty}\frac{\left[q_m^{(i-1)}-(-1)^n q_m^{(i)}\right] n \sin\frac{n\pi}{b}\beta^{(i)}\sin\frac{m\pi}{a}\alpha}{(m^2+\lambda^2 n^2)^2}$$

(d)

$$\frac{2b^2\pi}{N}\int_0^{\infty}\left(\sum_{n=1}^{\infty}\frac{\left[q^{(i-1)}(t)-(-1)^n q^{(i)}(t)\right] n \sin\frac{n\pi}{b}\beta^{(i)}\sin t\alpha'}{(t^2+n^2\pi^2)^2}\right)dt$$

(e)

$$\frac{2b^2\pi}{N}\int_0^{\infty}\left(\sum_{n=1}^{\infty}\frac{\left[q^{(i-1)}(t)-(-1)^n q^{(i)}(t)\right] n \sin\frac{n\pi}{b}\beta^{(i)}\cos t(\alpha'-\Xi')}{(t^2+n^2\pi^2)^2}\right)dt$$

TABLE III (Cont'd)

Case $k_o(\alpha, \beta^{(o)}; \Xi, H^{(o)})$

Original
$$\frac{4R^2\alpha_1^3}{\pi^4 N \beta_1} \sum_{m=1}^{\infty}\sum_{n=1}^{\infty} \frac{\sin\frac{m\pi}{\alpha_1}\alpha \sin\frac{n\pi}{\beta_1}\beta^{(o)} \sin\frac{m\pi}{\alpha_1}\Xi \sin\frac{n\pi}{\beta_1}H^{(o)}}{D_{mn}}$$

(a)
$$\frac{2R^2\beta_1^2}{\pi N} \sum_{n=1}^{\infty}\left[\pi_n(\alpha'-\Xi') - \pi_n(\alpha'+\Xi')\right] \sin(\tfrac{n\pi}{\beta_1})\beta^{(o)} \sin(\tfrac{n\pi}{\beta_1})H^{(o)}$$

(b)
$$\frac{2R^2\beta_1^2}{\pi N} \sum_{n=1}^{\infty}\left[\pi_n(\alpha'-\Xi')\right] \sin\frac{n\pi}{\beta_1}\beta^{(o)} \sin\frac{n\pi}{\beta_1}H^{(o)}$$

(c)
$$\frac{4a^3}{\pi^4 Nb} \sum_{m=1}^{\infty}\sum_{n=1}^{\infty} \frac{\sin\frac{m\pi}{a}\alpha \sin\frac{n\pi}{b}\beta^{(o)} \sin\frac{m\pi}{a}\Xi \sin\frac{n\pi}{b}H^{(o)}}{(m^2+\lambda^2 n^2)^2}$$

(d)
$$\frac{b^2}{2\pi^3 N} \sum_{n=1}^{\infty}\left(\left[1\mp\tfrac{n\pi}{b}(\alpha-\Xi)\right]e^{\pm\frac{n\pi}{b}(\alpha-\Xi)} - \left[1+\tfrac{n\pi}{b}(\alpha+\Xi)\right]e^{-\frac{n\pi}{b}(\alpha+\Xi)}\right)\frac{\sin\frac{n\pi}{b}\beta^{(o)}\sin\frac{n\pi}{b}H^{(o)}}{n^3}$$

(e)
$$\frac{b^2}{2\pi^3 N} \sum_{n=1}^{\infty}\left[1\mp\tfrac{n\pi}{b}(\alpha-\Xi)\right]e^{\pm\frac{n\pi}{b}(\alpha-\Xi)} \frac{\sin\frac{n\pi}{b}\beta^{(o)}\sin\frac{n\pi}{b}H^{(o)}}{n^3}$$

$\alpha > \Xi$ Lower sign

$\alpha < \Xi$ Upper sign

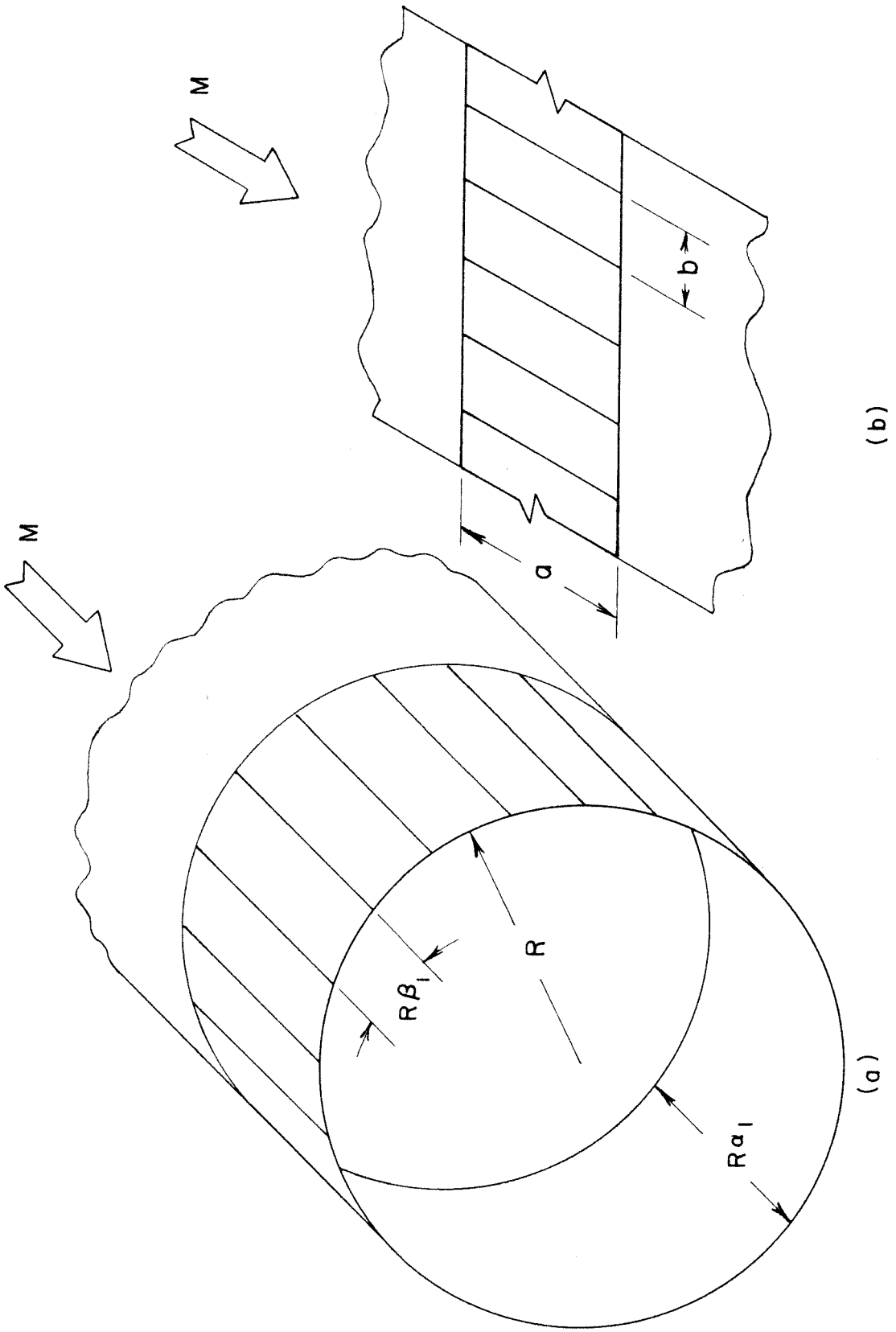

FIG. 1 THEORETICAL MODEL

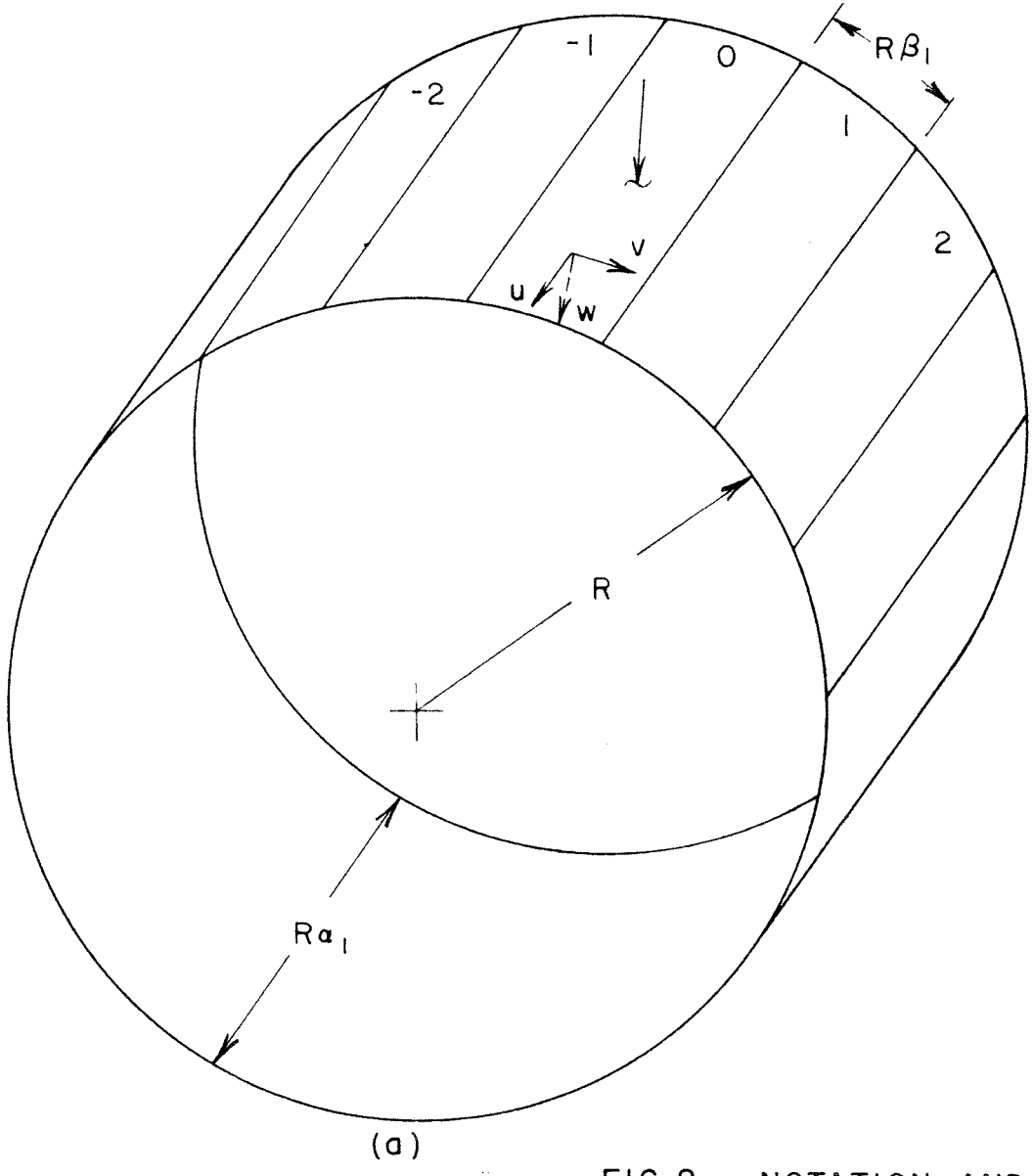

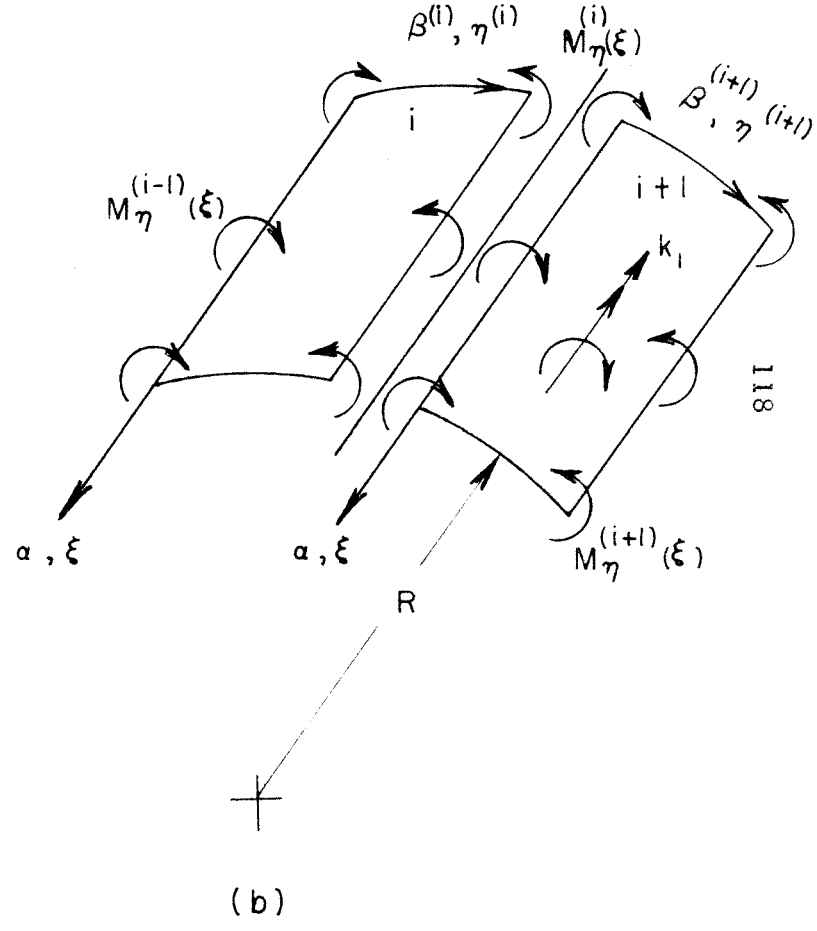

FIG. 2 NOTATION AND COORDINATE SYSTEM

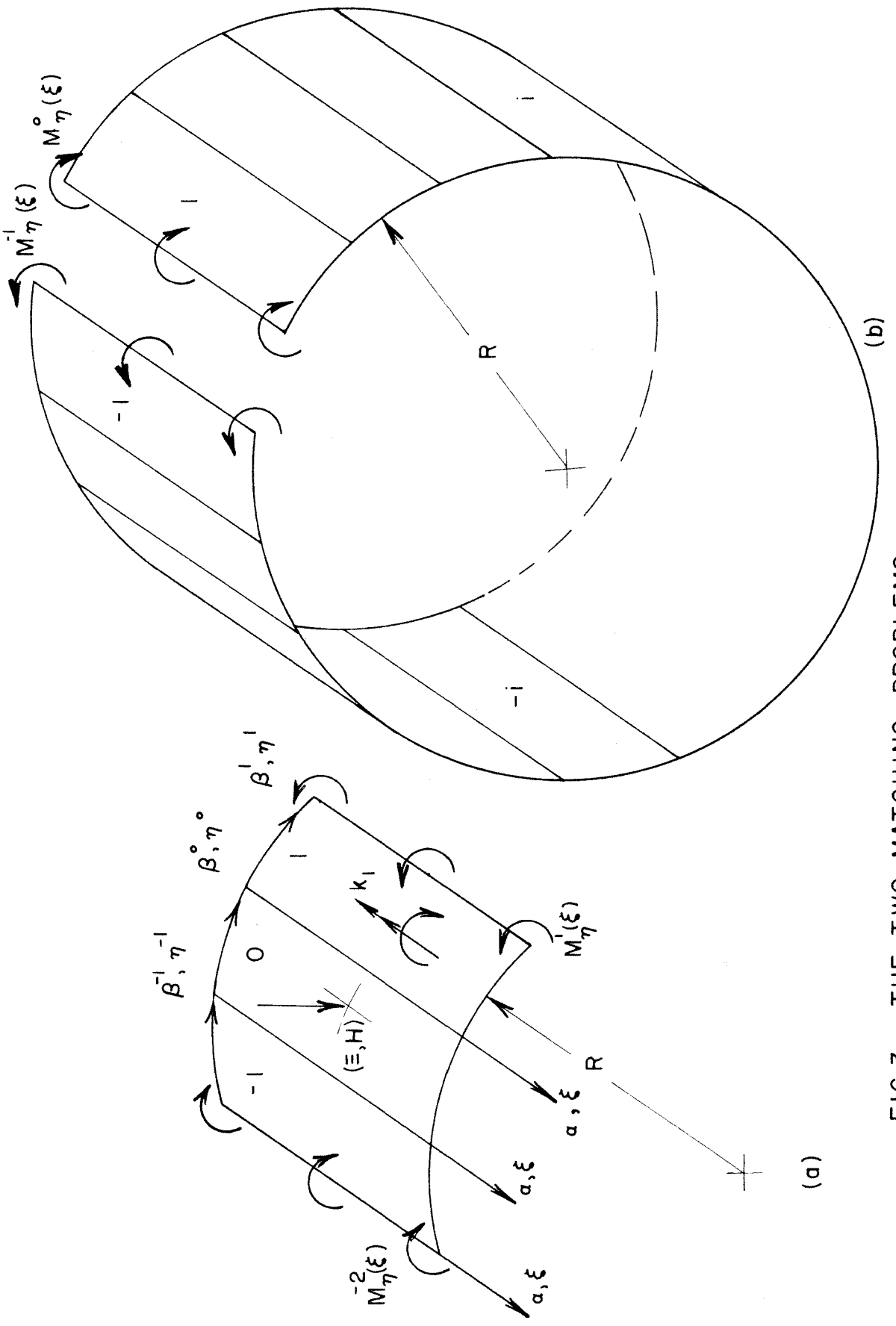

FIG.3 THE TWO MATCHING PROBLEMS

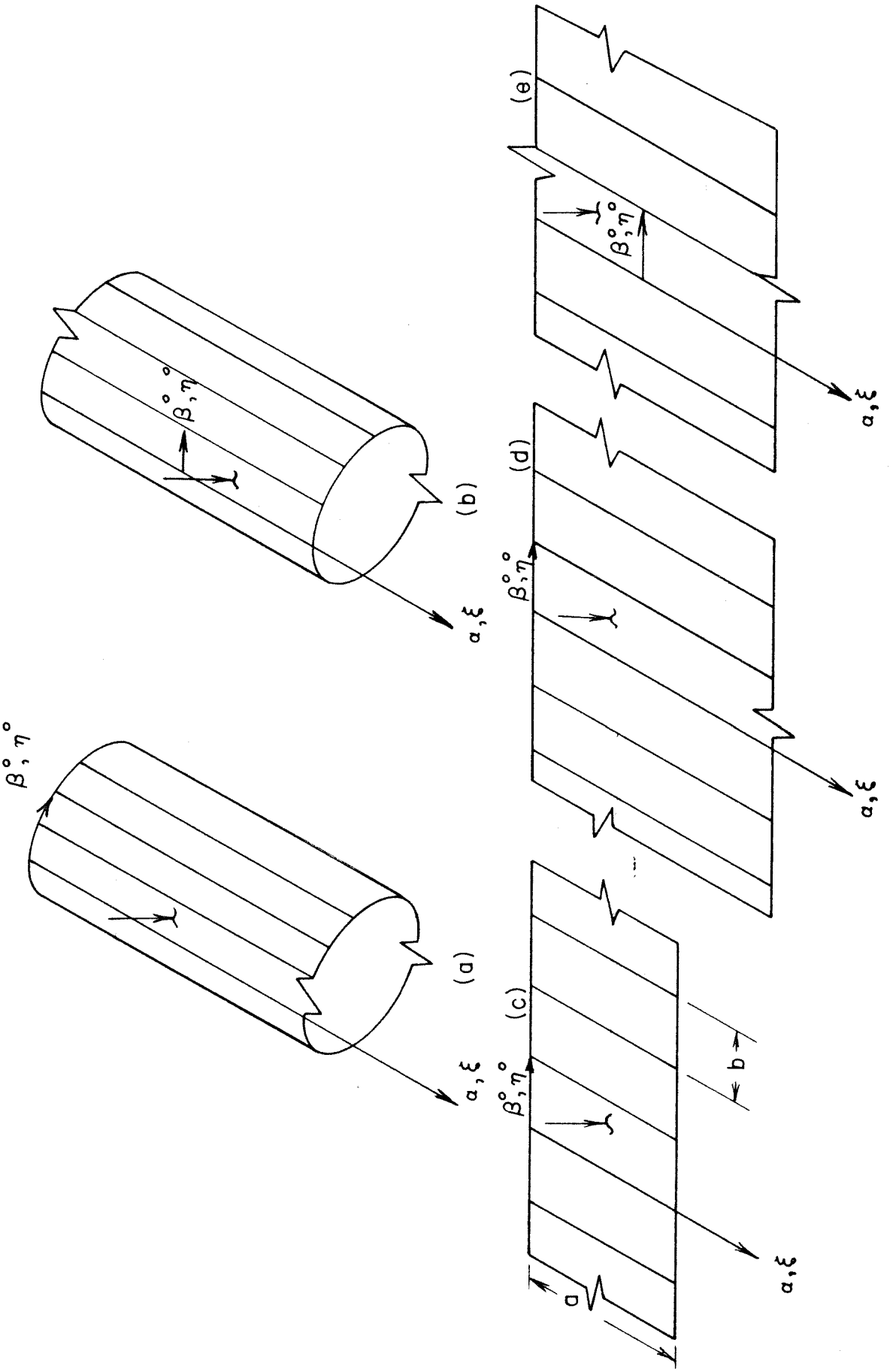

FIG. 4 LIMITING CASES

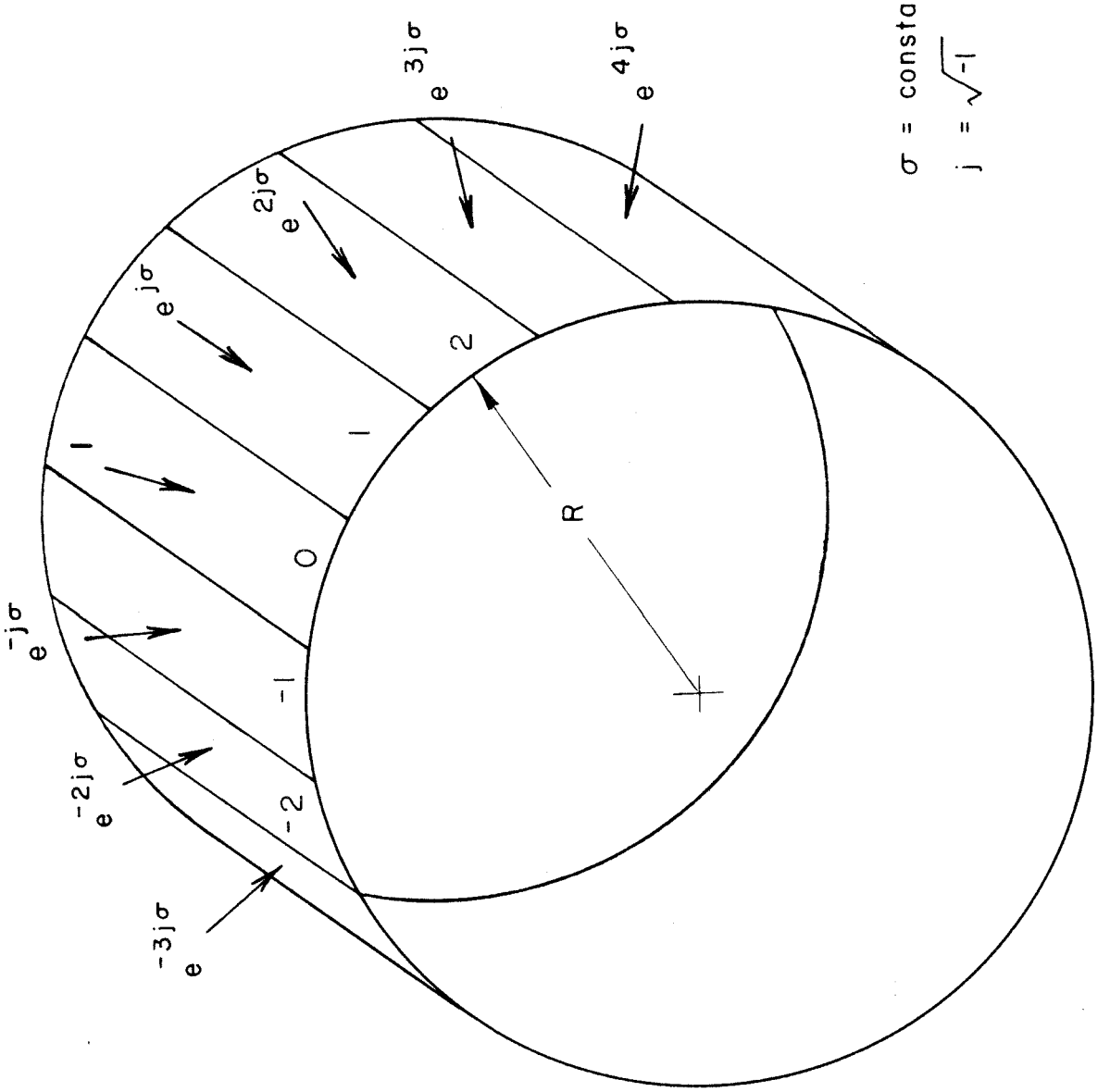

FIG. 5 EQUIVALENT LOADING FOR REDUCED PROBLEM

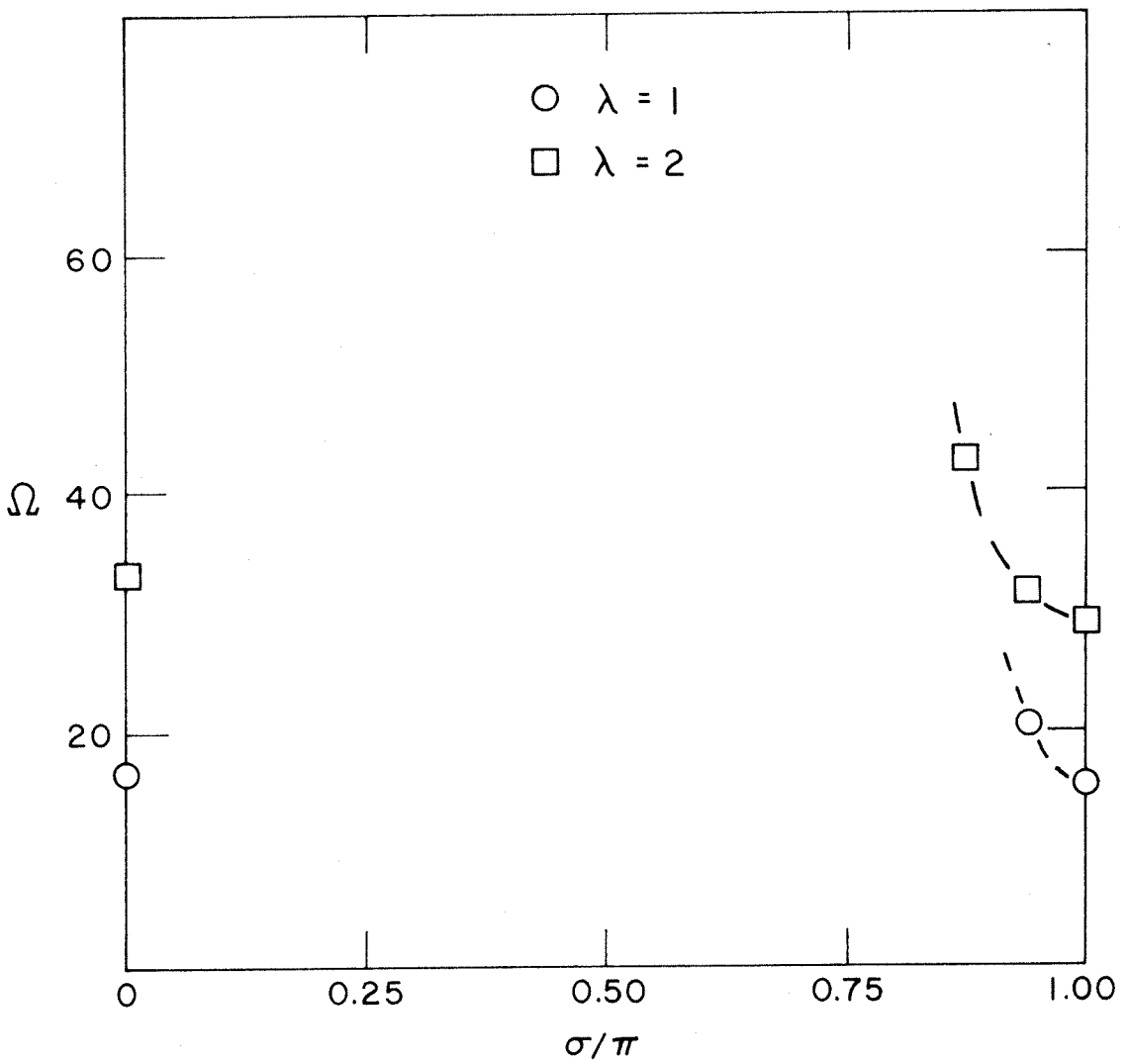

FIG. 6 EIGENVALUE VERSES INTERPANEL PHASE ANGLE